

THE ^{13}N COMPOUND NUCLEUS ABOVE 25 MeV EXCITATION

AND

THE ENERGY LEVEL STRUCTURE OF ^{57}Co , ^{59}Co AND ^{61}Co

by

Ian Garth Graham

A Thesis submitted to the Australian National University
for the degree of Doctor of Philosophy

Canberra, A.C.T.

August, 1971



To
my Parents
and
Helen

PREFACE

This thesis describes two experimental studies which were carried out within the Department of Nuclear Physics at the Australian National University using the 6 MV tandem Van de Graaff accelerator and associated experimental facilities.

The studies on the odd-mass cobalt nuclei were initiated by Mr. (now Dr.) K.L. Coop, and the experimental work was shared equally with him. About two-thirds of the data for chapter 6 and one-half of the data for chapter 7 were analyzed by myself. The main computer programs used in the analysis of the data were written by Dr. T.R. Ophel (γ -ray line shape fitting program), Dr. D.C. Kean (angular correlation fitting program) and myself. A further angular correlation investigation of ^{57}Co , in which I took part, is not presented in this thesis but has appeared in the publication:

"Angular correlation studies of the low-lying levels of ^{57}Co ", K.L. Coop, I.G. Graham and E.W. Titterton, Nucl. Phys. A149 (1970) 463.

The investigation of the ^{13}N compound system grew from a suggestion by Professor E.W. Titterton. The experimental work and the data reduction were shared equally with Dr. R.A.I. Bell and Mr. J.V. Thompson.

Some of the work reported here has appeared in the following publications:

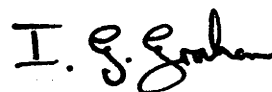
"Energy levels in $^{57,59,61}\text{Co}$ from the $^{60,62,64}\text{Ni}$ (p, α) reactions", K.L. Coop, I.G. Graham, J.M. Poate and E.W. Titterton, Nucl. Phys. A130 (1969) 223;

"An investigation of ^{59}Co and ^{61}Co using the $^{56}\text{Fe}(\alpha, p\gamma)$ and $^{64}\text{Ni}(p, \alpha\gamma)$ reactions", K.L. Coop, I.G. Graham and E.W. Titterton, Nucl. Phys. A150 (1970) 346; and "Cross-sections of $^{10}\text{B}(\tau, \gamma)^{13}\text{N}$ and $^{10}\text{B}(\tau, p\gamma)^{12}\text{C}$ reactions", R.A.I. Bell, I.G. Graham and J.V. Thompson, to be published.

During the course of this work, many people in the department have given assistance at one stage or another and it is not possible to name them all. However, I would particularly like to thank Ken Coop for his patience and guidance in my first two years at the laboratory, and Robin Bell and John Thompson for their help and generous, though at times somewhat light-hearted, advice in the later studies. Mr. T.A. Brinkley's willing and able assistance in the laboratory was also greatly appreciated. Many thanks are also due to Professor J.O. Newton, Dr. T.R. Ophel, Dr. P.B. Treacy and Dr. R.A.I. Bell for constructive criticism of parts of this manuscript, and to Miss Norma Chin for her able typing of the thesis.

Finally, I would like to thank Professor Sir Ernest Titterton for his supervision and support, and the Australian National University for the award of a Post-graduate Research Scholarship.

No part of this thesis has been submitted for a degree at any other university.



I.G. Graham

Canberra,

August 1971.

TABLE OF CONTENTS

	Page
PREFACE	i
ABSTRACT	vi
PART I	
THE ^{13}N COMPOUND NUCLEUS ABOVE 25 MeV EXCITATION	
CHAPTER 1 - INTRODUCTION	1
CHAPTER 2 - THE $(^3\text{He},\alpha)$, $(^3\text{He},d)$ AND $(^3\text{He},p)$ EXCITATION FUNCTIONS	8
2.1 THE $^{10}\text{B}(^3\text{He},\alpha)^9\text{B}$ REACTION	8
2.1.1 Experimental Details	8
2.1.2 Results	12
2.1.3 Discussion	14
2.2 THE $^{10}\text{B}(^3\text{He},d)^{11}\text{C}$ REACTION	16
2.2.1 Experimental Details	16
2.2.2 Results	18
2.2.3 Discussion	20
2.3 THE $^{10}\text{B}(^3\text{He},p)^{12}\text{C}$ REACTION	20
2.3.1 Experimental Details	21
2.3.2 Results	23
2.3.3 Discussion	24
2.4 SUMMARY	24
CHAPTER 3 - THE $(^3\text{He},p\gamma)$ AND $(^3\text{He},\gamma)$ MEASUREMENTS	26
3.1 INTRODUCTION	26
3.2 EXPERIMENTAL DETAILS	27
3.3 ANALYSIS AND RESULTS	31
3.4 DISCUSSION	34

TABLE OF CONTENTS (cont'd)

	Page
CHAPTER 4 - SUMMARY AND CONCLUSIONS	39
PART II	
THE ENERGY LEVEL STRUCTURE OF ^{57}Co , ^{59}Co AND ^{61}Co	
CHAPTER 5 - INTRODUCTION	47
CHAPTER 6 - ENERGY LEVELS IN $^{57,59,61}\text{Co}$ FROM THE $^{60,62,64}\text{Ni}(p,\alpha)$ REACTIONS	50
6.1 INTRODUCTION	50
6.2 EXPERIMENTAL DETAILS	53
6.3 RESULTS OF THE (p,α) EXPERIMENTS	56
6.3.1 ^{57}Co Results	58
6.3.2 ^{59}Co Results	58
6.3.3 ^{61}Co Results	59
6.4 DISCUSSION	61
CHAPTER 7 - THE $^{56,58}\text{Fe}(\alpha,p\gamma)$ AND $^{64}\text{Ni}(p,\alpha\gamma)$ MEASUREMENTS	65
7.1 INTRODUCTION	65
7.2 $^{56}\text{Fe}(\alpha,p)^{59}\text{Co}$ EXCITATION FUNCTIONS	66
7.3 PARTICLE-GAMMA-RAY COINCIDENCE MEASUREMENTS	68
7.3.1 Method A	68
7.3.2 Method B	71
7.3.3 Method C	74
7.4 ^{59}Co RESULTS	76
7.4.1 γ -ray Branching Ratios	76
7.4.2 Angular Correlation Measurements	79
7.5 ^{61}Co RESULTS	90

TABLE OF CONTENTS (cont'd)

	Page
7.6 DISCUSSION	99
CHAPTER 8 - CONCLUSIONS	101
APPENDIX - CONSIDERATIONS INVOLVED IN ANGULAR CORRELATION MEASUREMENTS	108
REFERENCES	114

ABSTRACT

Two independent studies of nuclear energy levels are described. In the first part of the thesis, the ^{13}N compound nucleus above 25 MeV excitation was investigated through $^{10}\text{B} + ^3\text{He}$ reactions. Excitation functions were measured for the $^{10}\text{B}(^3\text{He},\alpha)^9\text{B}$, $^{10}\text{B}(^3\text{He},\text{d})^{11}\text{C}$ and $^{10}\text{B}(^3\text{He},\text{p})^{12}\text{C}$ reactions in the region from 9 to 19 MeV bombarding energy (28.6 to 36.3 MeV excitation in ^{13}N). Both the $^{10}\text{B}(^3\text{He},\alpha_1)^9\text{B}^*$ (2.33 MeV) and $^{10}\text{B}(^3\text{He},\text{d}_{4,5})^{11}\text{C}^*$ (6.34 and 6.48 MeV) excitation functions measured at 150° (lab) showed increases in yield at about 13.5 MeV bombarding energy, indicative of a resonance in the ^{13}N compound system at 32 MeV excitation.

Excitation functions were also measured at 90° (lab) for the $^{10}\text{B}(^3\text{He},\text{p}\gamma)^{12}\text{C}$ ($E_\gamma = 12.71$ and 15.11 MeV) and $^{10}\text{B}(^3\text{He},\gamma)^{13}\text{N}$ reactions between 4 and 17 MeV ^3He energy. In contrast to previous measurements, the 15.11 MeV γ -ray yield from the $^{10}\text{B}(^3\text{He},\text{p}\gamma)^{12}\text{C}$ reaction showed the resonances at 26 and 28 MeV excitation already reported in previous $^{10}\text{B} + ^3\text{He}$ studies. The behaviour of the cross sections, and the smallness of the $(^3\text{He},\gamma_0)$ cross section, suggest that the 26, 28 and 32 MeV resonances are not associated with the ^{13}N giant dipole resonances.

The second part of the thesis describes an investigation of the odd-mass cobalt nuclei, ^{57}Co , ^{59}Co and ^{61}Co . The positions of levels below 3 MeV excitation in all three nuclei were measured using the $^{60,62,64}\text{Ni}(\text{p},\alpha)$ reactions and analyzing the α -particles with a broad range magnetic spectrograph. Particle- γ -ray coincidence measurements were performed on the $^{56,58}\text{Fe}(\alpha,\text{p}\gamma)$ and $^{64}\text{Ni}(\text{p},\alpha\gamma)$ reactions to determine γ -ray branching ratios in ^{59}Co and

^{61}Co , while $^{56}\text{Fe}(\alpha, p\gamma)$ angular correlations were measured for low lying states in ^{59}Co .

Branching ratios were obtained in ^{59}Co for many states below 2.6 MeV excitation, including the 1.744 MeV state which was found to have a branch to the 1.482 MeV state. Using the correlation data involving transitions from the 1.744 MeV state, J^π assignments of $9/2^-$ ($5/2^-$), $5/2^-$ and $7/2^-$ were made for the 1.190, 1.482 and 1.744 MeV states respectively. The measured correlations involving the 1.100 and 1.291 MeV states were consistent with $3/2^-$ assignments for both.

A number of previously unreported energy levels in ^{61}Co were identified, including the third excited state at 1.287 MeV. The decay properties of states below 2.3 MeV excitation were determined, and probable spin assignments of $7/2^-$, $5/2^-$ or $3/2^-$ and $5/2^-$ or $3/2^-$ were deduced for the states at 1.623, 1.655 and 2.015 MeV respectively.

The systematics of the level structure of the odd-mass cobalt isotopes were examined, and many similarities found.

PART I

THE ^{13}N COMPOUND NUCLEUS ABOVE 25 MeV EXCITATION

CHAPTER 1

INTRODUCTION

"In the case of nuclear transmutation caused by the impact of charged particles as well as for the nuclear disintegration produced by γ -rays, the formation of an intermediate semi-stable compound system seems decisive for the explanation of the great variety of the phenomena."

This extract from Bohr's original proposal [Bo 36] for the compound nucleus model of nuclear reactions is still true. The theory successfully describes most aspects of resonance behaviour in low energy nuclear reactions, and, in a modified form (the statistical model), can be used to interpret the features of reaction cross sections at higher energies.

The narrow resonances observed in reaction cross sections, which were one of the features that led Bohr to postulate the compound nucleus, only appear at low excitations. The energy dependence of these isolated resonances is usually described well by the Breit-Wigner dispersion formula, and at resonance the angular distributions of the reaction products are symmetric about 90° . As one goes higher in excitation, more channels for decay of the compound nucleus become available, so that the level width gets larger. At the same time the level density increases and the levels start to overlap. Interference between the states can then occur, and the angular distributions need no longer be symmetric about 90° . At even higher excitations, complete level overlap occurs and separate individual resonances are no longer observed. Instead, the cross

section is dominated by a large number of resonances, the amplitudes of which interfere strongly. In this region, the basic assumption of Bohr's model, that the formation and decay of the compound nucleus are independent, is invoked to postulate that the signs of the level amplitudes are random (the statistical model). The interference terms in cross sections averaged over energy intervals greater than the level width, then disappear, and the cross sections are smooth functions of energy, with angular distributions again symmetric about 90° . Thus, at low excitations, where the level width Γ is very much less than the average level spacing D , the compound nucleus theory can predict the fine structure present in excitation functions. However, at high excitations, where $\Gamma \gg D$, the model can only indicate the gross structure. A refinement of the statistical model [Er 63] postulates that if measurements are made with an energy resolution better than the average level width, then the excitation functions will exhibit peaks or fluctuations with average spacings of approximately twice the level width. Such peaks cannot be identified with individual resonances in the compound system.

Intensive experimental studies have been carried out on reactions in which the statistical concepts should have validity. In particular, studies of the compound system for A in the region of 30 and at excitations of approximately 20 MeV [e.g. He 70], have given strong support for the interpretation of excitation functions in terms of fluctuations. However there is also evidence [Si 66] that even at very high excitation, particular levels can be excited preferentially, giving rise to identifiable resonances.

Moldauer [Mo 67] has shown that when strongly absorbed channels are open, the distribution of widths and strengths for

excited states is so broad that, even when $\Gamma/D \gg 1$, it is possible that one state in the compound nucleus could dominate those underneath and around it. The resulting feature, when observed in an excitation function, will be recognized as an "intermediate resonance". Such an intermediate resonance will be associated with a definite orbital angular momentum in each channel. These resonances will therefore have characteristic angular distributions, especially in elastic scattering. Because of the strong absorption character of these states, reactions involving composite projectiles should exhibit this intermediate structure most strongly.

Similar properties are expected for the intermediate resonances arising from doorway states in the region of overlapping levels. These states have a configuration linking the incident particle and a simple excitation of the target nucleus, thus presenting a highly absorbing input channel. The doorway state can then quickly change to more complicated configurations in the compound nucleus before decaying. In the case of a single incoming nucleon, the doorway state is a two-particle, one-hole state [Le 64] which can quickly change through a three-particle, two-hole state to other less directly accessible configurations in the compound nucleus.

It is of interest to enquire whether statistical theories can be invoked for highly excited light nuclei. In previous work carried out in this laboratory [Os 64, Pa 65, Pa 65a, Pa 66, and Ba 66], intermediate structure was observed in the excitation functions of ^3He induced reactions on ^{10}B . These studies measured the ($^3\text{He},t$), ($^3\text{He},\alpha$), ($^3\text{He},d$), ($^3\text{He},p$), and ($^3\text{He},p\gamma_{15.11}$) excitation functions in the region between 2 and 12 MeV bombarding energy (23 to 31 MeV excitation in ^{13}N), and evidence was found for resonances

in the ^{13}N system at 22, 24.5, 26 and 28 MeV. Figure 1.1 shows the ^{13}N level scheme from the tabulations by Ajzenberg-Selove [Aj 69]; the general trend of some of the above excitation functions is indicated in the top left hand corner of the diagram. As can be seen, the observed peaks in the cross section have a width of about 1 MeV and are fairly strong, especially in the α_0 and p_0 exit channels.

Calculated level spacings and widths for neutron and proton emission at 24, 30 and 36 MeV excitation in ^{13}N are shown in table 1.1. Also shown are the calculated spacings of the two-particle, one-hole (doorway) states. These values were calculated from formulae derived from the Fermi gas model by Le Couteur [Po 67, Le 64]. The calculations are very sensitive to the value chosen for the density g of single nucleon states at the Fermi level; a value of the quantity:

$$a = A/8 \text{ MeV}^{-1} ,$$

$$\text{where } a \text{ is related to } g \text{ by } a = \pi^2 g/6 ,$$

was consistent with previous analyses in this mass region [Le 64], and was used in the present calculations (a value of $a = A/10 \text{ MeV}^{-1}$ generally tripled the level spacings and doubled the widths). With allowances for other decay modes, the total widths Γ should be approximately equal to $2 \Gamma_n$, so that, despite the above uncertainty, it is highly probable that we are in a region of overlapping levels where the statistical theory should be valid. This is rather a circular argument since the calculation of level widths and spacings depends on a statistical model theory. However, if the statistical

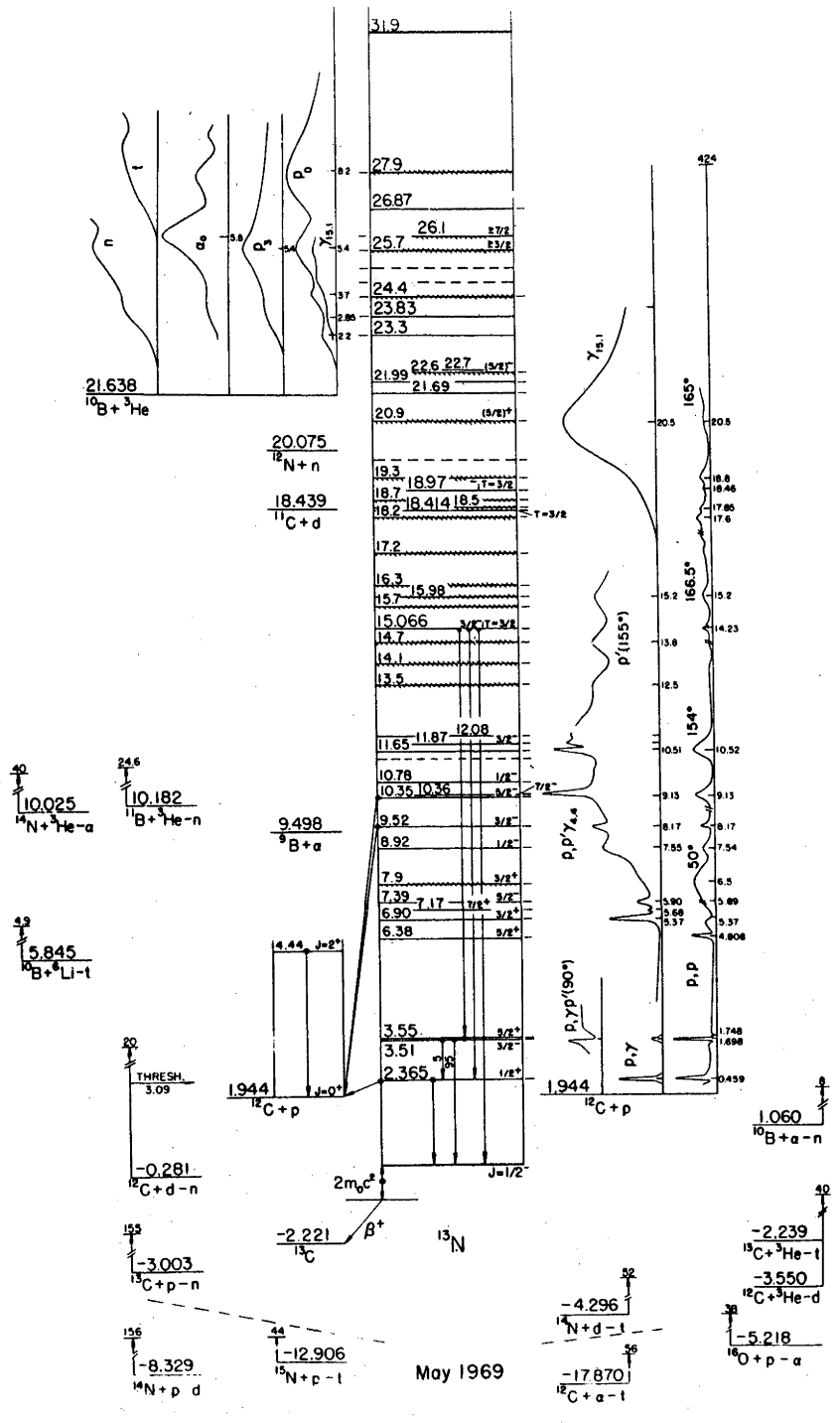


Figure 1.1: ^{13}N energy level scheme with reaction thresholds, taken from the compilations by Ajzenberg-Selove [Aj 69].

model holds for light nuclei, then it should be valid in this region of excitation in ^{13}N .

Table 1.1
Calculated level spacings and widths in ^{13}N

Excitation (MeV)	24	30	36
Level spacing, $D_{J=0}$ (keV)	8	3	1
Neutron width, Γ_n (keV)	70	150	260
Proton width, Γ_p (keV)	50	110	200
Doorway state spacing (keV)	32	26	22

To prove that intermediate structure in an excitation function does in fact arise from single resonant states of the compound nucleus is not easy. Such structure may arise from a number of different causes. As well as the highly absorbing states and fluctuation phenomena discussed above, local fluctuations in level densities, gross structure resonances and optical model effects can all give rise to yield peaks of various widths and spacings. However the last two causes give rise to fluctuations of greater spacing and widths than those observed in the ^{13}N system. Fairly good evidence that a peak in an excitation function did arise from a single resonant state of the compound nucleus would be given, if it could be shown that it occurred with the same energy and width in a number of different reaction channels. Careful measurements are necessary, since it might happen that a local fluctuation in level density or matrix elements could produce similar peaks in a number of channels.

The evidence that the four peaks observed in the $^{10}\text{B} + ^3\text{He}$ studies are individual resonances is fairly convincing. They appear in a number of exit channels with approximately the same excitation energy and width; also Girod *et al.* [Gi 70] have analyzed the available $^{10}\text{B}(^3\text{He},\alpha)^9\text{B}$ and $^{12}\text{C}(p,p)^{12}\text{C}$ reaction data between 20 and 30 MeV excitation in ^{13}N using an optical model formalism including resonant terms, and obtained reasonable fits. Their results indicate that the $^{10}\text{B} + ^3\text{He}$ reaction is exciting levels in ^{13}N at 22.7, 24.1, 25.9 and 27.9 MeV with spins of $5/2^-$, $7/2^-$, $7/2^-$ and $9/2^+$ respectively.

The previous studies on the $^{10}\text{B} + ^3\text{He}$ system were limited to 12 MeV bombarding energy by the attainable energy of the A.N.U. tandem accelerator and neutral injection system. With the installation of a lithium-exchange negative-ion source, it became possible to extend the previous measurements on the $^{10}\text{B}(^3\text{He},\alpha)$, $^{10}\text{B}(^3\text{He},d)$ and $^{10}\text{B}(^3\text{He},p)$ reactions to 19 MeV bombarding energy (36 MeV excitation in ^{13}N). Fisher *et al.* [Fi 63] have observed a broad resonance at 32 MeV in their $^{12}\text{C}(p,\gamma_0)^{13}\text{N}$ studies, so that it was of interest to see whether that state could be populated in the $^{10}\text{B} + ^3\text{He}$ reactions. If so, the channels it was observed in could give some clue to its structure. Another point of interest is that Easlea [Ea 62] has predicted that the $T = 3/2$ strength of the electric dipole resonance should occur at ~ 26 MeV (with a further small contribution at 37 MeV), and that the $T = 1/2$ strength should be divided over states at ~ 13 , ~ 20 and ~ 32 MeV. The recent commissioning of a 23.8 cm diam. \times 25.4 cm long NaI(Tl) γ -ray spectrometer enabled the $^{10}\text{B}(^3\text{He},\gamma)^{13}\text{N}$ and $^{10}\text{B}(^3\text{He},p\gamma)^{12}\text{C}$ ($E_\gamma = 15.11$ and 12.71 MeV) reactions to be studied. Provided that the state at 26 MeV has some $T = 1/2$ admixture, it might be populated by the $^{10}\text{B} + ^3\text{He}$ reactions and it

could then decay via the $T = 1$, 15.11 MeV level in ^{12}C . Also, any population of the $T = 1/2$ dipole state at 32 MeV should be noticeable in the $(^3\text{He}, \gamma)$ reaction.

Excitation functions were measured for the $^{10}\text{B}(^3\text{He}, \alpha)^9\text{B}$, $^{10}\text{B}(^3\text{He}, \text{d})^{11}\text{C}$, $^{10}\text{B}(^3\text{He}, \text{p})^{12}\text{C}$, $^{10}\text{B}(^3\text{He}, \text{p}\gamma)^{12}\text{C}$ ($E_\gamma = 15.11$ and 12.71 MeV), and $^{10}\text{B}(^3\text{He}, \gamma)^{13}\text{N}$ reactions up to 19 MeV bombarding energy. The particle reactions are described in chapter 2, and the γ -ray reactions in chapter 3. The results of these experiments and other experimental information on this region of excitation in ^{13}N , are summarized in chapter 4. The nature of the observed resonances is also discussed.

CHAPTER 2

THE ($^3\text{He},\alpha$), ($^3\text{He},d$), AND ($^3\text{He},p$) EXCITATION FUNCTIONS2.1 THE $^{10}\text{B}(^3\text{He},\alpha)^9\text{B}$ REACTION

This reaction is expected to proceed mainly through a direct pick-up mechanism. Transitions from the 3^+ ground state of ^{10}B to the $3/2^-$ ground state and $5/2^-$ 2.33 MeV state in ^9B can occur with the pick-up of a p shell neutron [La 66]; Taylor *et al.* [Ta 60] have confirmed that this process can be used to fit the $^{10}\text{B}(^3\text{He},\alpha)^9\text{B}$ reaction at forward angles. However, a previous study [Pa 65 and Po 67] in this laboratory of the $^{10}\text{B}(^3\text{He},\alpha)^9\text{B}$ reaction between 2 and 10 MeV bombarding energy, showed a large rise in the backward yield at 5.8 MeV, indicative of a compound nucleus resonance at 26 MeV in ^{13}N . Also, minor structure in the excitation functions was consistent with compound nucleus fluctuations of small amplitude. Thus it would seem that there is still some compound nucleus contribution to the reaction mechanism at these energies.

Patterson *et al.* [Pa 65 and Po 67] measured the ($^3\text{He},\alpha_0$) and ($^3\text{He},\alpha_1$) excitation functions between 2 and 10 MeV ^3He energy at 30° , 60° , 90° , 135° and 150° . The present experiment extended the measurements at 30° , 60° , 90° and 150° to 19 MeV. This covered the region in which a resonance had been observed in the $^{12}\text{C}(p,\gamma_0)^{13}\text{N}$ reaction. It was hoped that this resonance (32 MeV excitation in ^{13}N , corresponding to 13.5 MeV ^3He energy) would appear in either the α_0 or α_1 channel, and so give some clue as to its structure.

2.1.1 Experimental Details

The ^3He beams used in these experiments were obtained from

the A.N.U. accelerator (EN Tandem Van de Graaff). With the negative-helium-ion source using lithium vapour exchange, analyzed and collimated beams of ~ 150 nA of ${}^3\text{He}^{++}$ on target were available at most energies.

The measurements were carried out in the 50 cm scattering chamber described by Ophel [Op 70]. Beam collimation was provided by four tantalum discs of aperture 2.3 - 3.0 - 2.3 - 3.0 mm with the discs of larger aperture acting as anti-scatter baffles. The discs were spaced 10 cm apart in a brass tube, and the last anti-scatter baffle was 10 cm from the target. This collimating system limited the incident angular spread to less than 0.35° .

The detectors were mounted on blocks that were located in a 32 cm diameter annular groove in the base of the chamber. An angular scale on the base and a vernier scale on the detector block enabled the counters to be positioned reproducibly to within 0.1° . Checks on the alignment of the chamber and the accuracy of the angular scale [Op 70], indicated that an error of less than 0.2° could be expected from this system. Tantalum defining slits with rectangular apertures of 5 mm (vertical) \times 2 mm (horizontal) giving an acceptance angle of 0.6° , were located directly in front of the counters. Particular slits were always used at the same angles, although repeated comparisons of slit apertures by measuring the yield of the ${}^{12}\text{C}(p,p)$ reaction at 154° indicated that they were identical to 0.5%. The detectors were silicon surface barrier counters (manufactured by Ortec) with thicknesses chosen to just stop the most energetic α -particles expected. The counters were positioned at 30° (500 μ thick), 60° (500 μ), 90° (400 μ) and 150° (120 μ).

The amplifying electronics consisted of Ortec charge sensitive preamplifiers and linear amplifiers (models 109 - 410). Double delay line shaping and $0.1 \mu\text{s}$ RC integration were used to provide optimum resolution. The pulses were then routed into 4×512 channel segments in the IBM 1800 data acquisition system. This on-line computer system has been described in detail by Caelli *et al.* [Ca 69].

The self supporting ^{10}B foils used in these measurements were prepared by electron gun evaporation of enriched material (nominally $> 96.5\%$ ^{10}B , purchased from Union Carbide Nuclear Company, Oak Ridge, Tennessee) onto a glass slide previously coated with a thin layer of RBS25 detergent. The foils were then floated off the slide in distilled water, and picked up on an aluminium target frame. Using this technique, self supporting foils of up to $200 \mu\text{g}/\text{cm}^2$ thick could be obtained.

The following three techniques were used to determine the composition of the targets.

- (a) The shift in the $E_p = 1.881 \text{ MeV}$ threshold of the $^7\text{Li}(p,n)$ reaction. This was measured at 0° , and the target thicknesses were deduced using the dE/dx values of Williamson and Boujot [Wi 62].
- (b) Elastic proton scattering at $E_p = 2.45 \text{ MeV}$ and 154° (lab), using the (p,p) cross sections for ^{10}B , ^{11}B , ^{12}C , ^{14}N and ^{16}O reported by Overly and Whaling and other authors [Ov 62].
- (c) Rutherford scattering of α -particles at 1.4 MeV between 40° and 80° .

One target was measured using all three methods, and the ^{10}B composi-

tions obtained agreed within 10%. The mean value was near that derived from the elastic proton scattering. Since this method was also the most accurate one (the $^{10}\text{B}(p,p)$ cross sections are known to $\pm 7\%$), the rest of the target thicknesses were either measured directly using the (p,p) cross sections, or normalized by comparing the $^{10}\text{B}(^3\text{He}, p\gamma_{15.11})^{12}\text{C}$ yield (chapter 3) with that from a previously measured target. The composition of a typical target used in the experiments was found to be:

^{10}B	^{11}B	^{12}C	^{14}N	^{16}O	
100 ± 10	5 ± 1	6 ± 1	< 1	7 ± 1	$\mu\text{gm}/\text{cm}^2$

The measured ratio of ^{10}B and ^{11}B was approximately the same for all targets (19:1); slightly less than the nominal enrichment stated by the material suppliers. The ^{12}C , ^{14}N and ^{16}O impurities varied from target to target, and since the $^{16}\text{O}(^3\text{He}, \alpha)^{15}\text{O}$ reaction interfered with the $^{10}\text{B}(^3\text{He}, \alpha)^9\text{B}$ reaction at backward angles, targets with the least ^{16}O relative to ^{10}B were used in the $(^3\text{He}, \alpha)$ measurements. Targets of $\sim 100 \mu\text{gm}/\text{cm}^2$ ^{10}B were used in the $(^3\text{He}, \alpha)$, $(^3\text{He}, d)$ and $(^3\text{He}, p)$ measurements. This thickness was found to give a good compromise between yield and resolution. The target plane was set at 60° to the beam so that the 90° yield could be measured.

Two sets of measurements were made. In the first set, excitation functions were measured in 200 keV steps from 9.0 to 11.6 MeV, and in the second set they were measured from 11 to 19 MeV and then down from 15.9 MeV to 12.1 MeV in 200 keV steps, with the points at 15, 14, 13 and 12 MeV repeated as checks on the system. The charge was collected on an insulated and suppressed Faraday cup, and measured with an Elcor current integrator that had been cali-

brated before the runs, and was expected to be accurate to within 2%. Data were collected at each energy for 300 to 1000 μC integrated current to acquire adequate statistics in the peaks of interest. In the second set of measurements, a counter telescope was added at 150° to extract the deuteron spectra. The particle identification electronics are described in section 2.2.1.

2.1.2 Results

A typical spectrum taken at 150° with the counter telescope is shown in fig. 2.1. The two prominent α -particle groups corresponding to the ground and 2.33 MeV states of ${}^9\text{B}$, lie at the upper end of a background continuum due to α -particles from the multiparticle break-up of the ${}^{10}\text{B} + {}^3\text{He}$ system. In the other detectors, protons from this break-up were observed as a low energy edge, since most of them were not stopped in the detectors. Figure 2.2 shows some of the α identified spectra obtained between 11 and 19 MeV ${}^3\text{He}$ energy. The lower diagram in the figure indicates the identified contaminant peaks observed. It is drawn to the same scale as the upper diagram, but the particle energy is substituted for the channel number. The lines indicate the positions of the observed peaks at the various bombarding energies, and are labelled with the appropriate outgoing particle that arises from the reaction on the left hand side. The origin of the peak at a constant energy of 6.2 MeV that appears in all the spectra, is explained in section 2.2.2. It can be seen that the only contaminant peak that interferes with the α groups of interest is that due to the ${}^{16}\text{O}({}^3\text{He}, \alpha_0){}^{15}\text{O}$ reaction. At 90° the contaminant interferes with the α_1 peak around 17 MeV ${}^3\text{He}$ energy, while at 30° and 60° it is clear of the peaks of interest in the region studied.

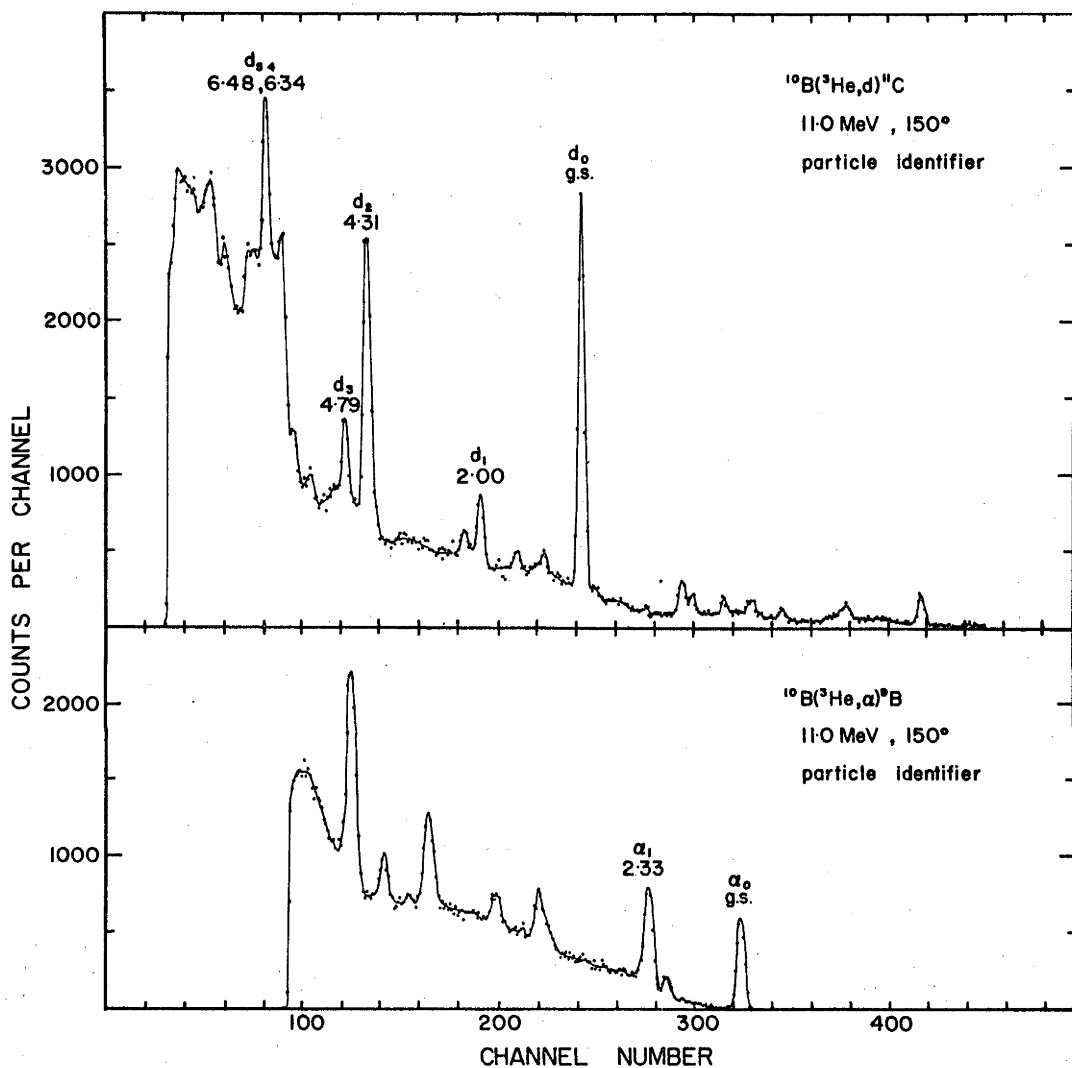


Figure 2.1: α -particle and deuteron spectra from the $^{10}\text{B} + ^3\text{He}$ reaction obtained with the counter telescope at 150° (lab). The bombarding energy was 11 MeV. The groups that were extracted are labelled with the excitation (in MeV) of the final nucleus. The contaminant peaks for the α -particle and deuteron spectra are identified in figures 2.2 and 2.5 respectively.

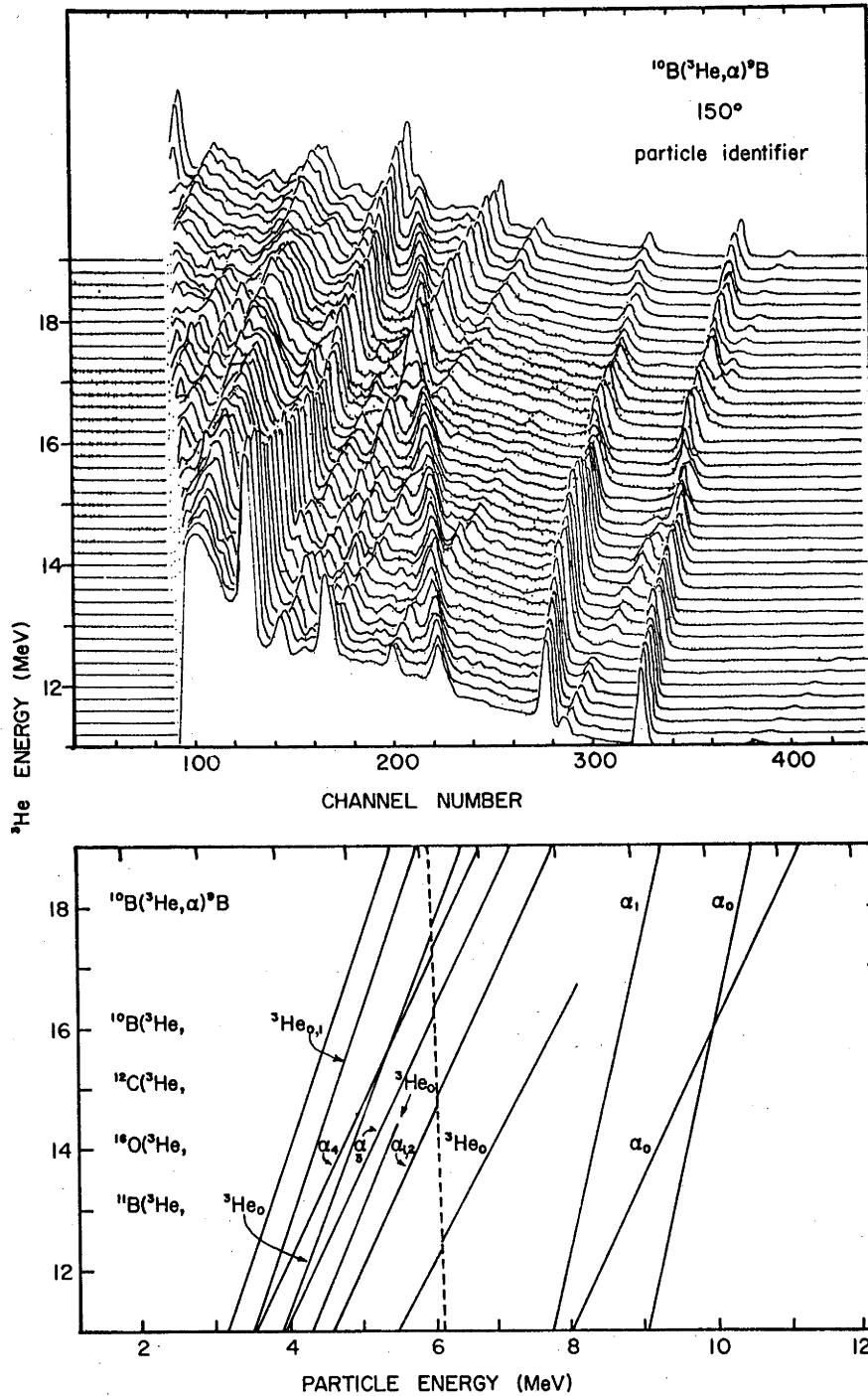


Figure 2.2: Some $^{10}\text{B}(^3\text{He}, \alpha)^9\text{B}$ spectra taken with the counter telescope at 150° (lab) from 11 to 19 MeV ^3He energy. Contaminant peaks that have been identified are indicated in the lower diagram.

There was no difficulty in subtracting the background underneath the α_0 peak. However, the subtraction was less accurate for the α_1 peak owing to the uncertainty of the background on the low energy side of the peak. This uncertainty can be associated with the weak state in ${}^9\text{B}$ at 2.71 ± 0.03 MeV which has a width of 710 ± 60 keV [Wi 66]. There is an additional uncertainty in the α_1 background at 60° due to the ground state α group from the ${}^{11}\text{B}({}^3\text{He}, \alpha){}^{10}\text{B}$ reaction. However, Poate [Po 67] has shown that the yield of the ${}^{11}\text{B}({}^3\text{He}, \alpha_0)$ reaction is approximately 1/3 the yield of the ${}^{10}\text{B}({}^3\text{He}, \alpha_1)$ reaction at lower energies. If this ratio obtains at higher energies, the contaminant peak would be less than 2% of the amplitude of the α_1 peak. In fact there is no sign of this reaction occurring in the 150° spectra (fig. 2.2), where the peak should appear between the α_0 and α_1 peaks.

The ground and 2.33 MeV states in ${}^9\text{B}$ have widths of 0.5 and 82 keV respectively [La 66], whereas fig. 2.1 shows that the α_0 and α_1 groups have the same widths (140 keV F.W.H.M.), indicating the observed width to be mainly due to experimental resolution. Subtraction of the background from the α_1 group was therefore effected by assuming the width to be the same as for the α_0 group, and drawing the background in by eye. An attempt to automate this process by fitting an exponential background and two Gaussians of fixed widths and slowly varying separation using a computer, gave approximately the same results. However, the introduction of another Gaussian when the ${}^{16}\text{O}$ contaminant peak was present, resulted in unsatisfactory fits. It was therefore decided to do the data reduction by "hand and eye" to be consistent. The uncertainty in the background subtraction and peak summing was estimated to be about 8% of the α_1 yield.

From fig. 2.2, it can be seen that the ^{16}O contaminant α_0 peak fluctuates considerably with energy. Therefore, when it overlapped with the α_1 peak, an appropriate proportion of the average yield of the contaminant was subtracted from the α_1 group. The yield of the ^{16}O peak was determined in the same way as the yield from the ^{10}B .

Excitation functions, measured at laboratory angles of 30° , 60° , 90° and 150° from 9 to 19 MeV, are shown in figs. 2.3 and 2.4. Cross sections are quoted in mb/sr. The main source of error arose from uncertainties in target thickness (10%). This dominated the other factors, such as beam current integration and geometry which were known to within 2%, and the counting statistics which were less than 4% for the α_0 peak. The absolute cross sections were therefore assigned errors of 12% for the α_0 yields and 15% for the α_1 yields. The error assigned to the α_1 yield was made larger to allow for any systematic error arising from the background subtraction. The results presented here match up very well with the ($^3\text{He}, \alpha$) results of Patterson *et al.* [Pa 65] who measured excitation functions at 30° , 60° , 90° and 150° up to 10 MeV ^3He energy. The bombarding energies shown in figs. 2.3 and 2.4 have not been corrected for the energy lost by the beam in the target, and should therefore be adjusted downwards by ~ 25 keV at the low energy end and ~ 15 keV at the high energy end.

2.1.3 Discussion

Inspection of the α_0 excitation functions (fig. 2.3) shows a general downward trend with increasing energy. In contrast to this the α_1 excitation functions (fig. 2.4) have considerable struc-

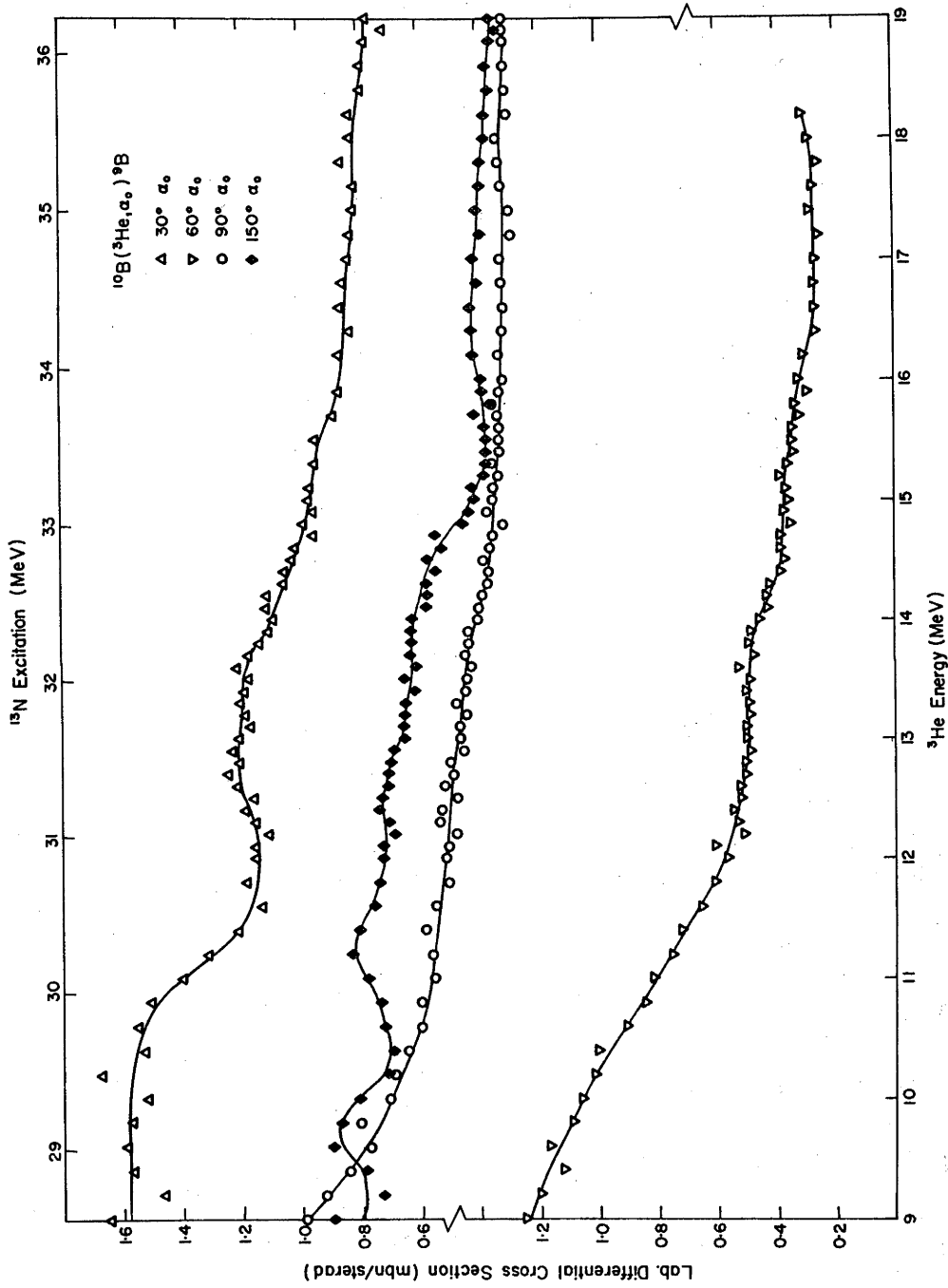


Figure 2.3: Differential excitation functions for the $^{10}\text{B}(^3\text{He}, \alpha_0) ^9\text{B}$ reaction at the lab. angles indicated. The relative errors are best shown by the spread in points. The cross section scale is assigned an error of $\pm 12\%$.

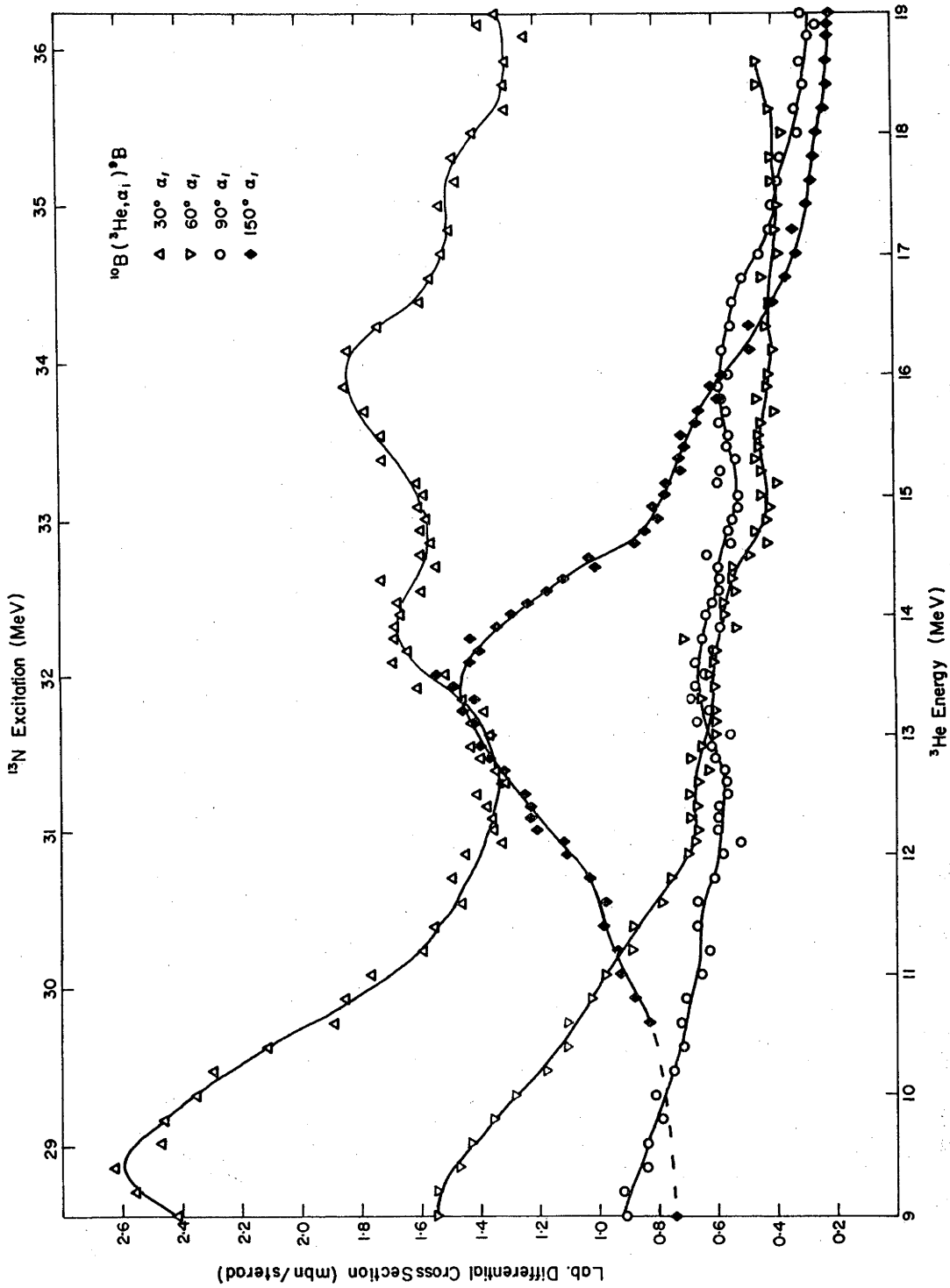


Figure 2.4: Differential excitation functions for the $^{10}\text{B}(^3\text{He}, \alpha_1)^9\text{B}^*$ (2.33 MeV) reaction at the lab. angles indicated. The relative errors are best shown by the spread in points. The cross section scale is assigned an error of $\pm 15\%$.

ture at 30° and 150° , with the yield at 150° as large as the yield at 30° around 13 MeV excitation. This peak in the α_1 yield at 150° is indicative of a compound nucleus resonance at ~ 13.3 MeV ^3He energy (~ 31.9 MeV excitation in ^{13}N). From fig. 2.2 it can be seen that there are no contaminant peaks running underneath the α_1 group that could cause a spurious rise in yield at this bombarding energy. However, a re-examination of the spectra indicated an increase in the yield to the 2.71 ($3/2^+$, $5/2^+$) state in ^9B of about 50% in the region of 13.3 MeV ^3He energy. This increase is likely to cause an error of less than 5% in the extraction of the α_1 yield over the region of the resonance, so that it appears that both the α_1 and α_2 yields at 150° peak at around 13.3 MeV bombarding energy.

As mentioned in the introductory chapter, the ^{13}N compound system should be in the region of strongly overlapping levels where fluctuations are expected to produce peaks with an average separation of about twice the level width. The positions of peaks in differential excitation functions should not then necessarily correlate with single levels in the compound system. The minor bumps observed in the excitation functions with a period of approximately 2 MeV, may have been due to such fluctuations. However, the peak in the α_1 150° yield at 13.3 MeV was a prominent feature on an otherwise fairly smooth curve and coincided with the resonance seen at 32 MeV excitation in the $^{12}\text{C}(p,\gamma_0)^{13}\text{N}$ studies of Fisher *et al.* [Fi 63]. This could have been mere coincidence, so the $^{10}\text{B} + ^3\text{He}$ studies were extended to observe other exit channels. The $^{10}\text{B}(^3\text{He},d)^{11}\text{C}$ investigations are discussed in the next section.

2.2 THE $^{10}\text{B}(^3\text{He},\text{d})^{11}\text{C}$ REACTION

The observation of a strong resonance-like feature in the α_1 differential cross section at backward angles initiated a study of the $^{10}\text{B}(^3\text{He},\text{d})^{11}\text{C}$ reaction, seeking to confirm the presence of the 13.3 MeV resonance in another channel. An investigation of the $(^3\text{He},\text{d})$ reaction is not an attractive way of studying compound nucleus phenomena, as the reaction has been shown to proceed mainly by a direct stripping mechanism [Pa 65a]. However, the 150° excitation function of the $^{10}\text{B}(^3\text{He},\text{d}_0)$ reaction between 3.5 and 10 MeV ^3He energy [Pa 65a], had shown a resonance at 5.8 MeV which could be identified with the resonance seen earlier in the $^{10}\text{B}(^3\text{He},\alpha_0)$ yield [Pa 65]. It therefore seemed possible that the 13.3 MeV resonance seen in $^{10}\text{B}(^3\text{He},\alpha_1)$ would appear in the deuteron exit channel.

In spectra from the previous experiment, the strong group from the $(^3\text{He},\text{d}_0)$ reaction stood out on top of the α -particle continuum. Normally though, to minimize the dead time, that part of the spectrum was biased out before storing in the IBM 1800. In any case, the deuteron groups going to higher excited states in ^{11}C were lost in a host of contaminant peaks. Therefore, in the second set of $(^3\text{He},\alpha)$ measurements, a counter telescope at 150° was added to the detector arrangement. If there were to be any compound nucleus contribution to the deuteron yields it would be expected to be more obvious at backward angles.

2.2.1 Experimental Details

These measurements were taken at the same time as the second series of $(^3\text{He},\alpha)$ measurements, so that the experimental arrangement was that described in section 2.1.1. The one exception

was the detector, which was a counter telescope mounted at 150° on the opposite side of the target chamber to the $120 \mu, \alpha$ detector. The telescope consisted of a 32μ transmission counter backed by a 1000μ surface barrier detector. This arrangement could stop the most energetic deuterons expected, but was not thick enough to stop the high energy proton groups.

No particle identifier unit was available at the time of these measurements, so that the identifying logic was built up using single channel analyzers (Ortec model 420). The system utilized the large difference in stopping power between the $Z = 1$ and $Z = 2$ particles. Figure 2.5 shows the energy deposited in a 32μ silicon detector plotted against both the total particle energy and the energy deposited in a stopping counter after transmission. It can be seen that after the particles are no longer fully stopped in the transmission counter, the energy loss (ΔE) steadily decreases with rising particle energy. The gap between the triton and ^3He energy loss curves can be approximated by a step function, which can then be used to set gates on the transmission counter signal (ΔE) and the stopping counter signal (E'). The total energy pulse, $E = E' + \Delta E$, can then be routed according to which side of this step function it occurred. The logic used in this instance (expressed in ALGOL notation) was:

if $\Delta E > 2.5 \text{ MeV}$ or ($\Delta E > 1.1 \text{ MeV}$ and $E' > 5 \text{ MeV}$) then $Z = 2$ else $Z = 1$

From fig. 2.5 it can be seen that the validity of this logic statement is limited to ^3He particles below 25 MeV. However, this is well above the highest energy expected for ^3He and α -particles at 150° .

The electronics required to perform these logic operations

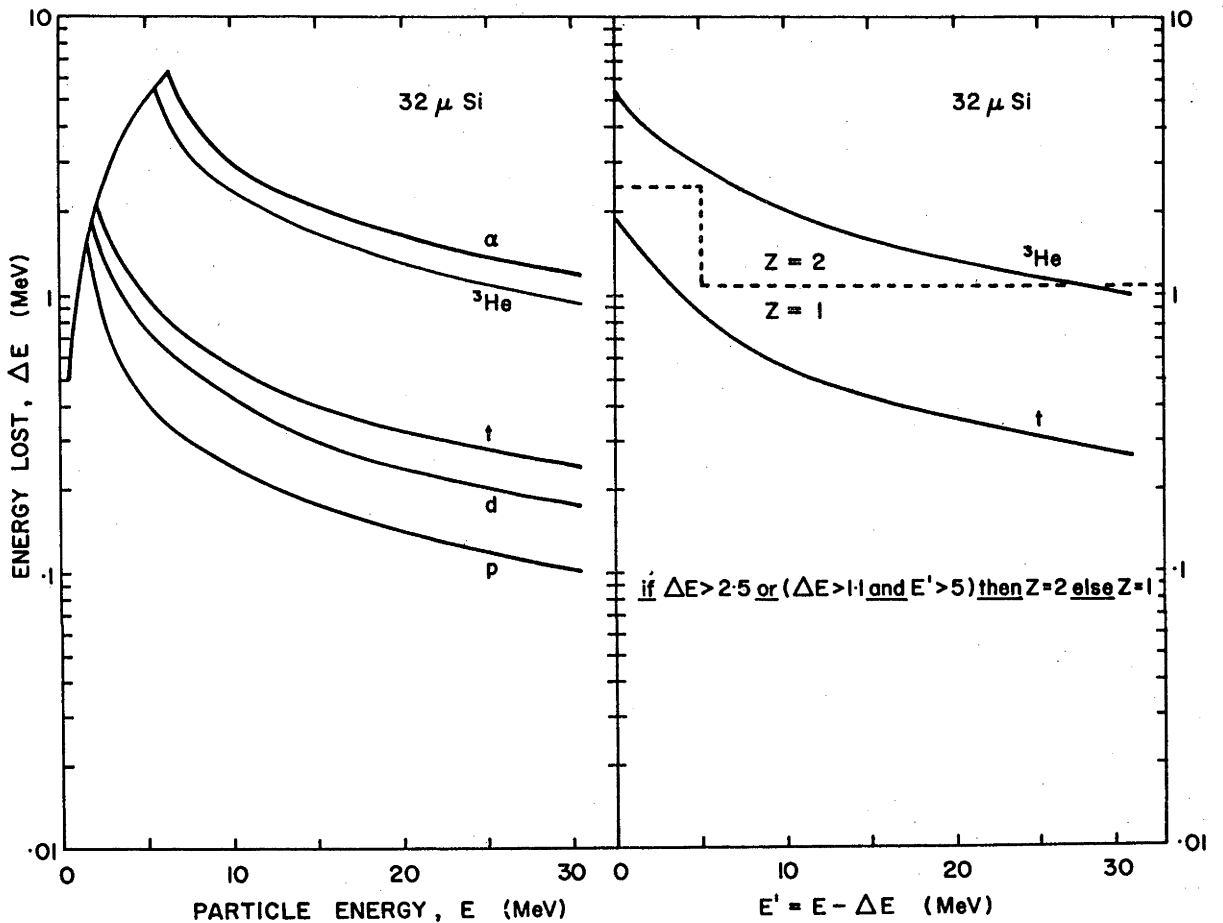


Figure 2.5: Energy deposited in a 32 μ silicon detector plotted against the particle energy before (E) and after (E') transmission. The curves for different types of incident particle are labelled accordingly.

The dashed line indicates the boundary of the particle identification criterion which is written symbolically on the same diagram.

The data for this diagram were obtained from Skyrme's tables of ranges and stopping powers of charged particles in silicon [Sk 67].

can be built up from basic Ortec modules, and the setting of the various levels is simple providing that the E' and $\Delta E'$ signals have been calibrated to the same gain. This is necessary to keep the total energy signal, $E = E' + \Delta E'$, linear. The $^{12}\text{C}(^3\text{He},^3\text{He})$ and $^{12}\text{C}(^3\text{He},\alpha)$ reactions were used to calibrate the ΔE amplifier, and the $^{12}\text{C}(^3\text{He},p)$ reaction was used to calibrate the E' amplifier. The levels were then set using a variable pulser.

The $Z = 1$ and $Z = 2$ identified groups were routed into another 2×512 channel segment in the IBM 1800 data acquisition system.

The excitation functions covered the range from 11.0 to 19.0 MeV as described for the second set of $(^3\text{He},\alpha)$ measurements (section 2.1.1).

2.2.2 Results

A typical deuteron spectrum taken at 150° with the counter telescope is shown in fig. 2.1. The deuteron peaks have been labelled with the final excitation of ^{11}C . It was not possible to tell whether the peak near channel 80 was due to the d_4 group to the 6.34 MeV state or the d_5 group to the 6.48 MeV state, or whether both were contributing. The proton continuum from the $^{10}\text{B} + ^3\text{He}$ system break up into 3 α -particles and a proton, can be seen rising in the same place as the α -particle continuum in the $(^3\text{He},\alpha)$ spectrum. There was also a fairly flat background due to protons that had not been stopped in the counter ($E_p > 12.4$ MeV).

Figure 2.6 shows some of the deuteron identified spectra obtained between 11 and 19 MeV ^3He energy. The lower diagram in the figure indicates the identified contaminant peaks observed. It can

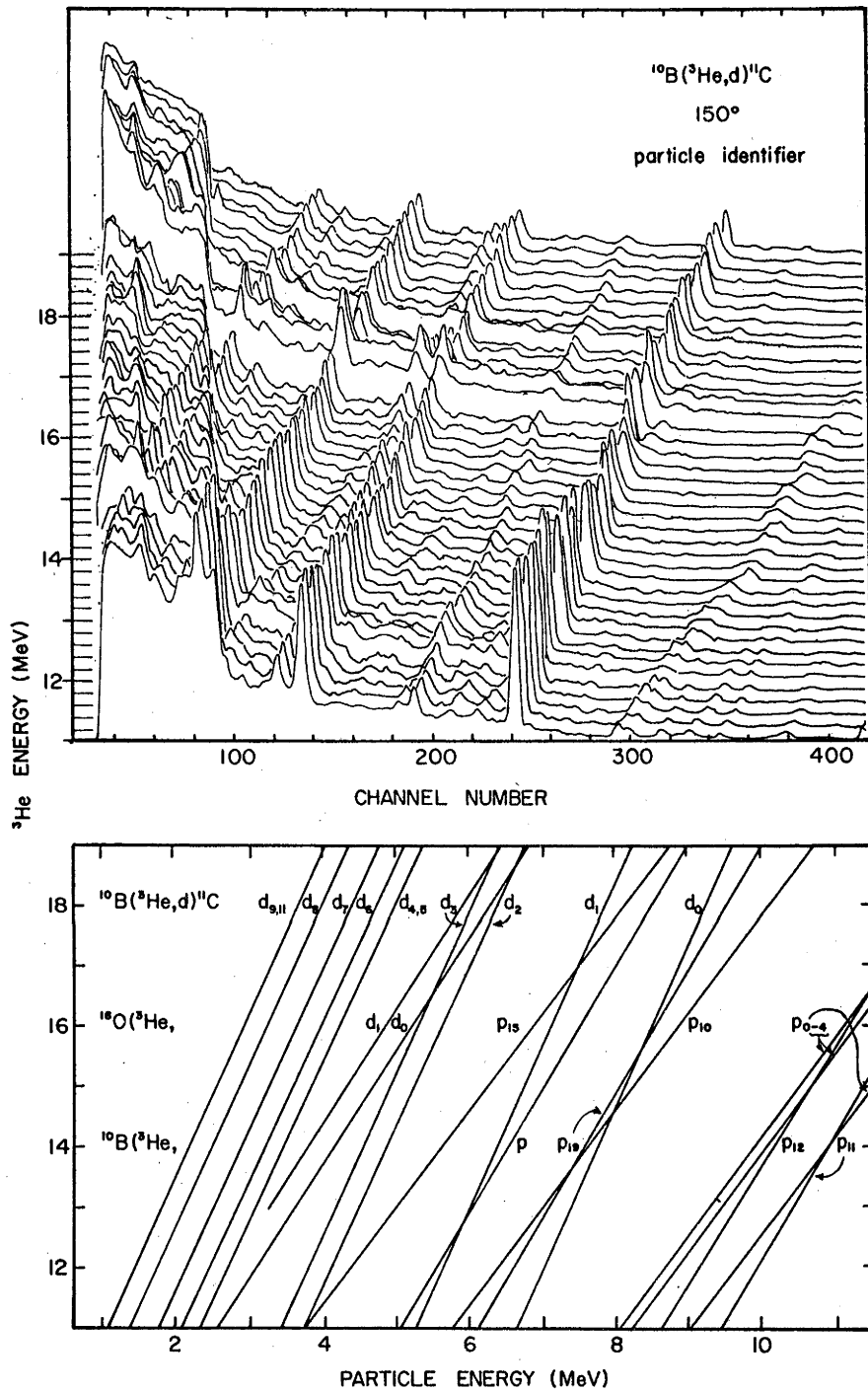


Figure 2.6: Some ${}^{10}\text{B}({}^3\text{He},d){}^{11}\text{C}$ spectra taken with the counter telescope at 150° (lab) from 11 to 19 MeV ${}^3\text{He}$ energy. Contaminant peaks that have been identified are indicated in the lower diagram.

be seen that all the deuteron peaks have contaminant peaks running through them at some energy, and this made the extraction of yields difficult. The amplitude of the contaminant peak underneath the peak of interest was estimated from its size and behaviour at higher and lower energies. The limitations of the particle identification can be seen in both figs. 2.2 and 2.6. In fig. 2.2 the peak at ~ 6.2 MeV that appears in all the spectra, is due to a discontinuity in the energy response of the system caused by dead layers at the back of the transmission counter and the front of the stopping counter; the 32 μ transmission counter just stopped 6.2 MeV α -particles. Other than this, the energy calibration of the system was linear. The low energy cut off at 2.5 MeV in fig. 2.2 is due to the first condition put on the routing logic. The α and ^3He particles below 2.5 MeV appear in fig. 2.6 where the cut off can be seen clearly.

The problems involved in estimating the backgrounds to the deuteron peaks again appeared to be too much for computer automation, so the data reduction was done by "hand and eye". The excitation functions measured at 150° (lab) from 11 to 19 MeV are shown in fig. 2.7. The errors assigned to the points in the d_1 and d_3 curves are 15 to 25%, worse than the spread in points would suggest. The errors in the other curves (5 to 10%) are mirrored in the spread of points. The smooth lines were drawn to aid the eye. The cross section scale was derived by normalizing the identified α -particle yields to those obtained at 150° with a single counter, and is assigned an error of $\pm 15\%$. As in the previous experiment, the bombarding energies have not been corrected for the energy lost by the beam in the target, and should be adjusted downwards by ~ 25 keV at the low energy end and ~ 15 keV at the high energy end.

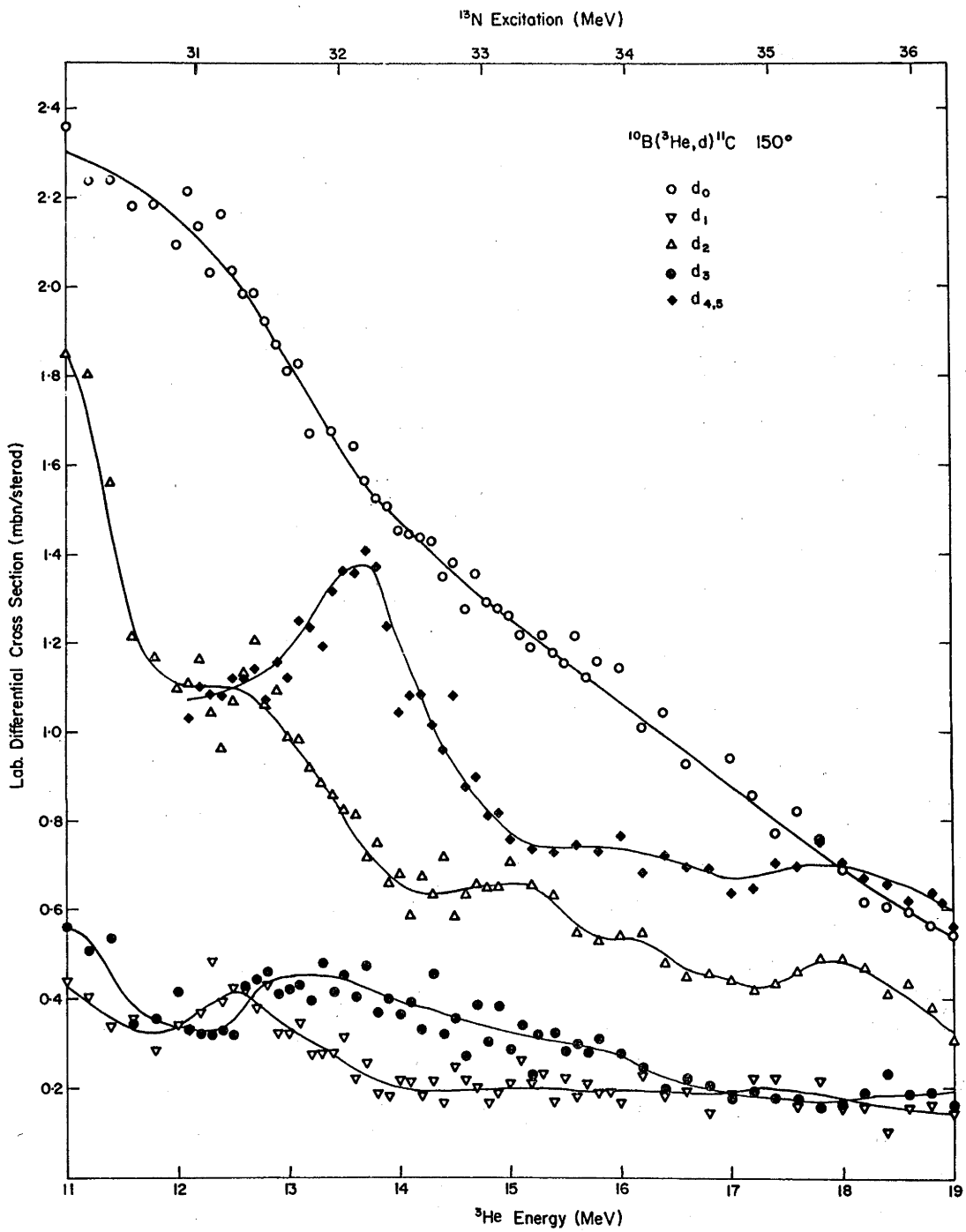


Figure 2.7: Differential excitation functions for the $^{10}\text{B}(^3\text{He},d)^{11}\text{C}$ reaction at 150° (lab). The cross section is assigned an error of $\pm 15\%$.

2.2.3 Discussion

Inspection of the deuteron excitation functions (fig. 2.7) shows a general downward trend with increasing energy. There appear to be a few minor fluctuations in the d_2 curve, but these could be due to inadequate compensation for underlying contaminant peaks. The $d_{4,5}$ yield to the 6.34 ($1/2^+$) or 6.48 ($7/2^-$) MeV state shows a peak at 13.6 MeV. With the large number of contaminant peaks around, this could have been due to a peak running underneath the $d_{4,5}$ peak. However, an examination of fig. 2.6 does not show any large background peaks in this region, and the bump in the yield curve shows up well in this display of the spectra.

Therefore, it would appear that there is a resonance in the $d_{4,5}$ yield corresponding to a state at 32.1 MeV excitation with a width of 1 MeV. It is debatable whether this can be identified with the resonance seen in the α channel at 31.9 MeV with a width of 1.5 MeV. Before drawing any conclusions on the nature of these resonances, an attempt was made to provide further information in this region by studying the $^{10}\text{B}(^3\text{He},\text{p})^{12}\text{C}$ reaction. This experiment is described in the next section.

2.3 THE $^{10}\text{B}(^3\text{He},\text{p})^{12}\text{C}$ REACTION

On simple arguments, the $^{10}\text{B}(^3\text{He},\text{p})^{12}\text{C}$ reaction, requiring the transfer of two nucleons for a direct process, would be expected to be a suitable reaction for studying any resonance behaviour, since the compound nucleus amplitude is expected to be enhanced relative to the direct amplitude. Indeed, the excitation function measurements of Patterson *et al.* [Pa 66] up to 12 MeV bombarding

energy, in which the proton transitions to the ground and first three excited states were studied at 150° , showed considerable resonance structure. In particular, the p_0 yield was dominated by resonances at 5.8 and 8.2 MeV ^3He energy (26 and 28 MeV excitation in ^{13}N), which had also been seen in the $(^3\text{He},\alpha)$ and $(^3\text{He},d)$ reactions [Pa 65 and Pa 65a].

The state at 26 MeV excitation has also been seen in the $(^{12}\text{C} + p)$ elastic scattering measurements of Dickens *et al.* [Di 63]. Unfortunately, these measurements did not cover the region of the 32 MeV resonance seen in the α -particle and deuteron channels in the present experiment. However, the $^{12}\text{C}(p,\gamma)^{13}\text{N}$ studies of Fisher *et al.* [Fi 63] did indicate a broad resonance ($\Gamma \approx 2$ MeV) at 32 MeV. Therefore it was reasonable to suppose that this resonance might also appear in the $^{10}\text{B}(^3\text{He},p)$ reaction.

The present work is an extension of the $^{10}\text{B}(^3\text{He},p)^{12}\text{C}$ studies of Patterson *et al.* [Pa 66] up to 19 MeV bombarding energy. Excitation functions for the p_0 and p_1 (4.43 MeV) groups were measured at 90° and 150° .

2.3.1 Experimental Details

The high Q value (19.7 MeV) of the $^{10}\text{B}(^3\text{He},p)$ reaction requires a very thick semiconductor counter to fully stop the energetic protons. The highest energy protons expected (p_0 at 90° with 19 MeV ^3He energy) were 31 MeV, which have a range of 5.2 mm in silicon. As no detectors of this thickness were available, instead of completely stopping the protons in a counter, the proton energy was degraded by tantalum foils before detection in 2 mm thick Si(Li) detectors. This meant that the protons had to be

degraded to lower than 18 MeV by the foils to be sure of fully stopping them in the detectors. Foils of thicknesses ranging from 0.08 to 0.51 mm were used.

The Si(Li) detectors were cooled by clamping them to a copper tube, through which refrigerated alcohol was circulated. As a result of the cooling (-20 to -30 °C), the detectors gave more stable operation and better resolution. Larger defining slits, 9 mm × 2 mm, were put in front of the detectors to increase the count rate; otherwise the experimental facilities were identical to those employed in the previous ($^3\text{He}, \alpha$) measurements. Two detectors were positioned at 90° and two at 150°, either side of the target chamber. The thicknesses of the foils on these counters were chosen so that one counter at one angle could stop the p_0 group, and the other counter at the same angle could stop the p_1 group throughout the range of energies expected in a particular series of runs. This meant that at all energies, both p_0 and p_1 could be extracted from the spectra; in most of the runs, both the p_0 and p_1 groups could be extracted from both of the counters at each angle. The excitation functions were measured in two accelerator runs. In the first series, measurements were made from 11.6 to 16.2 MeV ^3He energy, going up and down in 200 keV steps so that each point was measured twice. In the second run, the measurements were taken from 15.0 up to 18.6 MeV. The highest bombarding energy was limited by the accelerator performance at that time. Counts for each energy were measured for 600 to 900 μC , which normally gave statistics of better than 3% for the p_1 yield (< 8% for the p_0 yield) in each counter.

2.3.2 Results

Typical spectra obtained with 15.0 MeV ^3He energy are shown in fig. 2.8. It can be seen that even with a 0.6 mm thick tantalum foil (lower diagram), the first two proton groups are sufficiently well resolved to extract the yields accurately, although in this spectrum the protons to the ground state (initial energy 28.5 MeV) are not being fully stopped in the counter. The protons to the second, third and fourth excited states of ^{12}C were generally not well resolved, so that no yield curves could be obtained for them. The yields for p_0 and p_1 were extracted by hand calculator.

The excitation functions for p_0 and p_1 at 90° and 150° (lab) from 11.6 to 18.6 MeV are shown in fig. 2.9. The cross section scale in mb/sr was obtained from the known target thickness and experimental geometry, and is assigned an error of $\pm 13\%$. The main source of error arose from uncertainties in target thickness (10%), as in the determination of the α -particle cross sections in section 2.1. However, there is an additional uncertainty in the yield due to interactions of the high energy protons with nuclei in the degrading foils and the detectors, and therefore falling outside the main energy peak in the spectra. Cahill *et al.* [Ca 70] have measured the tail to peak ratio (number of counts outside a 3% resolution band/counts inside the 3% band) for 20 MeV protons stopped in a Si(Li) detector, and found the ratio to be 0.7%. For 30 MeV protons, the ratio is still less than 2%. The conditions in the present experiment were different to those of Cahill *et al.*, because the protons were first degraded by tantalum foil and the resolution with the thicker foils was greater than 3%. However, it is felt that a realistic upper limit of 2% can be put on the loss of

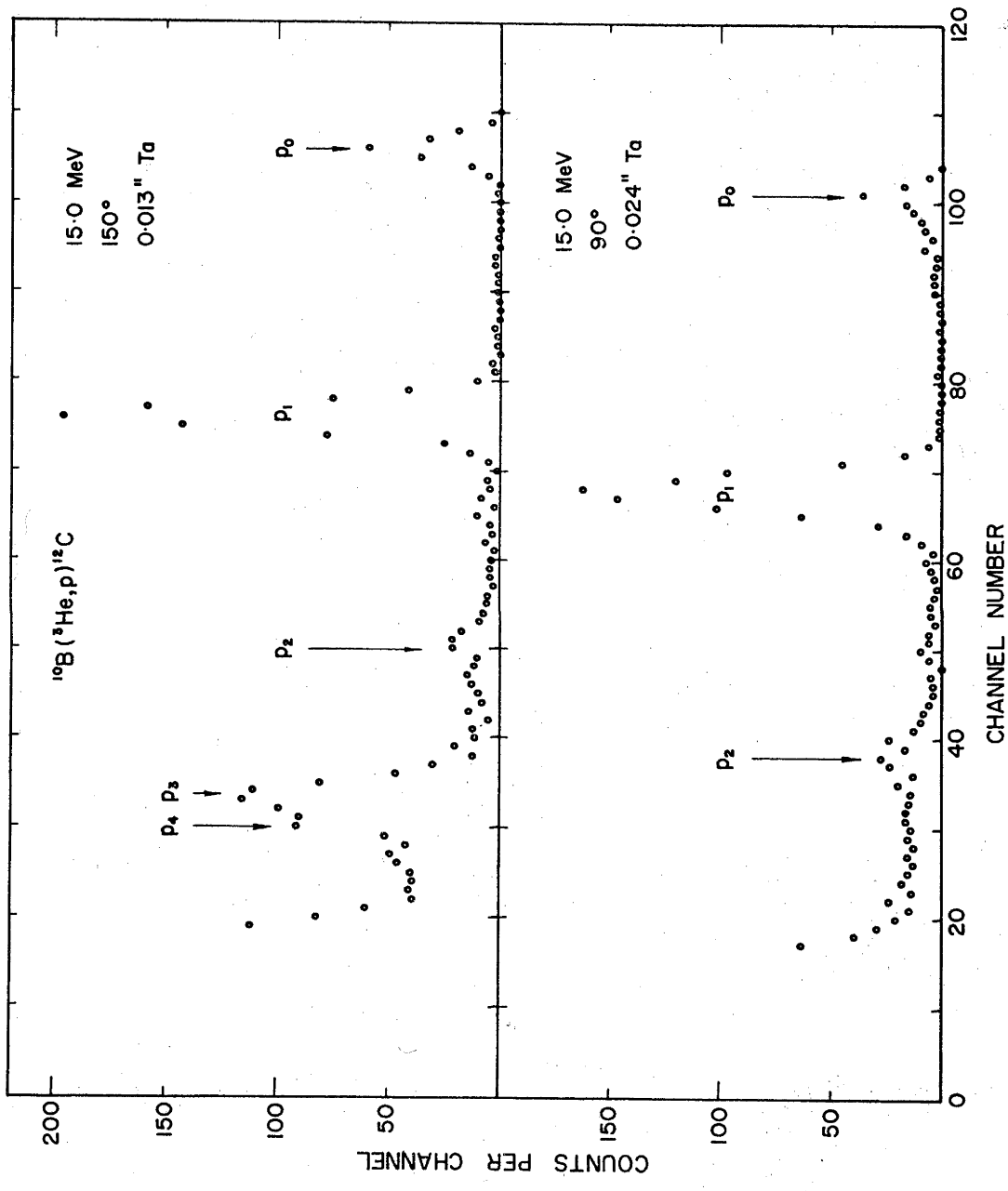


Figure 2.8: Proton spectra from the $^{10}\text{B}(^3\text{He},\text{p})^{12}\text{C}$ reaction at 15.0 MeV bombarding energy. States in ^{12}C populated are indicated by their excitation numbers. The detector angles and foil thicknesses used are shown in the diagrams.

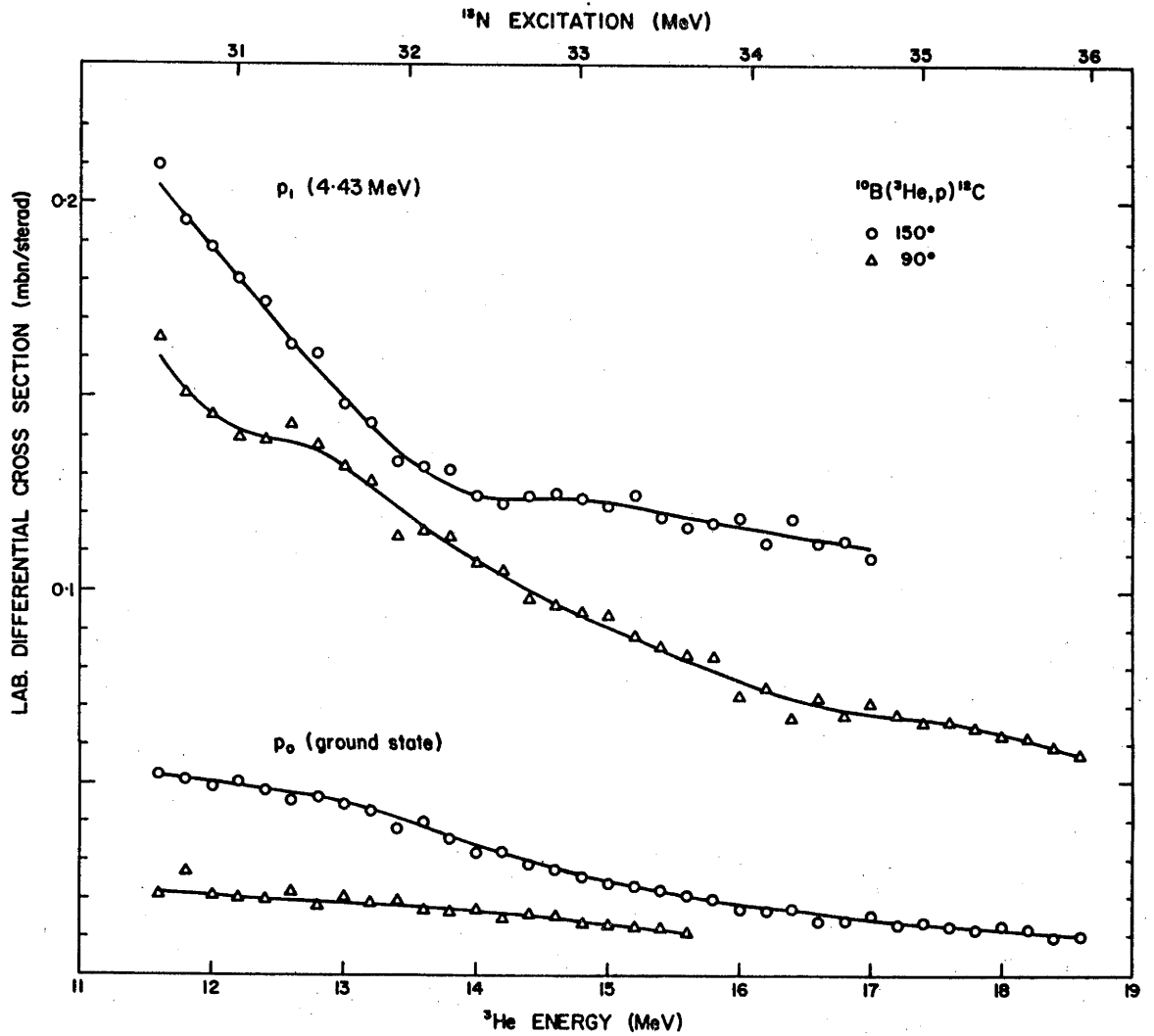


Figure 2.9: Differential excitation functions for the $^{10}\text{B}(^3\text{He},p)^{12}\text{C}$ reaction at 90° and 150° (lab). The cross section is assigned an error of $\pm 13\%$. The relative errors are best shown by the spread in points.

protons from the full energy peak due to nuclear interactions in both the tantalum foils and the Si(Li) detectors.

As in the previous experiments, the bombarding energies in fig. 2.9 have not been corrected for energy lost by the beam in the target. The mean bombarding energy is 25 keV lower than indicated for $E_{^3\text{He}} = 12$ MeV, and 15 keV lower for $E_{^3\text{He}} = 19$ MeV.

At 12 MeV, the 150° cross sections are approximately 30% lower than those measured by Patterson *et al.* [Pa 66]. Unfortunately, no other $^{10}\text{B}(^3\text{He},\text{p})$ cross sections have been measured in this region to cross-check the results. However, Schiffer *et al.* [Sc 56] have made measurements up to 5 MeV ^3He energy, and their results are also about 30% lower than those of Patterson *et al.*

2.3.3 Discussion

From fig. 2.9 it can be seen that the cross sections for both p_0 and p_1 decrease steadily with energy. The yield to the 4.43 MeV state at 90° dips slightly near 13 MeV ^3He energy where the 150° yield shows a slight rise. However, it is not possible to attach any significance to this feature because of the relatively large statistical errors (2% in this region). Thus the $(^3\text{He},\text{p})$ yields show no sign of the resonance structure observed in the $(^3\text{He},\alpha)$ and $(^3\text{He},\text{d})$ reactions in this energy range. This is in sharp contrast to the behaviour of the cross sections at lower energies [Pa 66], where marked resonance behaviour was observed.

2.4 SUMMARY

The particle yields from the $^{10}\text{B} + ^3\text{He}$ reactions observed

in the experiments described in this chapter, have generally shown a downward trend with increasing energy indicative of direct reaction processes. Both the α_1 group and the $d_{4,5}$ group showed a large increase in yield at 150° near 13.5 MeV ^3He energy. Evidence of compound nucleus fluctuations was seen in the α_1 excitation function at 30° and to a lesser extent in the other α and deuteron yields.

As discussed in chapter 1, intermediate structure in an excitation function can arise from a number of different causes. In this case, peaks in the yield curves corresponding to 32 MeV excitation in ^{13}N , have now been seen in three reactions: $^{10}\text{B}(^3\text{He},\alpha_1)^9\text{B}$, $^{10}\text{B}(^3\text{He},d_{4,5})^{11}\text{C}$, and $^{12}\text{C}(p,\gamma_0)^{13}\text{N}$, with much the same energy and similar widths, so that it appears reasonable to classify the peaks as resonances due to a state in ^{13}N . Further investigation of the $^{10}\text{B} + ^3\text{He}$ reactions to try to obtain the spin and parity of this state (e.g. angular distributions and angular correlations), is hindered by the large entrance channel spins ($5/2$ or $7/2$), and possible interference between the resonant state and the underlying background states.

Since the 32 MeV resonance seen in the $^{12}\text{C}(p,\gamma_0)^{13}\text{N}$ studies, coincides with a predicted $T = 1/2$ component of the ^{13}N giant dipole resonance, further investigations were made using the $^{10}\text{B}(^3\text{He},p\gamma)^{12}\text{C}$ and $^{10}\text{B}(^3\text{He},\gamma)^{13}\text{N}$ reactions. These reactions, especially the latter, were expected to be sensitive to any population of the dipole resonance by the $^{10}\text{B} + ^3\text{He}$ reactions. The experiments are described in chapter 3, and a discussion of all the $^{10}\text{B} + ^3\text{He}$ data and the conclusions that can be drawn from them is contained in chapter 4.

CHAPTER 3

THE ($^3\text{He}, p\gamma$) AND ($^3\text{He}, \gamma$) MEASUREMENTS

3.1 INTRODUCTION

The presence of states in ^{13}N at 26 and 32 MeV excitation has been established by the $^{10}\text{B} + ^3\text{He}$ reaction studies of Poate [Po 67] and the present work. It is therefore of interest to see whether these states can be identified with states in the ^{13}N giant dipole resonance. Easlea [Ea 62], using two-particle, one-hole excitations on a ^{12}C core, has calculated that most of the $T = 3/2$ strength of the mass 13 giant resonance occurs at ~ 25 MeV excitation, and that the $T = 1/2$ strength has a component at ~ 32 MeV excitation. The available experimental information from the $^{12}\text{C}(p, \gamma_0)$, $^{13}\text{C}(\gamma, n)$ and $^{13}\text{C}(\gamma, p)$ reactions (summarized by Measday *et al.* [Me 65] and Shin *et al.* [Sh 71]) does show resonances at 26 and 32 MeV, as well as others at lower energies. Measday *et al.* [Me 65] have shown that Easlea's predictions are substantially correct, but that there is some mixing between the $T = 3/2$ and $T = 1/2$ states. If this is so, it may be possible for the $^{10}\text{B} + ^3\text{He}$ reactions to populate both these resonances.

Because the $^{10}\text{B}(^3\text{He}, \gamma_0)^{13}\text{N}$ reaction should be particularly sensitive to the presence of $T = 1/2$ giant dipole state admixtures in the compound nucleus, the cross section of the reaction was measured over the region of the resonances under discussion. The 23.8 cm diam. \times 25.4 cm long NaI(Tl) γ -ray spectrometer, available in this laboratory, was particularly well suited to the study of the energetic γ -rays produced by this reaction (up to 35 MeV). Unfortunately, the yield of the ($^3\text{He}, \gamma$) reaction was found to be very low

(< 60 nb/sr), so that other likely modes of decay of the dipole states were also investigated. Barker *et al.* [Ba 66] have pointed out that the dipole states should have a similar structure to the $T = 1$, 15.11 MeV state in ^{12}C and possibly the $T = 0$, 12.71 MeV state, with an extra (2s,1d) proton. It was therefore expected that the ^{13}N giant resonance states should decay appreciably to either or both of these states in ^{12}C . The 15.11 MeV γ -ray dominated the spectra observed in the $^{10}\text{B}(^3\text{He},\gamma)$ experiments, and the 12.71 MeV γ -ray photopeak could be extracted fairly easily, so that excitation function measurements were made on the $^{10}\text{B}(^3\text{He},p\gamma)^{12}\text{C}$ reactions detecting the 15.11 MeV and 12.71 MeV de-excitation γ -rays.

Measurements on the $^{10}\text{B}(^3\text{He},p\gamma_{15.11})^{12}\text{C}$ reaction up to 9 MeV bombarding energy (29 MeV excitation in ^{13}N) have been made by Barker *et al.* [Ba 66]. They observed no structure in the excitation function, but their targets contained an appreciable amount of ^{11}B ($\approx 15\%$); the yield from the $^{11}\text{B}(^3\text{He},d\gamma_{15.11})^{12}\text{C}$ reaction, which has a threshold at ~ 6 MeV ^3He energy, could have masked out any resonance in the 15.11 MeV γ -ray yield from the ^{10}B reaction.

The experimental procedure is described in section 3.2, while the results are presented and discussed in sections 3.3 and 3.4 respectively.

3.2 EXPERIMENTAL DETAILS

The ^3He beams used in these experiments were obtained from the A.N.U. tandem accelerator, in conjunction with either the neutral-helium injector (1 MeV type J Van de Graaff), or the negative-helium-ion source using lithium vapour exchange. In

general, beam energies of 4 to 12 MeV were available with the former combination, and energies of 10 to 19 MeV from the latter. The beam was collimated by several apertures in the beam line, the last one, 2.3 mm diameter, being 1 m away from the target. After passing through the target, the beam was collected, 2 m from the target, in an insulated Faraday cup which was connected to a calibrated current integrator (accuracy $\pm 2\%$). In order to reduce background, the last aperture was insulated, and the current collected from it minimized with respect to the transmitted beam (usually better than 90% transmission was achieved). Self supporting ^{10}B targets, with thicknesses varying from 85 to 240 $\mu\text{gm}/\text{cm}^2$, were used in these experiments. The thicker targets were used to obtain adequate capture γ -ray yields with the beam currents used (~ 150 nA).

The γ -rays were collimated by a tapered lead annulus, and detected in a 23.8 cm diam. \times 25.4 cm long NaI(Tl) crystal placed at 90° to the beam direction, with the crystal face 30.5 cm from the target. The crystal was inside an NE102A plastic scintillator sheath surrounded by lead shielding. The plastic scintillator was operated in anticoincidence with the NaI detector to reject cosmic ray (muon) events, and also those γ -ray events accompanied by appreciable escape radiation, thus reducing background and improving the resolution. Both the accepted and rejected spectra were stored by routing to sections of 512 channels in the IBM 1800 data acquisition system. A detailed description of the 23.8 cm \times 25.4 cm NaI(Tl) crystal γ -ray spectrometer with the associated electronics is provided in an A.N.U. internal report [B1 69], and only relevant details and additions are noted below.

Because of the low yields, wide angle collimation ($\pm 20\%$)

was used, giving about 8% F.W.H.M. resolution. The photopeak yields were obtained by summing over \pm F.W.H.M.; detection efficiencies were estimated from the efficiencies obtained for a similar 24 cm \times 24 cm NaI(Tl) detector by Suffert *et al.* [Su 68]. Efficiencies ranged from $30 \pm 5\%$ at 15 MeV to $15 \pm 3\%$ at 30 MeV. γ -ray transmission by the wax and lithium carbonate neutron shielding inside the collimator, and by the plastic scintillator, was calculated from the photon absorption cross sections of Nijght *et al.* [Ni 59]; it was found to vary from 73 to $78 \pm 4\%$ for $E_{\gamma} = 15$ to 30 MeV. The resultant overall accuracy of the absolute cross sections was estimated to be $\pm 20\%$.

Energy calibrations were made using a RdTh γ -ray source ($E_{\gamma} = 2.61$ MeV), and the prominent ^{12}C γ -rays at 4.43 and 15.11 MeV in the reaction spectra. Further calibration points at 15.36 and 18.92 MeV were obtained using the $\text{T}(^3\text{He}, \gamma_0)^6\text{Li}$ reaction (Q value 15.79 MeV [Bl 68a]). Photopeaks, corresponding to the calculated energies (25.3 and 21.8 MeV) of the $^{10}\text{B}(^3\text{He}, \gamma)$ radiative capture transitions to the ground state and the 3.51 - 3.55 MeV doublet of ^{13}N , were observed in a spectrum obtained with a ^3He energy of 4.8 MeV, and lay on the extrapolation of the calibration line. Further extrapolation of the calibration line, by following these peaks as the ^3He energy was increased, resulted in a calibration that was linear to $\pm 2\%$ up to the maximum γ -ray energy observed ($E_{\gamma} = 32$ MeV), thus confirming the identification of the photopeak origins.

In early experiments, a pulsed light source, placed in the light pipe between the NaI crystal and the photomultiplier tube, was used to stabilize the gain of the photomultiplier. The amplitude of the pulse due to the light source (equivalent to $E_{\gamma} = 45$ MeV) was

fed to a feedback system that controlled the voltage applied to the dynode chain. However, the tail of the light pulse was so long that, at moderate count rates, significant broadening of the light pulser peak occurred, degrading the upper part of the spectrum. Stabilization was therefore abandoned, and the 15.11 MeV ^{12}C photopeak was used to monitor and to correct for any gain shifts (always less than 2%).

Two rejection circuits were used to minimize pile-up effects at high count rates. The first was a discriminator set at about 8 MeV on the delay line clipped leading edge of a fast anode signal from the photomultiplier. This discriminator was used to gate the linear signal from the ninth dynode. Outside a resolving time of about 90 ns, it prevented addition of two pulses (each below 8 MeV) from producing pulses in the 8 to 16 MeV region. However, at beam energies above 9 MeV, the fast neutron background was so high that pile-up of pulses below 8 MeV with the 15.11 MeV γ -ray pulses was a problem. Therefore a second circuit (fig. 3.1) was introduced. The clipped fast timing signal from the anode of the photomultiplier was amplified and fed to a fast discriminator set at 2 MeV. The resulting negative timing pulse was reflected by a shorted cable to produce a similar positive pulse delayed by 3 μs (corresponding to the length of the linear energy signals). Both pulses were integrated by a charge sensitive preamplifier to give a rectangular positive pulse of 3 μs duration. If two NaI events triggered the fast discriminator within 3 μs , the preamplifier output consisted of two overlapping (linearly summed) pulses. The integral discriminator was set to trigger a "veto" pulse only when overlap occurred. By utilizing a linear delay device and fast timing electronics

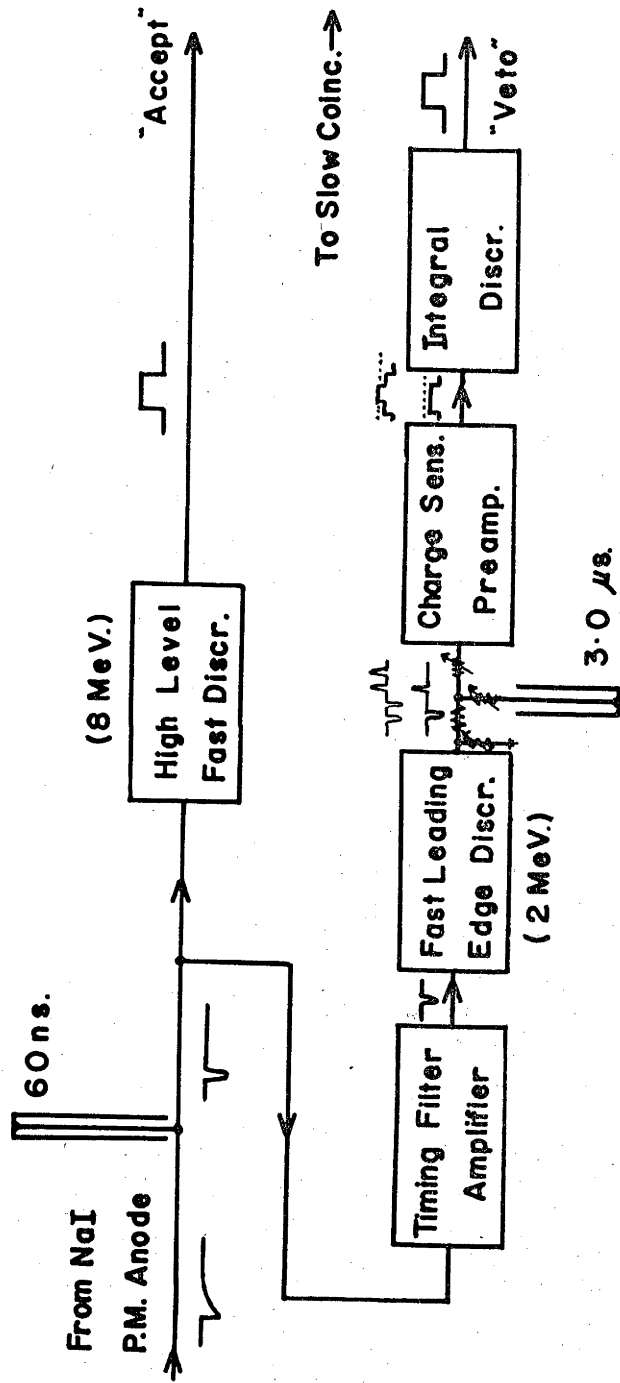


Figure 3.1: Pile up rejection electronics for the experiments using the 23.8 cm x 25.4 cm NaI(Tl) detector. The operation of the circuit is explained in the text.

(Ortec models 454, 417, 109A and 421), the circuit dead time was kept small at high count rates. With a resolving time of about 120 ns, this circuit prevented addition of any two pulses, each over 2 MeV. The resulting spectra were considerably improved.

3.3 ANALYSIS AND RESULTS

A typical spectrum obtained at 8.4 MeV ^3He energy is shown in fig. 3.2. The capture γ -ray transitions to the ground state (γ_0) and the 3.51 - 3.55 MeV doublet ($\gamma_{3.5}$) of ^{13}N are clear, as are the 15.11 \rightarrow 0, 12.71 \rightarrow 0, and 15.11 \rightarrow 4.44 MeV transitions in ^{12}C .

To minimize pile-up and dead time effects, low beam currents of about 30 nA on a 140 $\mu\text{g}/\text{cm}^2$ target were used for accurate measurements of the $^{10}\text{B}(^3\text{He}, p\gamma_{15.11})^{12}\text{C}$ cross sections. These were taken in 1 MeV steps from $E_{^3\text{He}} = 4$ to 17 MeV. All points were remeasured at least once with a different target; good agreement was obtained. In contradiction to previous measurements between 4 and 9 MeV bombarding energy [Ba 66], some structure was evident. Therefore the measurements in the region from 4 to 12 MeV were repeated twice in 100 keV steps (odd multiples with increasing energy, even when decreasing). The cross sections obtained ranged from 200 to 260 $\mu\text{b}/\text{sr}$ and they are shown in the top curve of fig. 3.3. As discussed in the previous section, the absolute errors in the cross section are estimated to be $\pm 20\%$.

Because the enriched ^{10}B targets contained about 5% of ^{11}B , a check was made on the $^{11}\text{B}(^3\text{He}, d\gamma_{15.11})^{12}\text{C}$ cross section at 8 MeV bombarding energy, using an enriched ^{11}B target (98%). The result (635 \pm 90 $\mu\text{b}/\text{sr}$) indicated a significant contribution to the

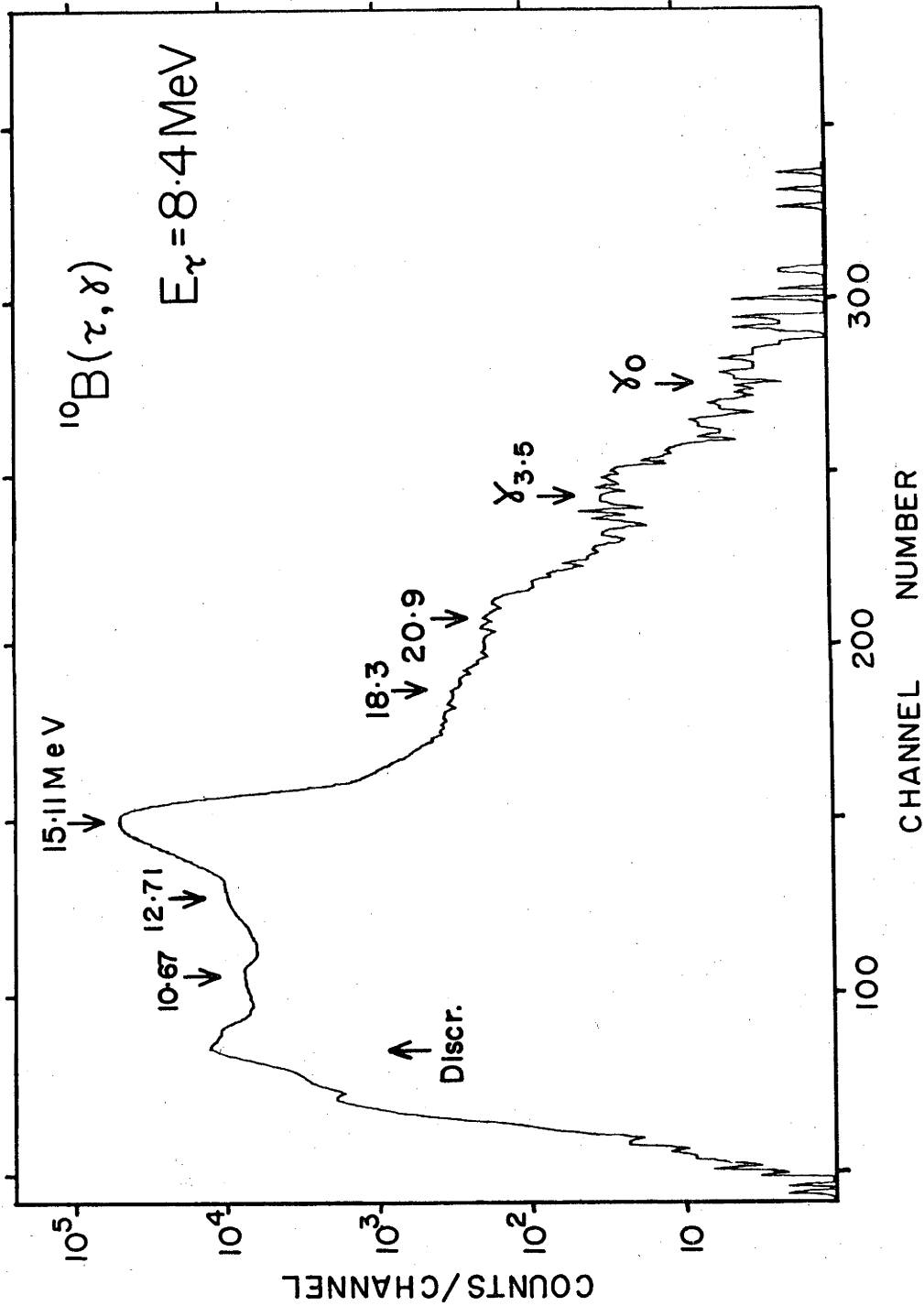


Figure 3.2: Typical γ -ray spectrum from the $^{10}\text{B} + ^3\text{He}$ reactions detected with the 23.7 cm \times 25.4 cm NaI(Tl) crystal.

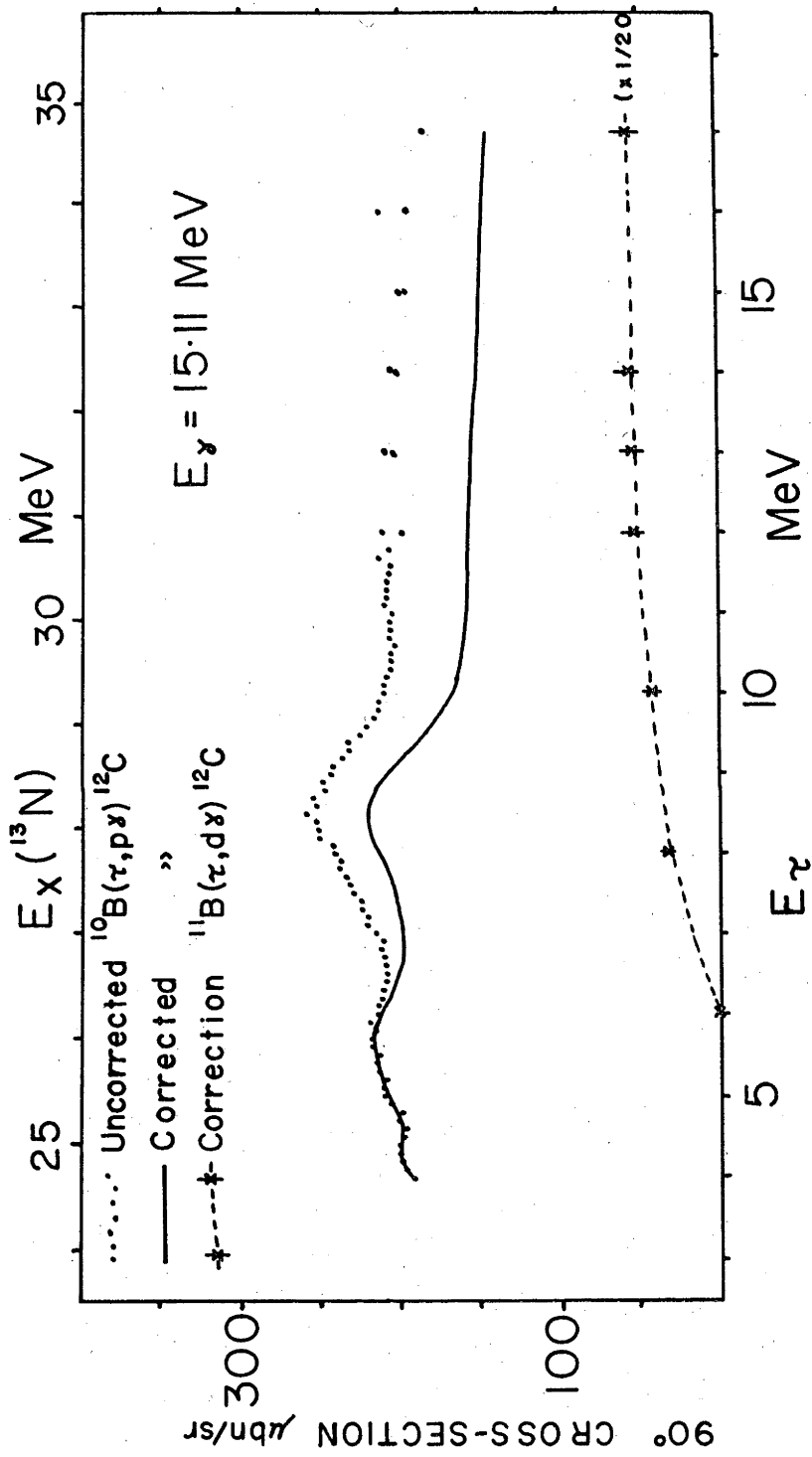


Figure 3.3: Differential cross sections of the $^{10}\text{B}(\text{}^3\text{He}, p\gamma_{15.11})^{12}\text{C}$ and $^{11}\text{B}(\text{}^3\text{He}, d\gamma_{15.11})^{12}\text{C}$ reactions. The relative error for the cross sections of the former reaction, is best shown by the spread in points. The absolute error is $\pm 20\%$. The smooth curve is the approximate shape of the 15.11 MeV γ -ray yield from ^{10}B after correction for the ^{11}B in the target.

15.11 MeV γ -ray yield in the ^{10}B measurements. Therefore the ^{11}B cross section was measured at a number of energies between 6 MeV (threshold) and 17 MeV, and the ^{10}B excitation function corrected accordingly. The results are collected in fig. 3.3 where the ^{11}B cross sections divided by 20 (the approximate contribution to the ^{10}B measurements) are shown, and the corrected ^{10}B excitation function is indicated by a smooth curve.

The much lower cross sections for the $^{10}\text{B}(^3\text{He}, p\gamma_{12.71})^{12}\text{C}$ and $^{10}\text{B}(^3\text{He}, \gamma)^{13}\text{N}$ reactions were measured with a thicker target (175 $\mu\text{g}/\text{cm}^2$) and beam currents up to 130 nA at energies from 4.8 to 14 MeV. To correct for dead time effects in the electronics (up to 15% at worst), the spectra were normalized to correctly reproduce the 15.11 MeV γ -ray yields measured with lower beam currents.

Extraction of the $^{10}\text{B}(^3\text{He}, p\gamma_{12.71})^{12}\text{C}$ cross sections was complicated by the uncertain background due to the low energy tail (bremsstrahlung escape) of the 15.11 MeV photopeak. The line shape improvement technique of Suffert *et al.* [Su 68] was therefore employed. For each run, a fraction (0.8 was found to be optimum) of the NaI(Tl) spectrum which had been rejected (because of coincident events in the plastic scintillator) was subtracted from the accepted spectrum. Figure 3.4 shows the result for $E_{^3\text{He}} = 8.4$ MeV. Despite the different scales, a comparison with the accepted spectrum in fig. 3.2 reveals a significant improvement in resolution. The ratio of the 12.71 and 15.11 MeV photopeak counts extracted from the "improved" spectrum at each energy, was then combined with the 15.11 MeV yields obtained from the "unimproved" spectra to give the true 12.71 MeV γ -ray yields.

As in the 15.11 MeV cross section measurements, the

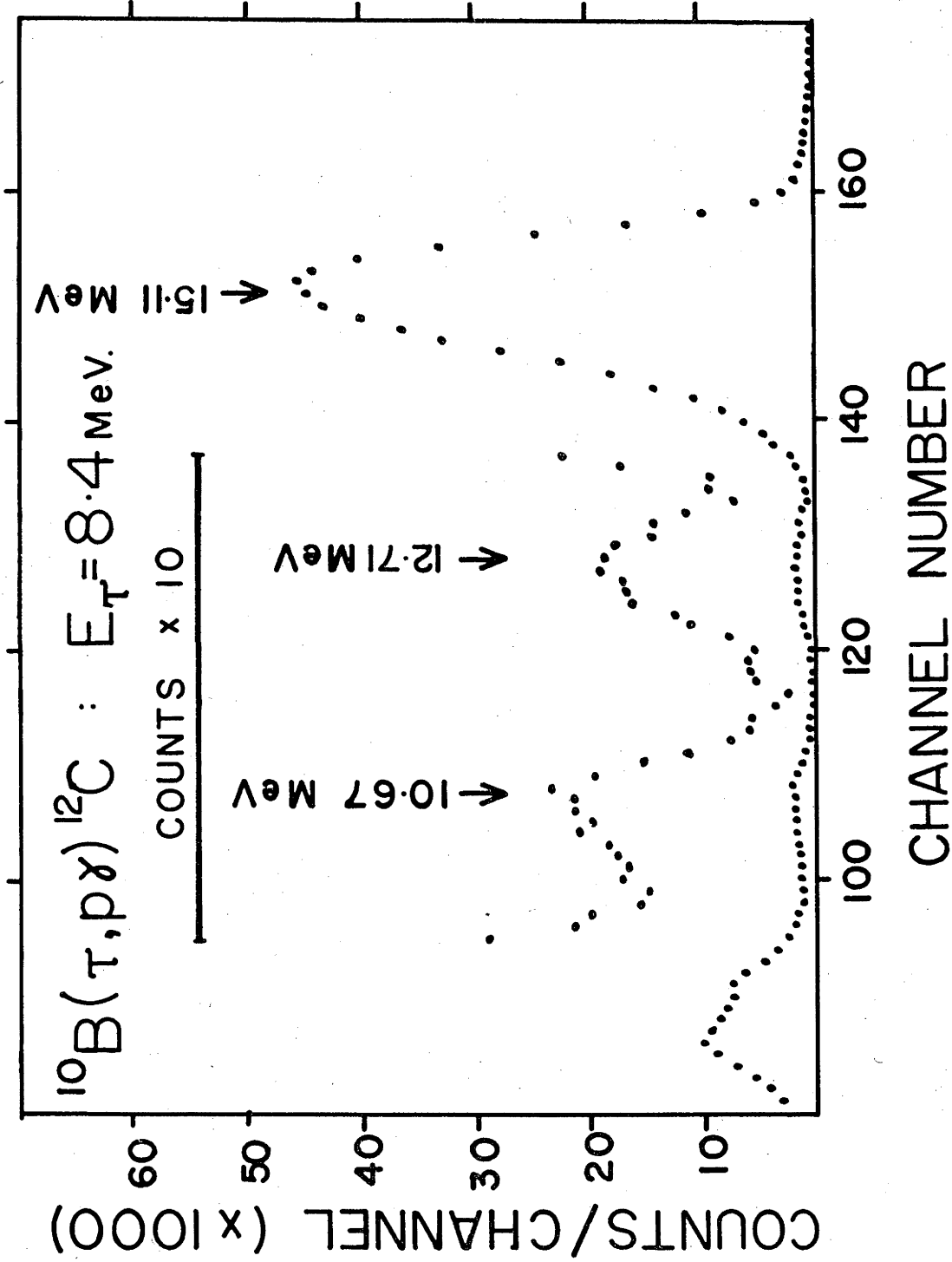


Figure 3.4: Typical γ -ray spectrum after "improvement" as described in the text.

$^{11}\text{B}(^3\text{He}, d\gamma_{12.71})^{12}\text{C}$ reaction was found to contribute significantly to the 12.71 MeV γ -ray yield. The 12.71 MeV cross sections were extracted from the ^{11}B data and they are presented with the uncorrected and corrected $^{10}\text{B}(^3\text{He}, d\gamma_{12.71})^{12}\text{C}$ results in fig. 3.5. The absolute errors in the cross sections are estimated to be $\pm 20\%$. It should be noted that these cross sections are for the production of the 12.71 MeV γ -ray. The 12.71 MeV level of ^{12}C decays primarily by α -emission (97.5%), so that the $^{10}\text{B}(^3\text{He}, p)^{12}\text{C}$ cross section to the 12.71 MeV state is actually about 50% greater than that to the 15.11 MeV state between 4.8 and 12 MeV bombarding energy.

Even with the thicker targets and higher beam currents, 6 to 10 hours were required to collect adequate statistics for the $(^3\text{He}, \gamma)$ reaction at each energy. As a check, three points were repeated with a different target; the results were in good agreement with the initial measurements. The γ_0 and $\gamma_{3.5}$ cross sections were evaluated by summing across the appropriate channels (\pm F.W.H.M.), and subtracting background estimates with generous error allowances. The results are shown in fig. 3.6. In no spectrum was there evidence of a transition to the 2.37 MeV first excited state of ^{13}N ; an upper limit of 20% of the γ_0 cross section is placed on this transition between 4.8 and 14 MeV ^3He energy.

The $^{11}\text{B}(^3\text{He}, \gamma)^{14}\text{N}$ reaction has a Q value only 0.9 MeV lower than that for ^{10}B radiative capture, so that any large contribution from this reaction would produce γ -rays that would be included in the ^{10}B yield. Therefore, a measurement of the $^{11}\text{B}(^3\text{He}, \gamma)^{14}\text{N}$ cross section was made at 8.4 MeV bombarding energy with an enriched ^{11}B target. This gave $\sigma(\gamma_0) = 210 \pm 90$ nb/sr and $\sigma(\gamma_{2,3}) < 400$ nb/sr. Black *et al.* [B1 70] have measured $\sigma(\gamma_0)$ from

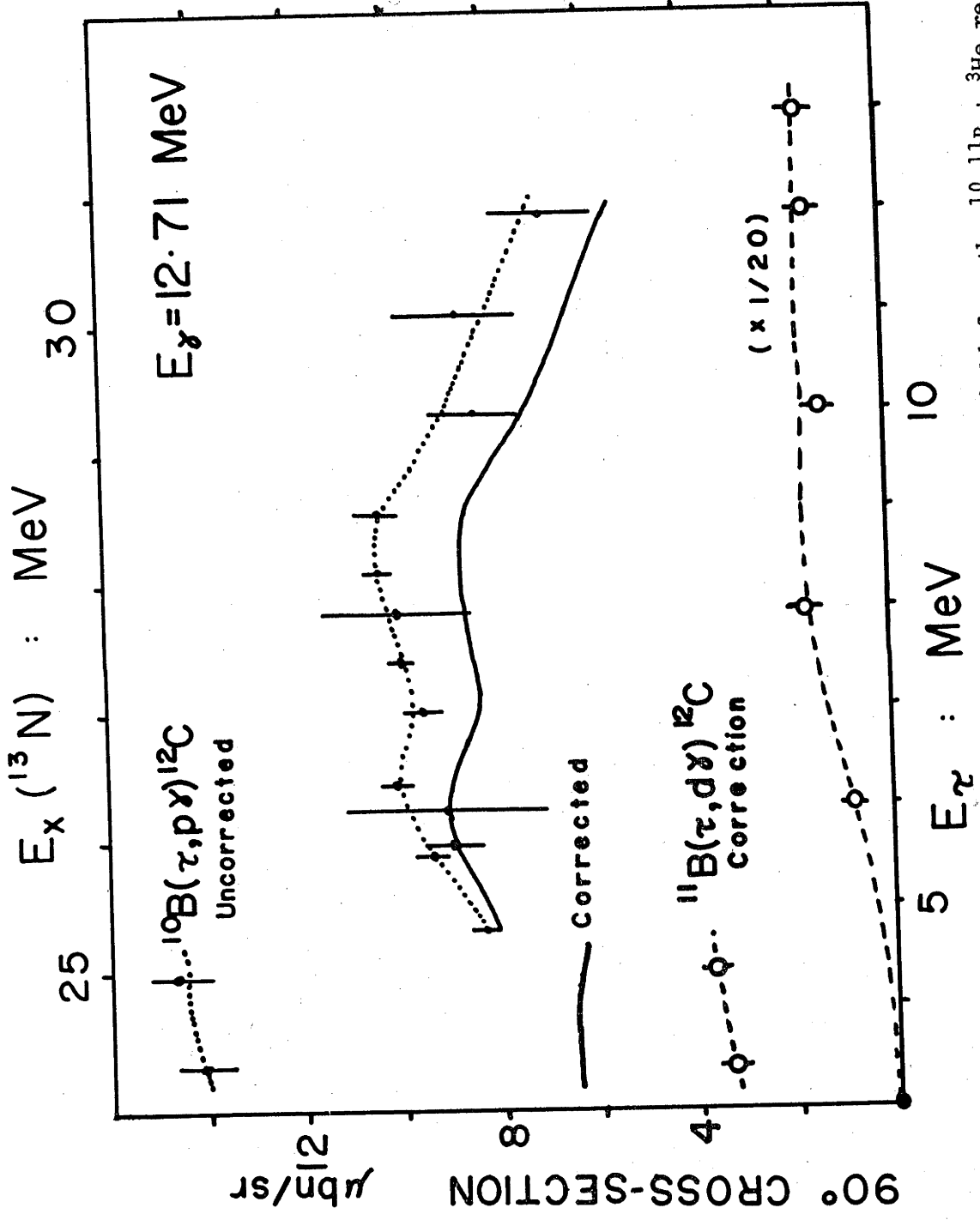


Figure 3.5: Differential cross sections for the 12.71 MeV γ -ray yield from the $^{10,11}\text{B} + ^3\text{He}$ reactions.

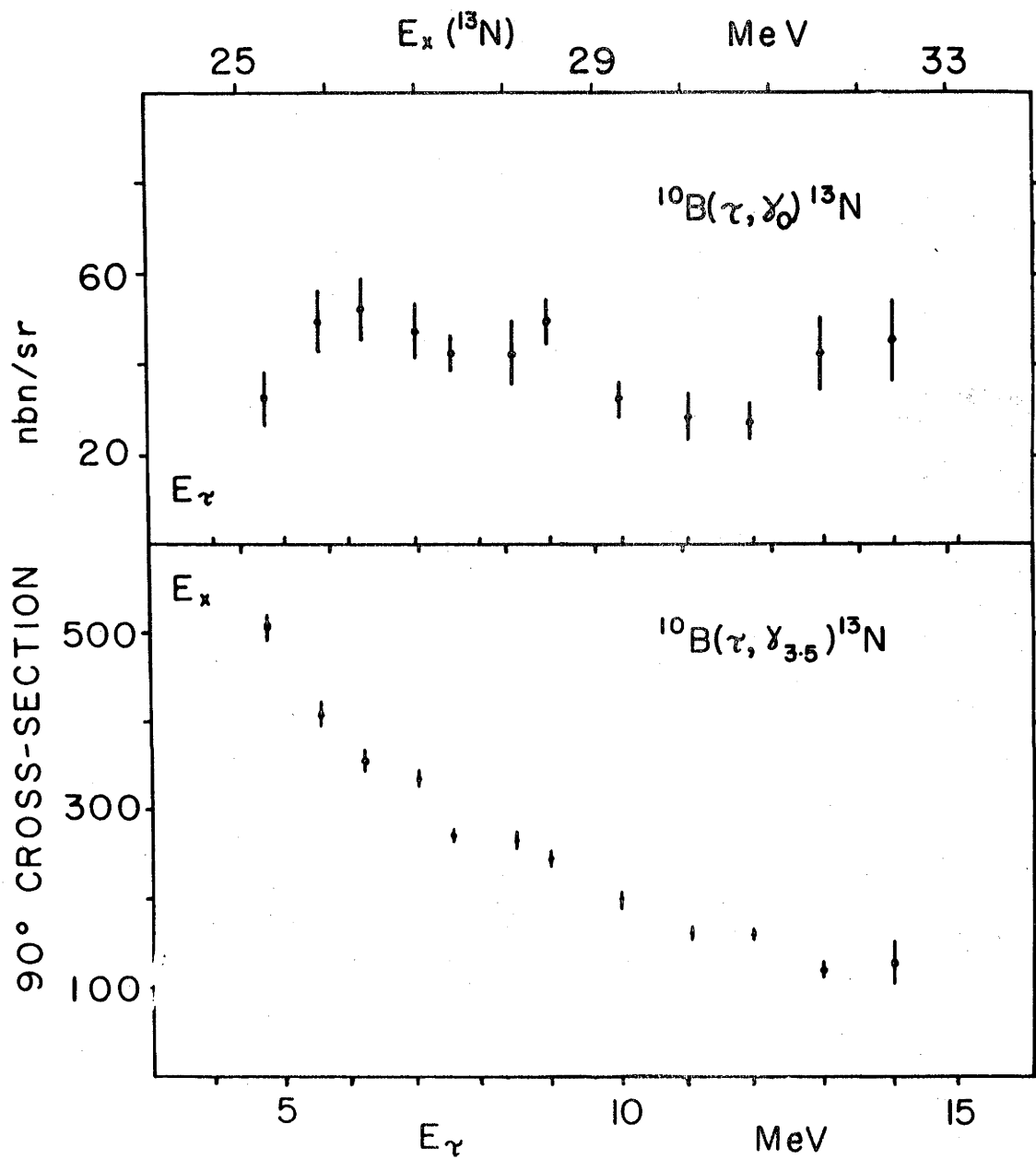


Figure 3.6: Differential cross sections for the $^{10}\text{B}(\text{}^3\text{He}, \gamma_0)^{13}\text{N}$ and $^{10}\text{B}(\text{}^3\text{He}, \gamma_{3.5})^{13}\text{N}$ reactions. The absolute error is $\pm 20\%$.

$E_{^3\text{He}} = 0.9$ to 2.6 MeV. At the latter energy, just above the Coulomb barrier, the cross section has risen to and levelled off at 300 ± 50 nb/sr. If these are typical $^{11}\text{B}(^3\text{He},\gamma)$ cross sections for the higher energy range studied in the present experiments, then the $^{10}\text{B}(^3\text{He},\gamma_0)$ and $^{10}\text{B}(^3\text{He},\gamma_{3,5})$ cross sections in fig. 3.6 are probably too large by 10 - 30% and 5 - 15% respectively.

Also visible, but less distinct, in the spectrum of fig. 3.2 are photopeaks at 20.9 ± 0.3 and 18.3 ± 0.6 MeV. These peaks were clearer for higher bombarding energies when they moved further above the high energy tail of the 15.11 MeV photopeak. They exhibited the correct shifts with beam energy to be capture γ -rays to states of ^{13}N at 7.25 ± 0.15 and 9.8 ± 0.3 MeV excitation, or possibly to states of ^{14}N at 6.35 ± 0.15 and 8.1 ± 0.3 MeV. The former origin seems more likely since these γ -rays were not obvious in the $^{11}\text{B}(^3\text{He},\gamma)$ spectrum at 8.4 MeV ^3He energy. Because of the appreciable background, it was not possible to extract accurate cross sections for these transitions over the full energy range, but $\sigma(\gamma_{7.2})$ was estimated to be ≈ 1.5 $\mu\text{b/sr}$ between 5 and 9 MeV bombarding energy, and $\sigma(\gamma_{9.8})$ was ≈ 2 $\mu\text{b/sr}$ at 9 MeV ^3He energy.

3.4 DISCUSSION

Several calculations have been made of the positive parity states of ^{13}C and ^{13}N produced by electric dipole absorption. Easlea [Ea 62] evaluated the dipole excitations of ^{13}C assuming the ^{13}C ground state to be a $1p_{1/2}$ neutron added to the ground state of ^{12}C which was assumed to be a pure j-j coupling state ($1p_{3/2}^8$). The dipole excitations were then described by single-particle excitation

of the ^{12}C core producing a two-particle, one-hole configuration, or by a single-particle excitation of the valence nucleon. This treatment admits the presence of $T = 3/2$ states, and a strong grouping of these states was found around 25 MeV excitation with a weaker component at 37 MeV. Likewise, groupings of $T = 1/2$ states were found around 13, 20 and 32 MeV. These isotopic spin assignments for the giant resonance states were supported by the $^{12}\text{C}(p,\gamma_0)$ data of Fisher *et al.* [Fi 63], in which the predicted $T = 1/2$ states were observed, but no resonance was observed corresponding to the $T = 3/2$ state at ~ 25 MeV. On the other hand, in the $^{13}\text{C}(\gamma,p)^{12}\text{B}$ measurements of Cook [Co 67], in which proton decay of $T = 3/2$ states in ^{13}C , to $T = 1$ states in ^{12}B was isospin allowed, a strong resonance was observed at ~ 26 MeV. However, there was no sign of the predicted $T = 3/2$ resonance at 37 MeV.

In a comprehensive survey of the electric dipole resonances of ^{13}C and ^{13}N by Measday *et al.* [Me 65], the relevant data were discussed and it was deduced that the 26 MeV state is predominantly $T = 3/2$ with some $T = 1/2$ admixture. Investigations of the giant resonance states were also carried out using a weak coupling model, essentially in the j - j coupling limit. The ^{13}C giant resonance states were described by core excitations of the form $lp_{3/2}^{-1} lp_{1/2}(2s,1d)$. Break-up of these states was expected to leave ^{12}C mainly in its $lp_{3/2}^{-1} lp_{1/2}$ states, which were taken to be those at 4.43, 12.71, 15.11 and perhaps 16.11 MeV.

If the ^{13}C and ^{13}N ground state configurations are obtained from the LS coupling limit, simple predictions can be made concerning the decay of giant resonance states. The ground states have the configurations $1s^4lp^9$ with symmetry [441] and E1 excitations will

produce states of the form $1s^4 1p^8 [431] (2s, 1d)$ - corresponding to core excitations - and $1s^4 1p^8 [44] (2s, 1d)$. Since the matrix elements for the dipole transitions are proportional to the fractional parentage coefficients of the form $\langle p^9 | p^8 p \rangle$, as given by Janh and van Wieringen [Ja 51], states of [431] symmetry will be produced five times as strongly as those of [44] symmetry. Therefore, nucleon emission from the E1 giant resonance states will then proceed preferentially to states of [431] symmetry. The lowest mass 12 states with predominantly the [431] symmetry are the $T = 1$ isospin triplet, consisting of the 15.11 MeV state of ^{12}C and the ground states of ^{12}B and ^{12}N , and possibly the $T = 0$, 12.71 MeV state of ^{12}C [Ku 71]. It is therefore expected that the ^{13}C (or ^{13}N) giant resonance states should decay appreciably to the 15.11 MeV state of ^{12}C .

The present excitation function measurements of the decay of the $^{10}\text{B} + ^3\text{He}$ system to the 15.11 and 12.71 MeV states in ^{12}C are shown in figs. 3.3 and 3.5 respectively. Some structure is evident in both of them at 26 and 28 MeV excitation, corresponding to the states seen in the $^{10}\text{B}(^3\text{He}, \text{particle})$ channels [Po 67]. If either of these states were associated with the $T = 3/2$ part of the ^{13}N giant resonance at 26 MeV, the $(^3\text{He}, p)$ yield should favour the $T = 1$ final state over the $T = 0$ one. This does not appear to be the case. There is no evidence in the 15.11 MeV γ -ray data for a resonance similar to those seen in the $(^3\text{He}, \alpha_1)$ and $(^3\text{He}, d_{4,5})$ reactions at 32 MeV.

The analogue of the $(^3\text{He}, p\gamma_{15.11})$ reaction is the $^{10}\text{B}(^3\text{He}, n_0)^{12}\text{B}$ reaction. Peterson and Glass [Pe 63] obtained evidence for the 26 MeV state in their total cross section measurement

of this reaction; however, it is not excited as strongly as would be expected for a giant resonance state. The measurements of Singh [Si 70] indicate some weak structure at about 32 and 34 MeV excitation, but the data points were so widely spread and the errors assigned so large, that it is not certain whether or not the reaction is populating the 32 MeV resonance seen in the other channels.

Further evidence for the weakness of the 26 and 28 MeV resonances in the channel to the 15.11 MeV state is available from the $^{12}\text{C}(p, p\gamma_{15.11})^{12}\text{C}$ reaction [Me 63] and its analogue, the $^{12}\text{C}(p, n)^{12}\text{N}$ reaction [Ri 68]. The 26 MeV resonance was seen in the former reaction, while both were observed in the latter. However, they were excited only weakly and in neither reaction was there any evidence for the 32 MeV resonance.

The $^{10}\text{B}(^3\text{He}, \gamma)^{13}\text{N}$ data obtained in the present studies are presented in fig. 3.6. The most striking feature of the results is the very small $(^3\text{He}, \gamma_0)$ cross section, which is typically 40 nb/sr between 25.3 and 32.4 MeV excitation. With the error bars applied to the data points it is only possible to say that there could be structure in the yield curve corresponding to the resonances seen in the other $^{10}\text{B} + ^3\text{He}$ studies at 26, 28 and 32 MeV. Using the principle of detailed balance to calculate the inverse reaction cross sections from these measurements and Fisher's $^{12}\text{C}(p, \gamma_0)^{13}\text{N}$ data, the following mean cross sections over the region from 25.3 to 32.4 MeV excitation are obtained:

$$\begin{aligned} ^{13}\text{N}(\gamma, p_0)^{12}\text{C} & : 296 \text{ } \mu\text{b/sr} \\ ^{13}\text{N}(\gamma, ^3\text{He}_0)^{10}\text{B} & : 5.3 \text{ } \mu\text{b/sr} . \end{aligned}$$

The $(\gamma, ^3\text{He}_0)$ cross section is thus typically 1.8% of the (γ, p_0)

cross section. This is strong evidence that the $^{10}\text{B} + ^3\text{He}$ system has little overlap with low multipolarity electromagnetic excitations of the ^{13}N ground state. In particular, with the $(^3\text{He}, p\gamma)$ results of the present experiment, it can be concluded that the various resonances seen in the $^{10}\text{B}(^3\text{He}, \text{particle})$ channels are not associated with the ^{13}N giant dipole resonance.

It is unfortunate that the low cross section precluded more accurate measurements of the $^{10}\text{B}(^3\text{He}, \gamma_0)$ yield; for the same reason, angular distribution measurements were not feasible in the (accelerator) time available. Increasing neutron background prevented the extension of the measurements above 14 MeV ^3He energy (32.4 MeV excitation in ^{13}N). However, with the data available, it can be seen that the 32 MeV resonance seen in the $^{12}\text{C}(p, \gamma_0)$ reaction is certainly not strong in the $^{10}\text{B}(^3\text{He}, \gamma_0)$ channel, if it is excited at all.

The $^{10}\text{B}(^3\text{He}, \gamma_{3.5})^{13}\text{N}$ cross section decreases smoothly over the measured range. The high value at 4.8 MeV ^3He energy might be associated with a resonance at a lower energy, but the difficulty in extracting the $\gamma_{3.5}$ photopeak from the tail of the 15.11 MeV photopeak prevented reliable measurements below 4.8 MeV.

In conclusion, the results presented in this chapter indicate that the resonances seen in the $^{10}\text{B} + ^3\text{He}$ reactions above 25 MeV excitation in ^{13}N can not be identified with the giant dipole resonance. A summary of all the data pertaining to the resonances seen in the $^{10}\text{B} + ^3\text{He}$ reactions above 25 MeV excitation is presented in chapter 4.

CHAPTER 4

SUMMARY AND CONCLUSIONS

The $^{10}\text{B} + ^3\text{He}$ studies described in this thesis have sought to establish the presence of levels in the ^{13}N compound system above 25 MeV excitation. Previous work had indicated resonances in the $^{10}\text{B} + ^3\text{He}$ and $^{12}\text{C} + \text{p}$ systems at 26 and 28 MeV excitation, while a resonance at 32 MeV had been observed in the $^{12}\text{C}(\text{p}, \gamma_0)$ reaction. In the present experiments, the $^{10}\text{B} + ^3\text{He}$ measurements were extended to include the region of the 32 MeV resonance, and additional studies were made of all three resonances using the $^{10}\text{B}(^3\text{He}, \gamma)^{13}\text{N}$ and $^{10}\text{B}(^3\text{He}, \text{p}\gamma)^{12}\text{C}$ ($E_\gamma = 15.11$ and 12.71 MeV) reactions.

A summary of the available data on the ^{13}N compound system above 25 MeV excitation is presented in table 4.1. The data were taken from the compilation by Ajzenberg-Selove [Aj 69] and the present work. If a given resonance has been seen in a particular reaction, the angle or angles at which it was observed is noted. Indications of changes in yield at the appropriate resonance energies are shown by parentheses. As discussed in chapter 1, whilst one should be wary of interpreting "bumps" in cross sections as resonances from individual states in the compound nucleus, there is substantial evidence in this instance, that resonances occur in the ^{13}N compound system at 26, 28 and 32 MeV.

The first two resonances have been observed in several channels, and their nature has been discussed by Scott *et al.* [Sc 67] and Girod *et al.* [Gi 70]. The latter authors have fitted the available $^{10}\text{B}(^3\text{He}, \alpha)$ data using the Humblet-Rosenfeld theory (in which the collision matrix is considered to be the sum of a smooth back-

Table 4.1
Yield resonances in reactions
going through the ^{13}N compound nucleus

^3He Energy (MeV)	5.6	8.5	13.5
^{13}N Excitation (MeV)	26	28	32
Reaction			
$^{10}\text{B}(^3\text{He},\alpha_0)^9\text{B}$	150°	(90°, 150°)	*
α_1	*	*	150°
α_2			(150°)
$^{10}\text{B}(^3\text{He},\text{t})^{10}\text{C}$	*	*	
$^{10}\text{B}(^3\text{He},\text{d}_0)^{11}\text{C}$	90°, 150°	*	*
d_1			*
d_2			*
d_3			*
$\text{d}_{4,5}$			150°
$^{10}\text{B}(^3\text{He},\text{p}_0)^{12}\text{C}$	150°	150°	*
p_1	*	*	*
p_2	150°	*	
p_3	150°	*	
$^{10}\text{B}(^3\text{He},\text{p}\gamma_{12.71})^{12}\text{C}$	90°	90°	*
$\text{p}\gamma_{15.11}$	90°	90°	*
$^{10}\text{B}(^3\text{He},\text{n})^{12}\text{N}$	(total)	*	*
$^{10}\text{B}(^3\text{He},\gamma_0)^{13}\text{N}$	(90°)	(90°)	(90°)
$\gamma_{2,3}$	*	*	*
$^{12}\text{C}(\text{p},\text{p})^{12}\text{C}$	135°, 145°	135°, 145°	
$^{12}\text{C}(\text{p},\text{p}\gamma_{15.11})^{12}\text{C}$	90°	*	*
$^{12}\text{C}(\text{p},\gamma_0)^{13}\text{N}$	*	*	90°
$\gamma_{2,3}$	90°	*	*
$^{12}\text{C}(\text{p},\text{n})^{12}\text{N}$	(total)	(total)	(total)

* Indicates no significant change in yield at that excitation.
Parentheses indicate a possible resonant change in yield.

The data for this table were taken from the compilation of Ajzenberg-Selove [Aj 69] and the present work.

ground term and a series of resonant terms) and have analyzed the $^{12}\text{C}(p,p)$ data using an optical model formalism modified by a resonance term. They proposed spins and parities of $7/2^-$ and $9/2^+$ for the states in ^{13}N giving rise to the resonances at 26 and 28 MeV respectively. The high spins postulated for these states are consistent with the γ -ray measurements of the present work (chapter 3), from which it was concluded that the resonances observed in the $^{10}\text{B} + ^3\text{He}$ reactions could not be identified with the electric dipole giant resonance states in ^{13}N (which have spins of $1/2^+$ and $3/2^+$).

The 32 MeV resonance has now been observed in three different reactions at the same energy and with similar widths. There is the possibility that the resonance observed in the $^{10}\text{B} + ^3\text{He}$ studies could be due to a strongly absorbing resonance in the input channel [Mo 67], that happens to coincide with a giant dipole state observed in the $^{12}\text{C}(p,\gamma_0)$ reaction. However, such a resonance should also appear strongly in the ^3He elastic scattering cross section, and, although it was not possible to extract the $^{10}\text{B}(^3\text{He},^3\text{He})$ yield accurately because of underlying background peaks, an inspection of the spectra taken at 150° , presented in fig. 2.2, reveals no sign of a large change in yield near 13.5 MeV bombarding energy (32 MeV excitation in ^{13}N). It appears reasonable therefore, to assume that the same resonance is populated in the three reactions, and that it can be classified as due to a state in ^{13}N .

Unfortunately, in the time available, it was not possible to measure angular distributions over the region in which the resonance was observed, so that no total cross sections could be deduced. Neither could an analysis similar to that of Girod *et al.*

[Gi 70] be applied. However, such an analysis is unlikely to provide a unique value of spin and parity because of the large entrance channel spin ($5/2$ and $7/2$), and the variety of possible angular momenta for the incoming particle. An extension of the $^{12}\text{C} + p$ experiments, which provide less complex input channel situations, might provide the necessary information.

One conclusion about the nature of the state at 32 MeV can be drawn from the data in table 4.1. The 32 MeV resonance is not seen in the same channels as either the 26 or 28 MeV resonances, although the deuteron yields to the fourth and fifth excited states of ^{11}C have not been measured over the region of the lower two resonances. This disparity suggests that the state has a substantially different structure to the other two resonance states at 26 and 28 MeV.

In an effort to see whether the character of the 32 MeV state could be deduced from the configurations of the outgoing channels, the predominant symmetries of the wave functions of the final states were examined. The wave functions for the negative parity states were calculated by Kumar [Ku 71] from the parameters of Cohen and Kurath [Co 65a] (using the 2BME parameters for $A = 9$, and the POT parameters for $A = 11, 12$ and 13). The predominant symmetries of the positive parity states were deduced from the Nilsson configurations of El-Batanoni and Kresnin [El 66]. The configurations are presented in table 4.2. Both the $(^3\text{He}, \alpha_2)$ and $(^3\text{He}, d_4)$ reactions lead to positive parity states in the final nucleus. Loosely binding an α -particle and a deuteron respectively to these states, leads to compound states that have similar configurations to one of the possible ^{13}N giant dipole configurations ($1s^4 1p^8$ [44] ($2s, 1d$)). How-

ever, there are several objections to this interpretation of the nature of the resonance. The calculated dipole resonances above 30 MeV result mainly from excitation of a 1s nucleon [Ea 62] giving a configuration predominantly of the form, $1s^3 1p^{10}$ [442]; although it could be possible to have some small admixture of the $1s^4 1p^8$ [44] (2s,1d) term. The main objection is the absence of any appreciable resonance in the ($^3\text{He},p$) reactions. Both the ground and first excited states of ^{12}C have mainly [44] symmetry (see table 4.3), and if the $^{10}\text{B} + ^3\text{He}$ system is populating the [44] symmetry components of the ^{13}N giant resonance states, the emission of a proton from the (2s,1d) shell to the first two states in ^{12}C would be favoured.

Table 4.2

Configurations of the outgoing channels
from the 32 MeV resonance in ^{13}N

Reaction	Configuration	Final Spin State
$^{10}\text{B}(^3\text{He},\alpha)^9\text{B}$	$\alpha_1 + 1s^4 1p^5$ [41]	$5/2^-$
	$\alpha_2 + 1s^4 1p^4$ [4] (2s,1d)	$3/2^+, 5/2^+$
$^{10}\text{B}(^3\text{He},d)^{11}\text{C}$	$d_4 + 1s^4 1p^6$ [42] (2s,1d)	$1/2^+$
	and/or $d_5 + 1s^4 1p^7$ [43]	$7/2^-$
$^{10}\text{B}(^3\text{He},\gamma)^{13}\text{N}$	$\gamma_0 + 1s^4 1p^9$ [441] and [432]	$1/2^-$

Wave functions for the negative parity final states were calculated from the parameters of Cohen and Kurath [Co 65a] by Kumar [Ku 71]. Only the predominant symmetries (contributing > 80% to the strength of the wave function) are listed.

The predominant symmetries of the positive parity states were deduced from ref. [E1 66].

Table 4.3

Wave functions for the ground and first excited states of ${}^9\text{B}$ and ${}^{12}\text{C}$, calculated [Ku 71] from the parameters of Cohen and Kurath [Co 65a]

Nucleus	Energy (MeV)		J^π	Symmetry terms (amplitudes)										
	exp.	calc.		[41] ${}^{22}\text{P}$	[41] ${}^{22}\text{D}$	[41] ${}^{22}\text{F}$	[32] ${}^{22}\text{D}$	[44] ${}^{11}\text{S}$	[44] ${}^{11}\text{D}$	[431] ${}^{13}\text{P}$	[431] ${}^{13}\text{D}$	[431] ${}^{13}\text{F}$	[422] ${}^{11}\text{S}$	[422] ${}^{15}\text{D}$
${}^9\text{B}$	0.0	0.0	$3/2^-$	0.922	0.325		-0.155							
	2.33	2.68	$5/2^-$		0.941	-0.259	0.105							
${}^{12}\text{C}$	0.0	0.0	0^+	0.890		0.402						0.158	-0.125	
	4.44	4.64	2^+		0.937	-0.211	-0.212	0.142						

Terms are in LS coupling notation (e.g. [1p symmetry] ${}^{2T+1, 2S+1}L$).
 Terms with |amplitude| less than 0.1 have been omitted.

A further problem which applies to all three of the resonances, is the appearance of each resonance in only one of the (${}^3\text{He}, \alpha_0$) or (${}^3\text{He}, \alpha_1$) channels. As can be seen from table 4.3, the ground and first excited states of ${}^9\text{B}$ have similar configurations, with an extra unit of angular momentum added to the latter. Also, in a strong coupling rotational model approach [El 66], the 2.33 MeV state can be described as the first level in a rotational band based on the ground state in a $1^4 3^4 2^1$ Nilsson configuration. If the 26 MeV state has a spin of $7/2^-$, as suggested by Girod *et al.* [Gi 70], then there is no apparent reason why it should not decay to the $5/2^-$ first excited state of ${}^9\text{B}$ as well as to the $3/2^-$ ground state. Similar inconsistencies occur in the decay of the 26 MeV state to the ground state of ${}^{12}\text{C}$ and not to the first excited state, and in the α -decay of the 32 MeV state. It is apparent therefore, that the resonances cannot be described simply as configurations of the outgoing particles and the state of the final nucleus.

In their analysis of the 20.9, 22.5 and 25.5 MeV resonances that appear in the ${}^{12}\text{C}(p, p'){}^{12}\text{C}^*$ (15.11 MeV) reaction, Scott *et al.* [Sc 67] successfully explained the behaviour of the cross sections using DWBA theory and a three-quasi-particle model for the intermediate levels in ${}^{13}\text{N}$. In this interpretation, the temporary capture of an outgoing nucleon, subsequent to the initial direct reaction, creates a long-lived configuration of three-quasi-particles. These levels are more complex excitations than the giant dipole states, which are essentially one-quasi-particle states, and may be identified as "doorway states" that can propagate into increasingly complex excitations which constitute a true compound nucleus. Since the 32 MeV level cannot be described by any simple

excitation, it could well be another example of such a doorway state.

The $^{10}\text{B} + ^3\text{He}$ studies presented in this thesis have confirmed the existence of a state in ^{13}N at 32 MeV excitation. Three states in ^{13}N above 25 MeV excitation have now been observed as resonances in excitation functions of the $^{10}\text{B} + ^3\text{He}$ reactions measured in this and previous work [Po 67]. It has been shown that none of the three states at 26, 28 and 32 MeV excitation can be identified with E1 giant resonance states in ^{13}N . The nature of these states is not clear, and more work, both experimental and theoretical, is required to elucidate their character. In particular, the spin and parity of the 32 MeV state is unknown, and needs to be determined before further conclusions can be drawn.

PART II

THE ENERGY LEVEL STRUCTURE OF ^{57}Co , ^{59}Co AND ^{61}Co

CHAPTER 5

INTRODUCTION

In nuclear spectroscopy, systematic changes in nuclear parameters and level structure with changing nucleon numbers are of interest to both theoretical and experimental investigators. An obvious example of this is the striking systematic variation in the energies of the first excited states of even-even nuclei which provided early evidence for shell structure of nuclei. On a smaller scale, the degree of similarity in the level structures of a sequence of nuclei can suggest an appropriate nuclear model to describe these and neighbouring nuclei. Such systematics can also be used to infer the existence or the properties of corresponding levels in nuclei of the series. While information derived in this way is not conclusive, it can provide a valuable guide to the direction of further research.

A number of interesting similarities between the positions and properties of levels in the odd mass cobalt nuclei (^{57}Co , ^{59}Co , ^{61}Co , and ^{63}Co) were noted by Blair and Armstrong [Bl 66] in their (t, α) studies. They observed that many of the features of the α -particle spectra were common to all four Co nuclides. Grench *et al.* [Gr 67], in their β decay studies, also commented on the similarity of the levels of ^{59}Co and ^{61}Co populated in β decay, and arrived at a ratio of 1.07 linking the excitation energies of corresponding states in the two nuclei. In each of the above studies, the number of states observed was restricted by the reaction mechanism involved and the experimental resolution. The experiments reported here were undertaken to supply more comprehensive informa-

tion on the positions, properties and systematics of the energy levels in the three neighbouring odd mass cobalt nuclei, ^{57}Co , ^{59}Co and ^{61}Co .

Since the appropriate nickel and iron isotopes are stable and enriched targets could be made, it was possible to study states in ^{57}Co , ^{59}Co and ^{61}Co using the $\text{Ni}(p,\alpha)$ and $\text{Fe}(\alpha,p\gamma)$ reactions. Both these reactions were expected to be primarily compound nuclear reactions, so that a large variety of final states would be populated. It would also have been possible to investigate ^{55}Co using the $^{58}\text{Ni}(p,\alpha)$ reaction; however, this nucleus has a closed neutron shell ($N = 28$) and the energy level spectrum was already known to be quite dissimilar to that of the higher mass cobalt nuclei. ^{63}Co could not be investigated through these reactions since the appropriate target nuclei are not stable.

The positions of the low lying levels of $^{57,59,61}\text{Co}$ were initially determined using the $^{60,62,64}\text{Ni}(p,\alpha)$ reactions. A broad range magnetic spectrograph was used to identify the α -particle groups and to provide adequate resolution. The experiment is described in chapter 6.

Subsequently, the decay schemes and J^π values of levels in ^{59}Co and ^{61}Co were measured using the $^{56,58}\text{Fe}(\alpha,p\gamma)$ and $^{64}\text{Ni}(p,\alpha\gamma)$ reactions. Particle- γ -ray coincidence measurements were performed using the geometry of Litherland and Ferguson Method II [Li 61]. The outgoing particles were detected at 0° by a double focusing magnetic spectrometer and a position sensitive detector, or near to 180° by an annular solid state detector. Coincident γ -rays were detected using NaI(Tl) crystals and a Ge(Li) detector. The angular correlation theory of Rose and Brink [Ro 67a] used to analyze the

$^{56}\text{Fe}(\alpha, p\gamma)$ data is discussed briefly in the Appendix, along with several related experimental features. The experiments and results are reported in chapter 7.

Decay schemes and angular correlations in the $^{54}\text{Fe}(\alpha, p\gamma)^{57}\text{Co}$ reaction have been measured by Coop *et al.* [Co 70] at this laboratory. That experiment is not reported here, but the results are discussed in relation to the level schemes of ^{59}Co and ^{61}Co in chapter 8. The observed similarities in the level properties of the three nuclei are examined, and compared with the available theoretical predictions.

CHAPTER 6
ENERGY LEVELS IN $^{57,59,61}\text{Co}$ FROM THE
 $^{60,62,64}\text{Ni}(p,\alpha)$ REACTIONS

6.1 INTRODUCTION

When these reaction studies were made, little information on the spins and parities of the energy levels of the three odd-mass isotopes, $^{57,59,61}\text{Co}$, was available. The low lying levels of ^{57}Co had been investigated by a number of experimentalists, but disagreements as to the existence of some levels, and the J^π of others, appeared in their results. These disagreements have been summarized by Bouchard and Cujec [Bo 68], and will be discussed in the light of subsequent data (section 6.3.1). ^{59}Co is the only stable cobalt isotope, and the positions of the levels up to a few MeV excitation have been determined by (p,p') studies, as well as through various other reactions summarized conveniently in the Nuclear Data Sheets [N.D.S.]. Published information on the energy levels of ^{61}Co was less plentiful, and comes entirely from (t, α), (t,p) and β decay studies [Hu 71 and N.D.S.]. Again there were discrepancies in the β decay results and these will be discussed later in the context of the present results (section 6.3.3).

The purpose of the present experiment was to resolve these earlier disagreements and to provide accurate level schemes for the $^{57,59,61}\text{Co}$ nuclei. The availability of highly enriched nickel isotopes of mass 60, 62 and 64 made the (p, α) reaction a convenient method for populating states in the cobalt isotopes of interest. This was especially so, since the (^3He ,d) and (t, α) reactions, and the β decay studies used previously, tended to selectively populate

states in the final nuclei, while the (p, α) reaction was expected to be primarily compound nuclear in nature, and therefore populate a large variety of final states. Relevant target enrichments and reaction Q values are shown in tables 6.1 and 6.2 respectively.

Table 6.1
Isotopic abundances of enriched
iron and nickel target materials

Enriched isotope	Isotopic abundance (%)				
	^{58}Ni	^{60}Ni	^{61}Ni	^{62}Ni	^{64}Ni
^{60}Ni	0.21	99.79	< 0.05	< 0.05	< 0.05
^{62}Ni	0.38	0.51	0.09	99.02	< 0.05
^{64}Ni	0.61	0.43	0.14	0.26	98.56
	^{54}Fe	^{56}Fe	^{57}Fe	^{58}Fe	
^{56}Fe	0.03	99.93	0.03	< 0.02	
^{58}Fe	0.45	15.83	1.6	82.12	

The target material and analyses were obtained from Oak Ridge National Laboratories. Other elements present have individual abundances of 0.1% or less.

Preliminary experiments performed in this laboratory with solid state counters [Co 69] showed that, between 9 and 11 MeV bombarding energy, the $^{62,64}\text{Ni}(p,\alpha)$ differential cross sections fluctuated rapidly with energy. Also, only the ground state groups showed the marked forward peaking in the angular distributions which is characteristic of direct reaction mechanisms. Kumabe *et al.* [Ku 63], who observed similar characteristics in the $^{58,60}\text{Ni}(p,\alpha)$

Table 6.2
 Ground state Q values (MeV)
 for (p, α) and (α ,p) reactions of interest

Target nucleus	(p, α) Q value	(α ,p) Q value
^{58}Ni	-1.35	
^{60}Ni	-0.27	
^{61}Ni	0.48	
^{62}Ni	0.35	
^{64}Ni	0.69	
^{54}Fe		-1.77
^{56}Fe		-3.24
^{57}Fe		-3.39
^{58}Fe		-4.09
^{12}C	-7.55	-4.96
^{13}C	-4.06	-7.43
^{16}O	-5.22	-8.11

reactions in the same range of bombarding energies, explained the fluctuations in cross section on the basis of Ericson's theory of statistical compound nucleus decay [Er 60]. For the corresponding excitation energies in the compound system (≈ 15 MeV), states would be expected to be closely spaced and overlapping. Thus many different J^π states would be populated in the final nucleus, while angular distribution effects, due to single compound nuclear states, would be smeared out.

The yield for states above a few MeV excitation rapidly decreased due to the Coulomb barrier (≈ 10 MeV for α -particles in Fe). However, typical differential cross sections for the low lying states were of the order of 20 $\mu\text{b}/\text{sr}$ which made experiments with a

magnetic spectrograph feasible. Because of the independent fluctuations of the reaction cross sections to different states, measurements were made at several different incident energies in order to detect as many final states as possible.

6.2 EXPERIMENTAL DETAILS

The A.N.U. broad range magnetic spectrograph is a uniform field spectrograph similar to that described by Browne and Buechner [Br 56]. It has a pole radius of 65 cm and a useful focal plane length of 107 cm. The particles are deflected through approximately 90° and may be detected in the focal plane with either photographic plates or position-sensitive solid state detectors. The maximum solid angle subtended, decreases from 0.6 msr at the low energy end of the focal plane to 0.35 msr at the other end. The magnetic field is measured and stabilized using a proton nuclear magnetic resonance system. In principle, a resolution of $E/\Delta E > 1000$ can be obtained, but in practice, this figure is not achieved because of effects due to finite target thickness, beam spot size, kinematic shifts, aberrations, etc. The associated target chamber has a sliding band seal to the entrance of the spectrograph, allowing the detection angle of the magnet, with respect to the beam direction, to be varied from 0° to 153° . Further details of the magnet and associated equipment have been given by Scarr [Sc 66].

Proton beams of approximately $0.2 \mu\text{A}$ intensity from the A.N.U. tandem Van de Graaff accelerator were used to bombard the various Ni targets (each being $\sim 30 \mu\text{gm}/\text{cm}^2$ of enriched isotope on $\sim 20 \mu\text{gm}/\text{cm}^2$ carbon foil). From 10,000 to 25,000 μC of beam were

collected for each plate exposure, and, as far as was possible, the parameters of the steering elements of the accelerator, (the electrostatic steerers and magnetic quadrupoles on the high energy side of the accelerator), were not changed during each run to minimize movement of the beam spot and to prevent variations in the beam energy. The outgoing α -particles were detected with 25 μm Ilford K minus-1 photographic emulsions located in the focal plane of the spectrograph.

Successful exposures were made at the energy-angle combinations shown in table 6.3. In addition a ^{58}Ni target was bombarded at several different energy-angle combinations but the low yields precluded study of the energy levels of ^{55}Co , which is therefore not discussed further. The overall energy resolution achieved was generally 20 - 30 keV. Groups due to contaminants were identified through their kinematic shifts with changing angle and bombarding energy.

Table 6.3

Bombarding energies and detection angles for the successful exposures in the (p, α) experiments

Target	Detection angle		
	9.50 MeV	10.0 MeV	10.5 MeV
^{60}Ni		140°	30°
^{62}Ni		40°, 140°	
^{64}Ni	30°	30°, 40°, 140°	

After the Ni(p, α) exposures, the spectrograph was recalibrated with a thin ThB(ThC + ThC') α source. Forty calibration points were obtained from the 8.78 and 6.05 MeV α groups at 29 different frequency settings. The calculated radii of the α -particle trajectories were then fitted to the positions of the groups on the plates using a quadratic polynomial. This was necessary since some level energies (known accurately from β decay studies with Ge(Li) γ -ray spectrometers), disagreed with the previous ThB and $^{12}\text{C}(p,p')$ calibrations of the magnetic spectrograph. This disagreement was probably due to a slight shift of the plate holder alignment with respect to the focal plane, and insufficient recycling of the magnet between field changes at the time of the experiment. The latter would have resulted in an inhomogeneous field due to differential hysteresis; although before delivery, Spectromagnetic Industries measured most of the effective field to be uniform to 1 part in 2000.

The energy levels determined with the new calibration fitted better with the published β decay results (typically less than 5 keV difference), lending support to the hypothesis that the alignment had changed. However, the results still differed amongst themselves (10 keV at worst) at the low energy end of the α -particle spectra. The number of accurately known levels was not sufficient to calibrate each exposure internally, so that the dominant source of error in the energy measurements is due to the uncertainty in the magnet calibration. Estimates of these errors were made by comparing the results obtained at different energy-angle combinations, and by comparisons with those level energies already accurately established by other experimentalists.

Peak centres for both the (p, α) and calibration data were

determined by a least squares fit of a Gaussian curve to the peak. Doublets and triplets were fitted by combining two or three Gaussian distributions of fixed width but with individually variable heights and positions. To correct for α -particle energy losses in the target, small corrections (< 2 keV), derived from the range-energy tables of Williamson and Boujot [Wi 62], were made to the (p, α) level energies.

Q values for the (p, α) reactions calculated from the results were typically within 10 keV of the published values listed in table 6.2. However, because of uncertainties in bombarding energy and target thicknesses, more accurate Q values could not be obtained. The energy calibration of each α -particle spectrum was normalized to zero ground state energy to obtain the level excitations.

6.3 RESULTS OF THE (p, α) EXPERIMENTS

Representative spectra of α -particle groups populating states in the three cobalt isotopes are shown in figs. 6.1, 2 and 3. Above about 3 MeV excitation, both the level spacing and the particle yields decreased, so that individual levels could not in general be resolved. For these spectra, a field of 10 mm height and 0.4 mm width was scanned at 0.5 mm intervals along the plate. Selected additional spectra for some closely spaced levels in the three isotopes were scanned at 0.4 mm intervals, and these are shown in fig. 6.4.

The energy levels deduced from the experiments are listed in table 6.4 and are shown in fig. 6.5. The estimated standard

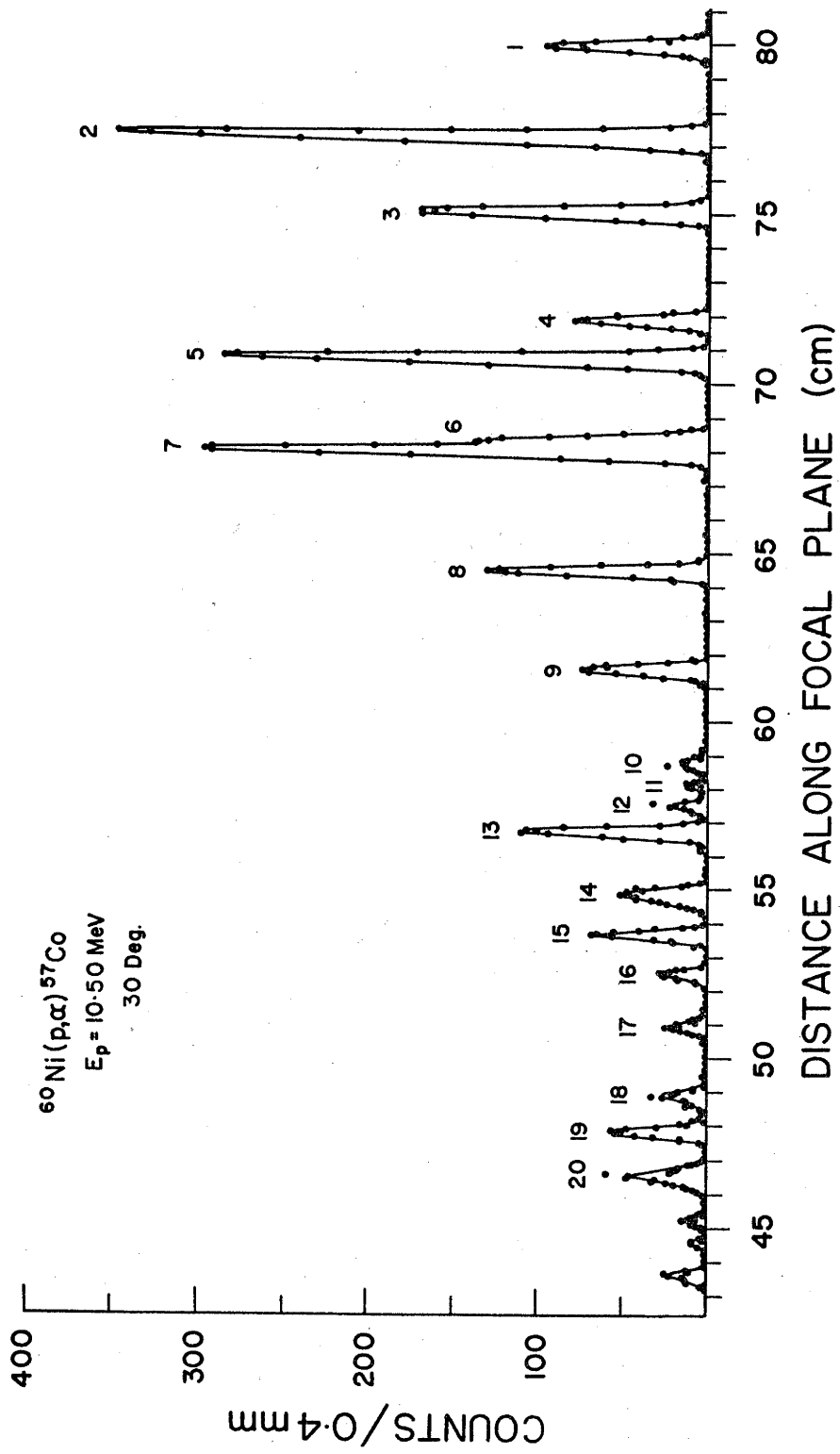


Figure 6.1: $^{60}\text{Ni}(p,\alpha)^{57}\text{Co}$ spectrum from the first excited state of ^{57}Co to 3.5 MeV excitation. The numbered α -particle groups correspond to excited states in ^{57}Co whose energies are listed in table 6.3.

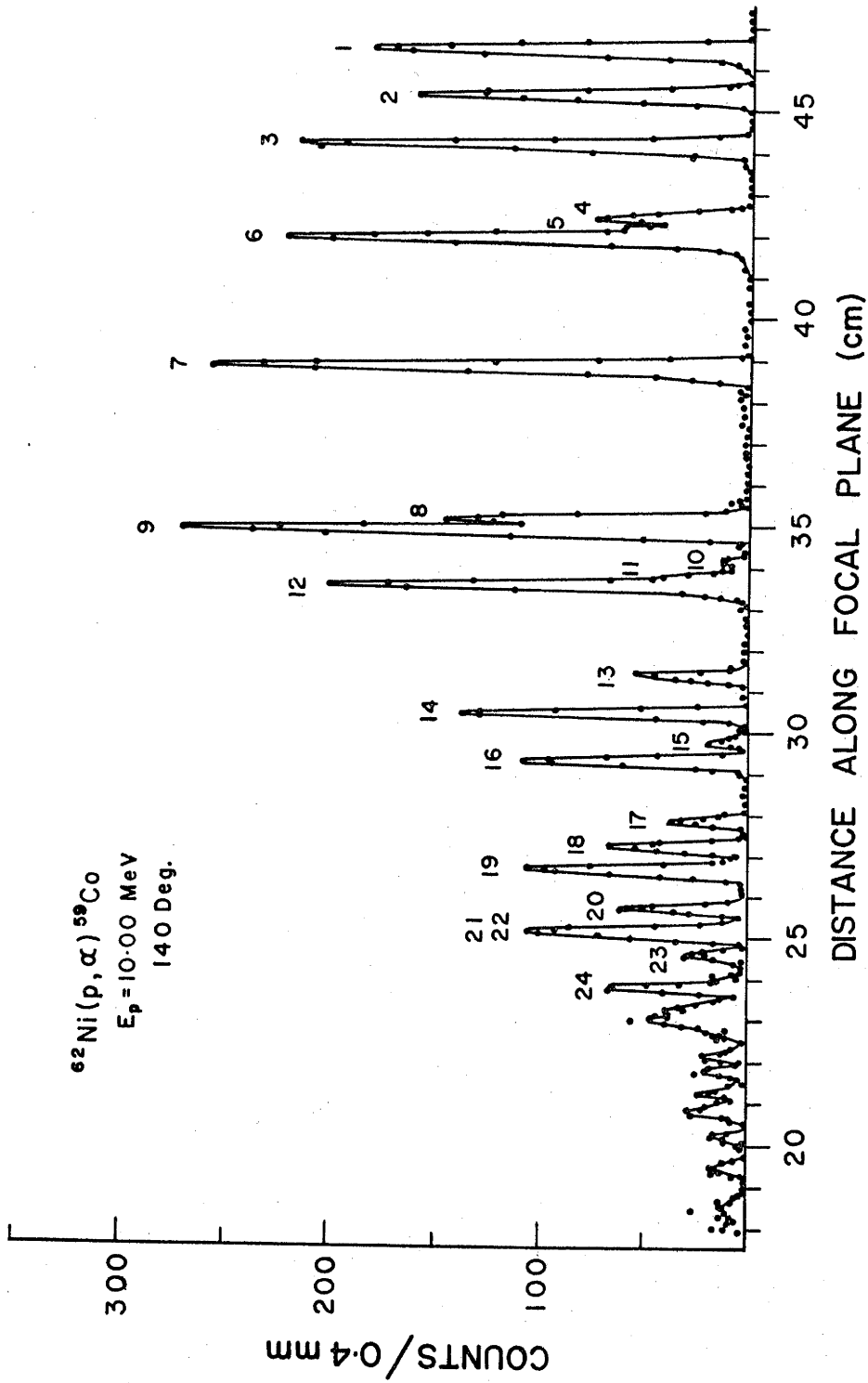


Figure 6.2: $^{62}\text{Ni}(p, \alpha)^{59}\text{Co}$ spectrum from the first excited state of ^{59}Co to 3.5 MeV excitation. The numbered α -particle groups correspond to excited states in ^{59}Co whose energies are listed in table 6.3.

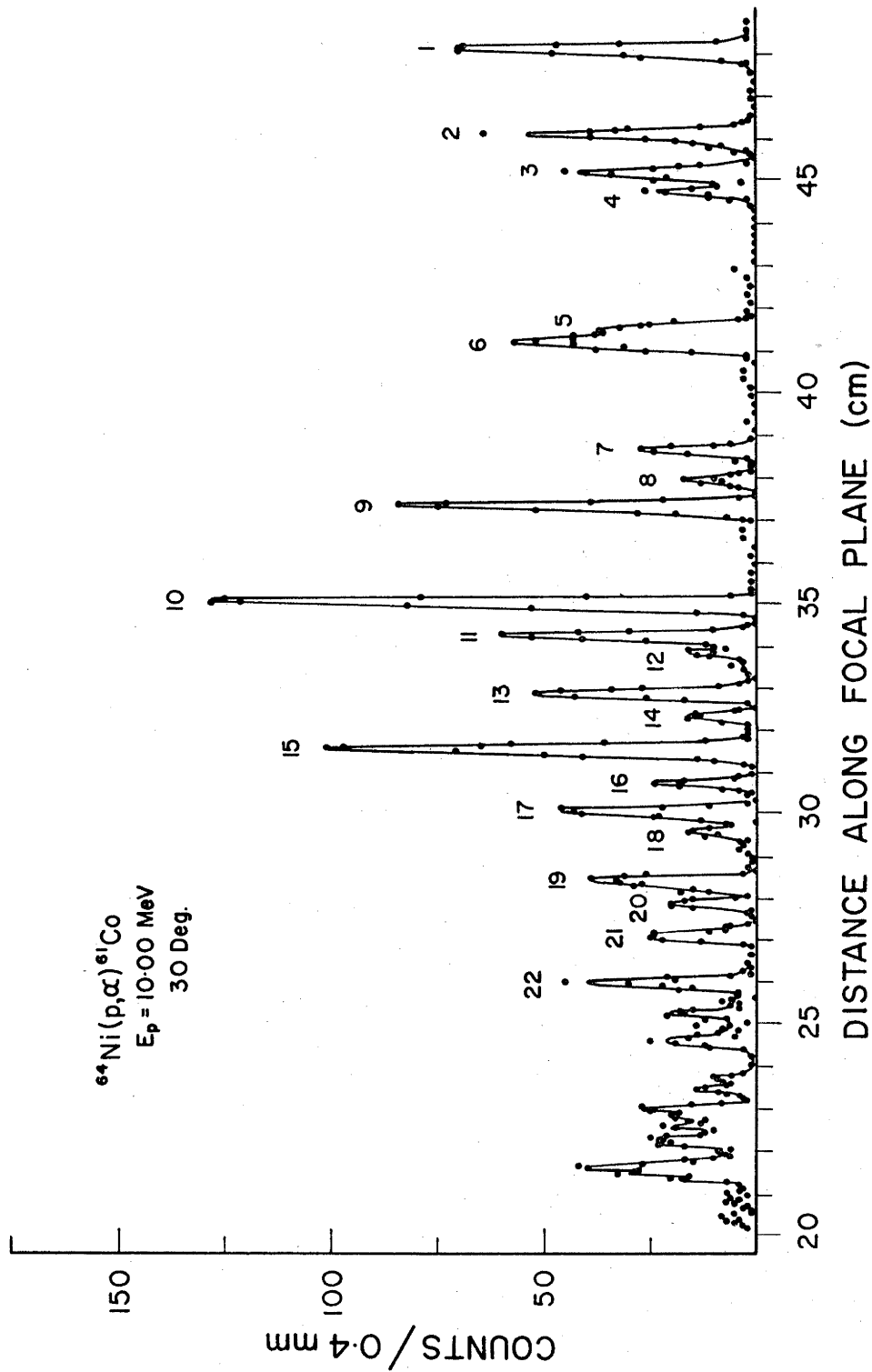


Figure 6.3: $^{64}\text{Ni}(p,\alpha)^{61}\text{Co}$ spectrum from the first excited state of ^{61}Co to 3.6 MeV excitation. The numbered α -particle groups correspond to excited states in ^{61}Co whose energies are listed in table 6.3.

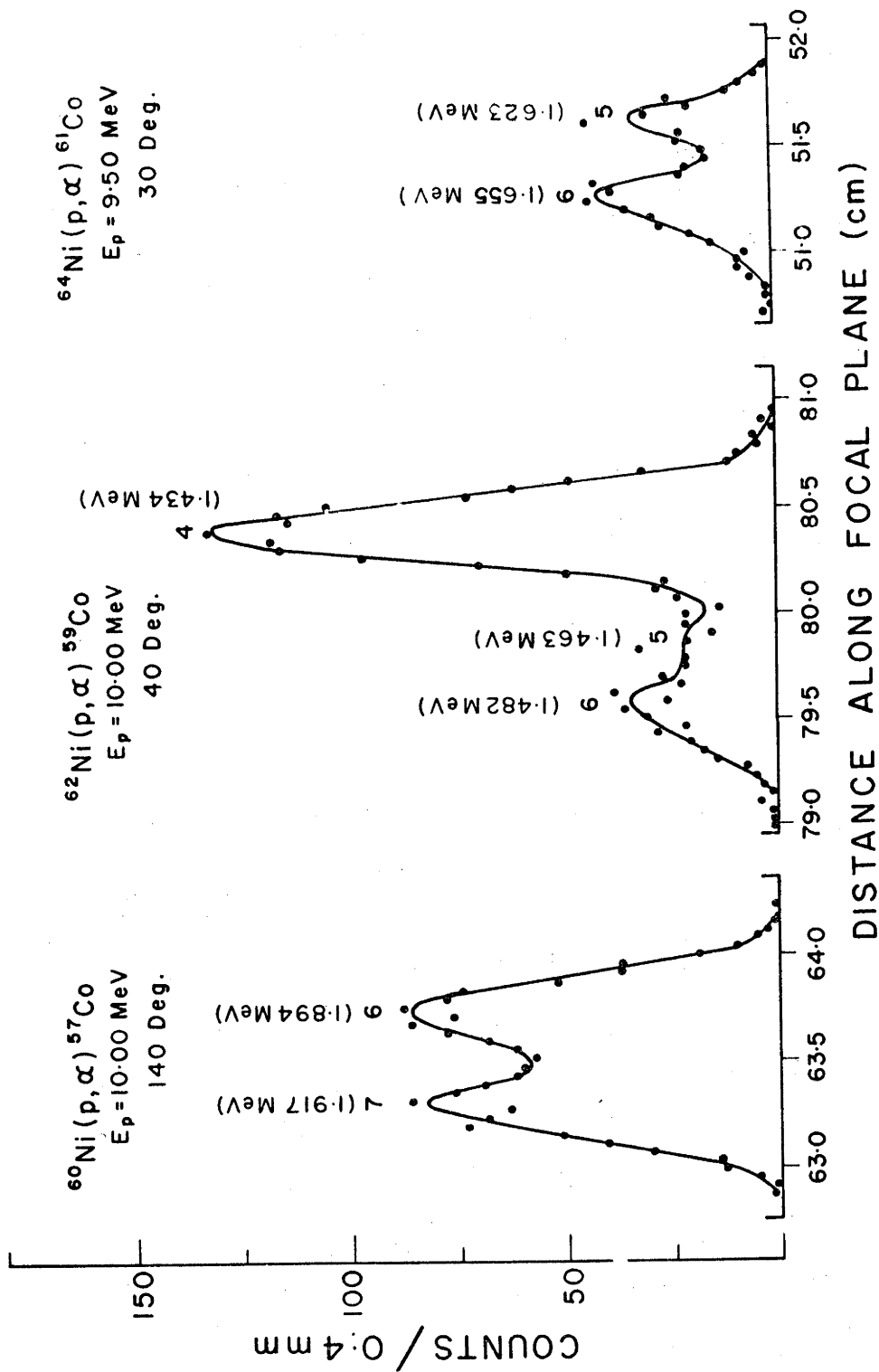


Figure 6.4: Spectra for some closely spaced groups from the (p,α) reactions. The numbers and energies near the groups correspond to the excited states in the appropriate cobalt isotope.

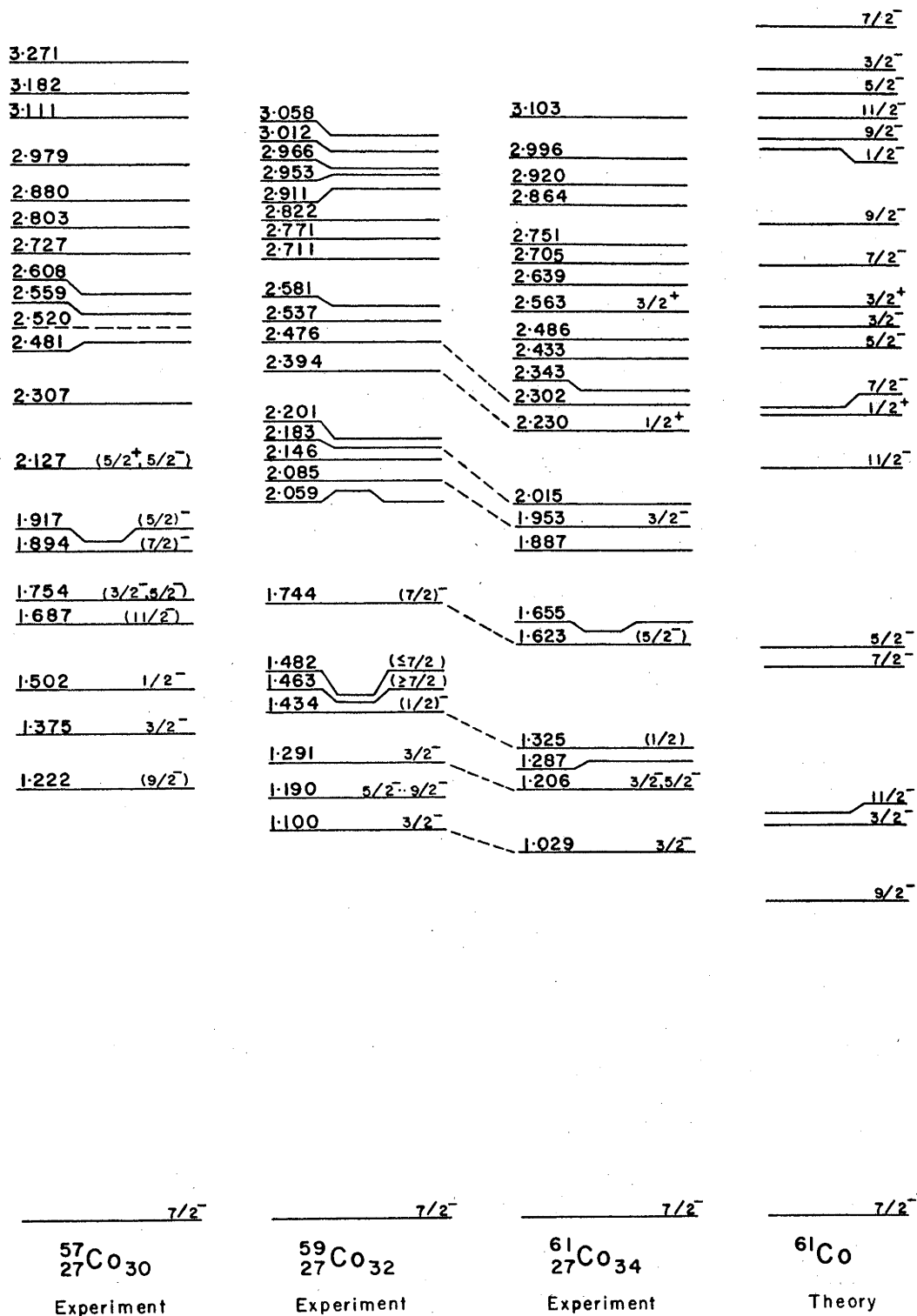


Figure 6.5: Energy levels of ^{57}Co , ^{59}Co , ^{61}Co deduced in the present experiments. Spins and parities are taken from ref. [Bo 68 and N.D.S.]. The theoretical level scheme for ^{61}Co is that calculated by Satpathy and Gujrathi [Sa 68].

Table 6.4
Energy levels (in MeV) of ^{57}Co , ^{59}Co , ^{61}Co

Group	^{57}Co a)	^{59}Co b)	^{61}Co c)
1	1.222	1.100	1.029
2	1.375	1.190	1.206
3	1.502	1.291	1.287
4	1.687	1.434	1.325
5	1.754	1.463	1.623
6	1.894	1.482	1.655
7	1.917	1.744	1.887
8	2.127	2.059	1.953
9	2.307	2.085	2.015
10	2.481	2.146	2.230
11	2.520 d)	2.183	2.302
12	2.559	2.201	2.343
13	2.608	2.394	2.433
14	2.727 e)	2.476	2.486
15	2.803	2.537	2.563
16	2.880	2.581	2.639
17	2.979	2.711 e)	2.705
18	3.111	2.771 e)	2.751
19	3.182	2.822 e)	2.864
20	3.271 e)	2.911	2.920
21		2.953	2.996
22		2.996	3.103
23		3.012	
24		3.058	

- a) Estimated standard errors are ± 4 keV for groups 1 - 5, ± 7 keV for groups 6 - 19 and ± 10 keV for group 20.
- b) Estimated standard errors are ± 4 keV for groups 1 - 7, ± 7 keV for groups 8 - 16 and ± 10 keV for groups 17 - 24.
- c) Estimated standard errors are ± 4 keV for groups 1 - 4, ± 7 keV for groups 5 - 14 and ± 10 keV for groups 15 - 22.
- d) Clearly seen at only one angle.
- e) Possible doublets.

errors for the energies of the excited states are indicated in the footnotes to the table. The spins and parities shown in fig. 6.5 are taken from work published previously [N.D.S. and Bo 68]. The theoretical predictions of Satpathy and Gujrathi [Sa 68] for levels in ^{61}Co are also shown for later comparison with the experimental results (section 6.4).

6.3.1 ^{57}Co Results

The (p, α) results for the ^{57}Co energy levels were in good agreement with values published previously. Exceptions to this were the two levels at 1.59 MeV and 1.46 MeV reported by Bakhru and Preiss [Ba 67] in β decay studies. These levels were not seen in other β decay investigations [Pi 66, Li 67 and Ga 69], nor were they seen by Bouchard and Cujec in their $^{54}\text{Fe}(\alpha, p)$ studies [Bo 68], so that their existence is doubtful.

The latter (α, p) studies indicated probable doublets at 1.75, 1.90 and 2.30 MeV with about 20 keV separation. The present work resolved clearly the doublet at 1.90 MeV (fig. 6.4), but there was no evidence for doublets at the other energies. At no energy-angle combination was there a significant increase in the widths of the groups from these states, so that if either is a doublet, the separation is probably < 5 keV. Also the $^{54}\text{Fe}(\alpha, p\gamma)$ correlation studies of Coop *et al.* [Co 70] involving these levels, indicated that only single levels were present.

6.3.2 ^{59}Co Results

The level energies in ^{59}Co obtained from the present experiment agreed well with those reported previously [N.D.S.]. All

levels below 3 MeV seen in other reactions appeared in the (p, α) spectra; no new levels were observed. This indicated that the (p, α) reaction, at the energies used, should also have populated all levels below a few MeV in the adjacent odd mass nuclei. High spin states, which require a large angular momentum transfer, would have been inhibited by penetrability factors. Of course, such spin states were also unlikely to appear in the other experiments reported.

6.3.3 ^{61}Co Results

Several previously unreported levels were observed in the $^{64}\text{Ni}(p,\alpha)^{61}\text{Co}$ reaction. The third excited state at 1.287 MeV had not been reported before, although the (t, α) data of Blair and Armstrong [Bl 66] suggested a number of weakly populated states near 1.3 MeV. Subsequently, Hudson and Glover [Hu 71] observed the state at 1.286 MeV in the (t,p) reaction, and also saw it weakly in their (t, α) spectra as a 15 keV doublet (1.272 and 1.287 MeV). There was no evidence in the present experiment for a level at 1.272 MeV. Levels at 1.4 and 1.8 MeV reported in only some of the various β decay studies [N.D.S.], were not observed in the present experiment and their existence must be regarded as doubtful.

The 1.65 MeV doublet has been seen in all the reaction studies, but which state is populated in β decay, or whether both are populated, is unclear. The energy of the level populated in β decay has been variously reported as 1.650 ± 0.015 MeV [Gr 67], 1.65 MeV [St 66], and 1.610 ± 0.020 MeV [Cr 64]. The compilers of Nuclear Data Sheets [N.D.S.] have assumed that the lower level of the doublet is the one populated, and have therefore tentatively

assigned a spin of $(5/2^-)$. However, both the (t,p) and (t, α) investigations indicated an $\ell = 3$ transition to the upper level, and the (t,p) work showed an $\ell = 0$ transition to the lower level. On the basis of this, Hudson and Glover [Hu 71] assigned a J^π of $7/2^-$ to the 1.623 MeV level, and a tentative $(5/2^-)$ to the 1.655 MeV level. Thus the excitation of the 1.655 MeV state in β decay would be more likely. Further evidence to support this assignment will be presented below (section 7.5).

The 2.015 MeV level was not seen in either the (t, α) or (t,p) studies, but again it is uncertain whether this or the 1.953 MeV level is excited in β decay. An unweighted average of the β decay results (1.950 ± 0.020 MeV [Cr 64], 1.98 MeV [St 66], and 1.995 ± 0.020 MeV [Gr 67]) favours the 1.953 MeV level. Blair and Armstrong, in their (t, α) studies [Bl 66], assigned a spin of $3/2^-$ to the 1.953 MeV level. Thus it could be populated by an allowed β decay; while the 2.015 MeV level, which might be suspected to have high spin (since it was not seen in either the (t,p) or (t, α) reactions), would not be favoured. Evidence in contradiction of the above considerations will be presented below (section 7.5).

The rest of the observed levels were in agreement with the other reaction results. Hudson and Glover [Hu 71] have noted a tendency for the level energies above 2.5 MeV excitation obtained in the present experiment, to be lower than those from the other experiments (up to 20 keV lower for the 2.996 MeV state). This trend was not evident in the ^{57}Co and ^{59}Co results, and since the exposures for all three isotopes were made under the same conditions, the initial spectrograph calibration was retained.

6.4 DISCUSSION

The calculations of Satpathy and Gujrathi [Sa 68] using an intermediate coupling approach to the unified model, are the only calculations available that attempt to describe the odd-mass cobalt nuclei ($^{57,59,61,63}\text{Co}$). One-, two- and three-phonon states of the adjacent even-mass nickel cores were coupled to proton holes in the $1f_{7/2}$, $1d_{3/2}$ and $2s_{1/2}$ orbits. The phonon energy was taken as the energy of the first excited 2^+ state of the corresponding nickel isotope, while the coupling strength and the single hole excitation energies of the $1d_{3/2}$ and $2s_{1/2}$ states with respect to the $(1f_{7/2})_p^{-1}$ state were treated as variable parameters. The spectra obtained for the three isotopes $^{57,59,61}\text{Co}$ were similar below 3 MeV. In particular, the negative parity states remained in the same order, and maintained proportional spacing, since the only variable parameter was the coupling strength. Thus, only the predicted energy levels of ^{61}Co are shown in fig. 6.5. There was a general similarity between the experimental and theoretical level schemes, but below 2 MeV many observed levels were not predicted theoretically. Some of these would probably appear if higher proton orbits were included in the calculations. Satpathy and Gujrathi also obtained a reasonable agreement with the relative spectroscopic factors for the $7/2^-$, $1/2^+$ and $3/2^+$ states measured in the (t,α) experiments of Blair and Armstrong [Bl 66].

Corello and Manfredi [Co 71] extended the above studies in their investigation of the lowest five collective states of ^{57}Co , by including an octupole phonon excitation of the ^{58}Ni core. The single-hole energies and the deformation parameters were taken from experimental data, leaving no adjustable parameters. They found

that the octupole contribution was very small, and their level scheme was very similar to that obtained by Satpathy and Gujrathi [Sa 68]. The calculated E2/M1 mixing ratios agreed well with the experimental results of Coop *et al.* [Co 70].

Gatrousis *et al.* [Ga 69] have also performed some calculations on the ^{57}Co level scheme using an inert ^{40}Ca core and distributing the remaining nucleons in the $1f_{7/2}$, $2p_{3/2}$, $2p_{1/2}$, and $1f_{5/2}$ orbits. Figure 6.6 compares the calculations of Satpathy and Gujrathi and of Gatrousis *et al.* with the experimental level scheme of this work. The J^π values are those derived by Coop *et al.* [Co 70] from the $^{54}\text{Fe}(\alpha, p\gamma)$ reaction and from previous reaction data [Bo 68 and Ga 69]. It is clear that the calculations of Gatrousis *et al.* provide the better agreement with the level energies and J^π values. However, their model produced wave functions containing many admixed configurations. In no case was there any one shell model component that constituted as much as 50% of the wave function. This contrasted with the $(^3\text{He}, d)$ reaction data of Rosner and Holbrow [Ro 67]. The $(^3\text{He}, d)$ reaction is expected to proceed largely via a simple stripping mechanism, so that the reaction would tend to preferentially populate those states with a strong single-particle character. Rosner and Holbrow found that the 1.375 ($3/2^-$), 1.502 ($1/2^-$), 2.127 ($5/2^-$) and 2.307 ($7/2^-$) MeV states were strongly populated in the $(^3\text{He}, d)$ reaction, while all the other states below 3 MeV excitation were either weakly populated or not seen at all. If one accepts the 1.754 MeV level as the low lying $3/2^-$ state, then the above four states are also missing from the predictions of Satpathy and Gujrathi [Sa 68], who have suggested that some of these states could be accounted for by including the $2p_{1/2}$, $2p_{3/2}$ and $1f_{5/2}$

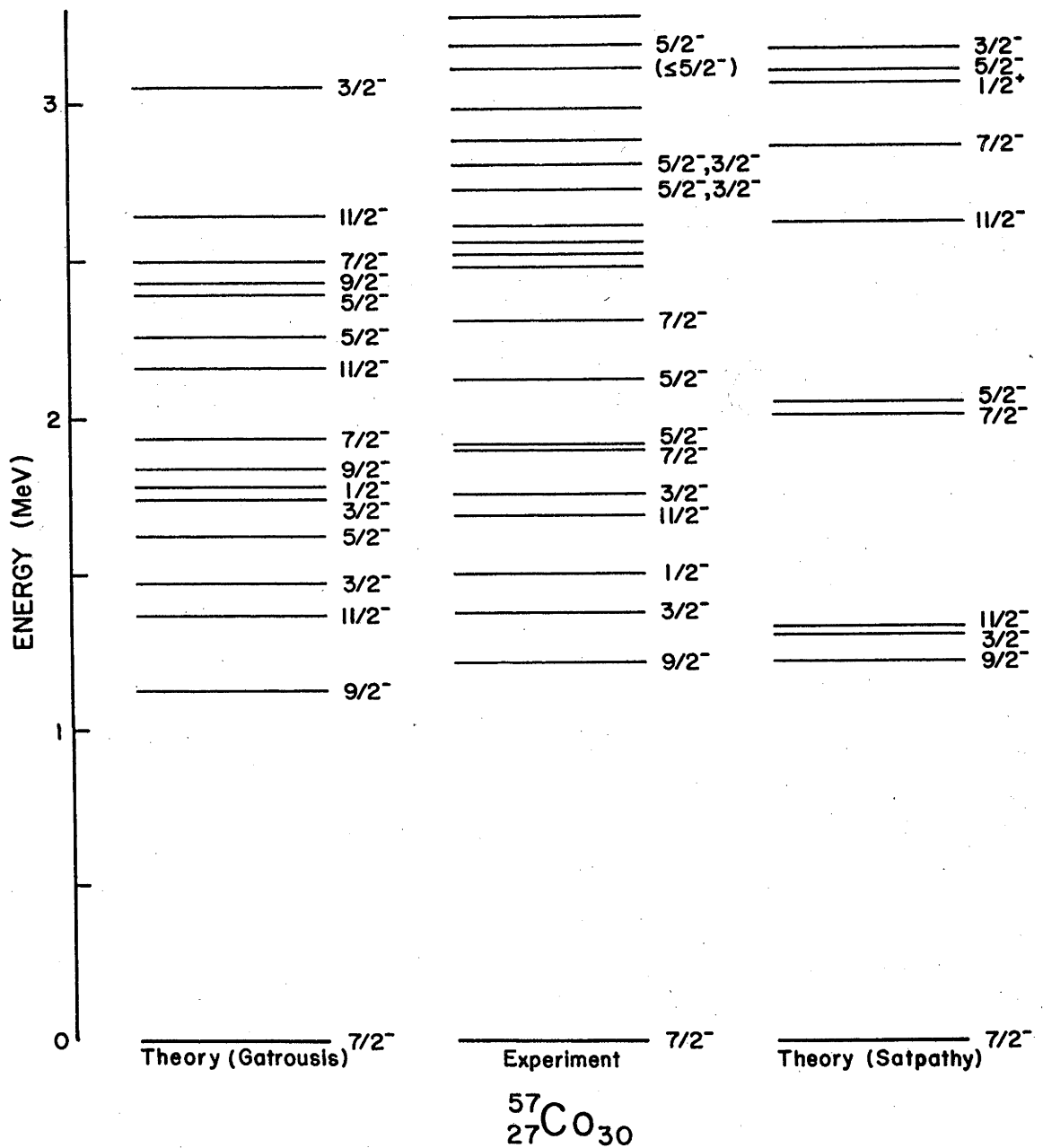


Figure 6.6: Experimental and calculated energy levels of ^{57}Co .

The experimental level energies are from the present experiment and the J^π values are those deduced by Coop *et al.* [Co 70].

The calculated energy level diagrams are from Gatrouris *et al.* [Ga 68] and Satpathy and Gujrathi [Sa 68].

orbits in their calculations. If successful, the same modification could also account for some of the discrepancies between theory and experiment in ^{59}Co and ^{61}Co .

Grench *et al.* [Gr 67] have pointed out an interesting similarity between the positions of some known states in ^{59}Co and the positions of states in ^{61}Co observed in their β decay studies. They noted that the lowest three states populated in β decay in both nuclei had similar properties, and that the ratios of the energies of the three corresponding excited states were approximately constant (1.07). Using the results of the present experiment, it was found that below 2.5 MeV excitation in the two nuclei, eight pairs of levels have energy ratios $E(^{59}\text{Co})/E(^{61}\text{Co}) = 1.076 \pm 0.007$. These levels have been connected by dashed lines in fig. 6.5. As far as is known, most of these pairs of levels have the same spins and parities and similar γ -ray decay schemes.

It was obvious that further information on the J^π values of states in both ^{59}Co and ^{61}Co was required before a detailed comparison with theory and any discussion of systematics could be made. The 1.190 MeV and 1.463 MeV states in ^{59}Co seemed likely candidates for the predicted $9/2^-$ and $11/2^-$ levels, but the $5/2^-$ member of the doublet, which appeared in both ^{57}Co and ^{61}Co at 1.9 and 1.6 MeV respectively, was not seen. In ^{61}Co the most serious discrepancy was the absence of any known high spin state at low excitation. The 1.287 MeV state is a possible candidate since it is not populated in β decay. However, if any of the other reported states were in fact a closely spaced doublet (≤ 5 keV), the members would not have been resolved in the (p, α), (t, α), or (t,p) experiments. The $^{56,58}\text{Fe}(\alpha, p\gamma)$ and $^{64}\text{Ni}(p, \alpha\gamma)$ experiments described in the next

chapter, were undertaken to try to further clarify the experimental level schemes of ^{59}Co and ^{61}Co .

CHAPTER 7

THE $^{56,58}\text{Fe}(\alpha, p\gamma)$ AND $^{64}\text{Ni}(p, \alpha\gamma)$ MEASUREMENTS

7.1 INTRODUCTION

The experiments described in this chapter were undertaken to resolve the discrepancies mentioned in the previous chapter, and to obtain further information regarding the J^π values and decay properties of levels in ^{59}Co and ^{61}Co . Previous information on the γ -ray decay of ^{59}Co had been reported in studies using the ($^{16}\text{O}, ^{16}\text{O}'\gamma$) and ($n, n'\gamma$) reactions [No 67 and Da 68], as well as from β decay studies [N.D.S.]. The decay modes of states in ^{61}Co had only been observed in β decay. These data, with subsequently published results, will be discussed with respect to the results from the present experiments in the relevant sections (^{59}Co - 7.4, ^{61}Co - 7.5).

Initially, it was hoped that angular correlation measurements could be made for states in both ^{59}Co and ^{61}Co . A combination of low yields from the $^{58}\text{Fe}(\alpha, p\gamma)$ reaction and interference from the $^{56}\text{Fe}(\alpha, p\gamma)$ reaction made measurements on ^{61}Co impracticable, although it was still possible to obtain γ -ray branching ratios from the (α, p) reaction as well as the $^{64}\text{Ni}(p, \alpha)$ reaction (section 7.5). E2/M1 mixing ratios for the γ -ray decay and J^π values for low lying states of ^{59}Co were obtained from angular correlation measurements involving the decay of the first three excited states and the 1.744 MeV state. Further information on these states, and some other states, was obtained from γ -ray branching measurements. These results are reported in section 7.4.

Preliminary measurements of the $^{56}\text{Fe}(\alpha, p)^{59}\text{Co}$ yield and

excitation functions were made to determine the feasibility of the proton- γ -ray coincidence measurements, and also to find suitable bombarding energies at which the yields of groups of interest were enhanced (section 7.2).

The particle- γ -ray coincidence measurements were made in the geometry of Method II of Litherland and Ferguson [Li 61]. The particles were detected either at 0° with a double focusing magnetic spectrometer, or near 180° with an annular surface barrier detector. 12.7 cm diam. \times 10.2 cm long NaI(Tl) crystals or a 40 cc Ge(Li) detector were used to detect the coincident γ -rays. The various configurations with the appropriate timing electronics are described in section 7.3.

7.2 $^{56}\text{Fe}(\alpha, p)^{59}\text{Co}$ EXCITATION FUNCTIONS

Preliminary measurements of the $^{56}\text{Fe}(\alpha, p)^{59}\text{Co}$ reaction yields were made to ensure that proton- γ -ray coincidence measurements were feasible with a reasonable investment of accelerator time. Rough excitation functions were taken between $E_\alpha = 10$ and 11 MeV to determine the energies at which the yields of the proton groups of interest were maximized. The bombarding energies are near the top of the Coulomb barrier (~ 10 MeV), so that at lower energies the proton yields would be expected to decrease. At higher energies, the value of increased proton yields would be offset by the increased neutron and γ -ray backgrounds from (α, n) reactions.

Self supporting ^{56}Fe targets were made from isotopically enriched material obtained from Oak Ridge National Laboratories; the relative isotopic abundances are listed in table 6.1. The

method used in making the self supporting iron targets has been described in some detail by Coop [Co 69]. Basically, the enriched iron oxide was reduced under a hydrogen atmosphere and then evaporated onto copper foil which had been preheated to reduce stress in the iron coating on cooling. The copper was etched away using an ammonia-trichloroacetic acid mixture. Targets of thickness of $\sim 200 \mu\text{g}/\text{cm}^2$ were used in the present experiment.

The measurements were made in the 50 cm diameter scattering chamber described earlier (section 2.1.1). Surface barrier detectors, 1000 μ thick, were located at 12° , 20° , 32° and 52° to the incident beam direction. Aluminium foils (~ 0.01 cm thick) were placed in front of the detectors to stop the elastically scattered α -particles. Vacuum tube preamplifiers and amplifiers (Ortec models 103 and 203) were used to amplify the energy pulses, which were analyzed and stored in two R.I.D.L. and two R.C.L. analyzers.

A typical spectrum obtained at 32° is shown in fig. 7.1. The large knock-on proton peak was thought to be due to protons present in the target as absorbed oil and water. Only a small amount of hydrogen in the target would account for the observed peak intensity, since the $p(\alpha,p)\alpha$ reaction has a large cross section (≈ 0.1 b/sr). The excitation functions obtained at 12° for the ground state and 1.74 MeV state proton groups are shown in fig. 7.1; the average cross section for the 1.74 MeV group is of the order of 0.1 mb/sr. The proton groups were not well resolved (the measured resolution was ≈ 100 keV F.W.H.M.) because of the foils placed in front of the detectors. However, from a close examination of the spectra, it was possible to determine where each of the states had a maximum yield.

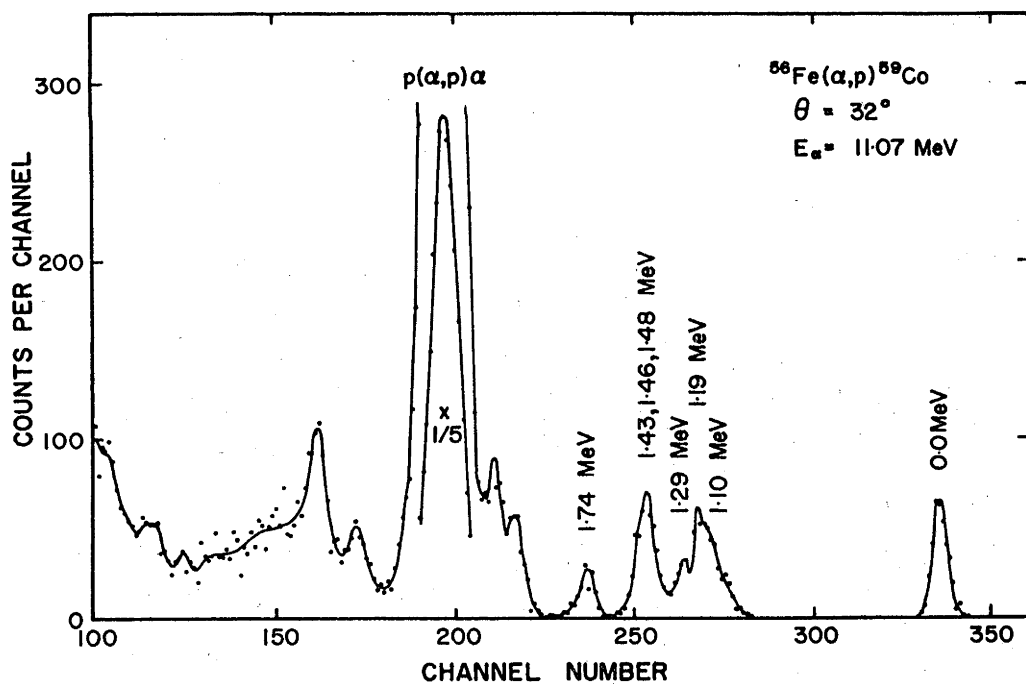
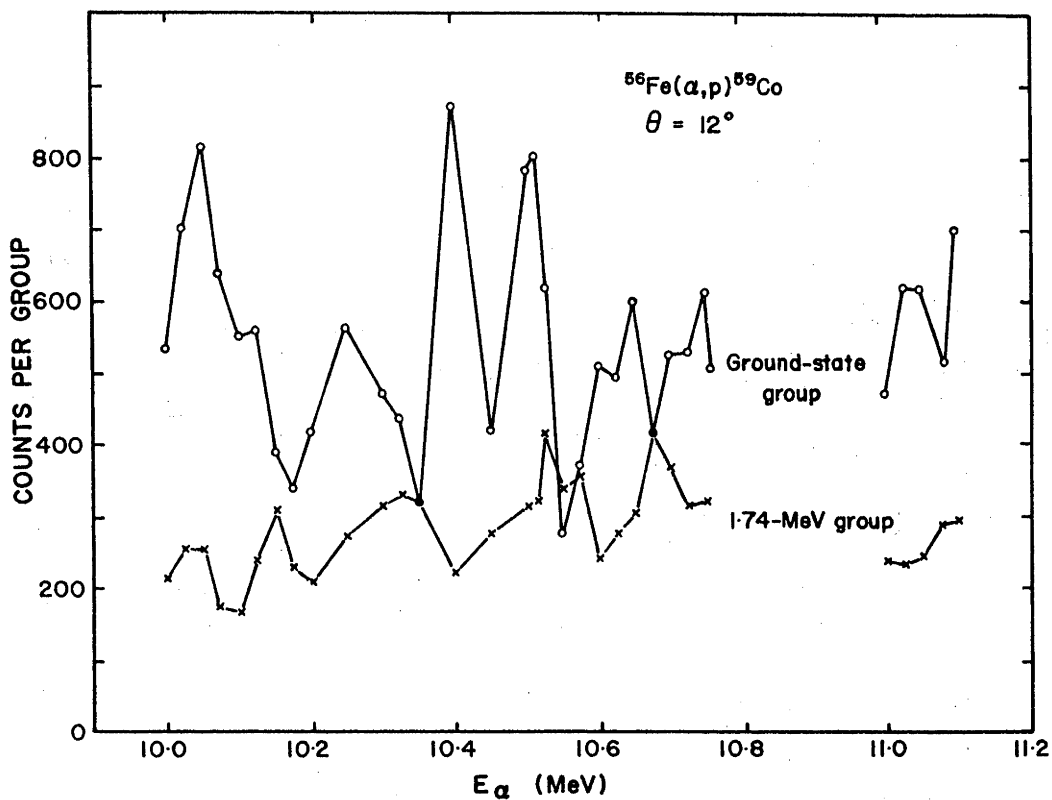


Figure 7.1: $^{56}\text{Fe}(\alpha, p)^{59}\text{Co}$ excitation functions for the proton groups populating the ground state and 1.744 MeV state. A typical particle spectrum is also shown. The proton groups are labelled by the excitation energy of the state populated in ^{59}Co .

The yield at 12° was assumed to be similar to the yield at zero degrees, as a coherence angle of about this magnitude is expected in this mass region for bombarding energies of ~ 10 MeV [Br 64]. This assumption is supported by the high degree of similarity between the yield curves measured at 12° and 20° . The measurements at 0° , reported in the following section, were made at the maxima of these excitation functions.

7.3 PARTICLE-GAMMA-RAY COINCIDENCE MEASUREMENTS

7.3.1 Method A

The first particle- γ -ray coincidence measurements were made using the A.N.U. double focusing magnetic spectrometer to detect the outgoing particles at 0° . This spectrometer is vertically mounted, and can be rotated in a horizontal plane from 0° to 153° with respect to the beam direction. Particles are deflected through 180° with a central radius of curvature of 61 cm, and are focused in both the vertical and horizontal planes. Ordinary solid state detectors or position-sensitive detectors may be positioned in the focal plane. Adjustable rectangular slits at the entrance to the spectrometer may be set to subtend a solid angle of 0 to 13 msr at the target. Measurements [E1 68] with a thin 8.78 MeV α -particle source have indicated that resolutions ($E/\Delta E$ @ F.W.H.M.) of 760 to 1100 can be achieved. A more detailed description of the properties of the double focusing spectrometer has been given by Elliott *et al.* [E1 68].

For these measurements, the outgoing particles were detected at 0° with a 5 cm long position-sensitive detector located

on the focal plane of the spectrometer. Aluminium foil, 0.007 to 0.012 cm thick, was placed in front of the detector to prevent α -particles from entering it: α -particles of the same magnetic rigidity as the proton groups of interest arise from scattering in the target and off the slits and inner walls of the magnet. The beam was dumped in a cup inside the spectrometer so that γ -ray backgrounds were minimized. In addition, the γ -ray detector, a 12.7 cm diam. \times 10.2 cm long NaI(Tl) crystal, was shielded with about 1 cm of lead.

For the branching ratio measurements, the NaI detector was mounted vertically on top of the target chamber so that its face was 4 cm from the beam spot on the target. A schematic diagram of the electronics used is shown in fig. 7.2. Resolving times of approximately 180 ns were obtained with double delay line shaping and Cosmic fast-slow coincidence equipment. The energy resolution obtained with the particle detector arose mainly from the difference in the target thickness for the incoming α -particles and outgoing protons (≈ 25 keV per $100 \mu\text{g}/\text{cm}^2$ of Fe at $E_\alpha = 10$ MeV). With the approximately $100 \mu\text{g}/\text{cm}^2$ self supporting targets used in these measurements, the resolution was typically 30 keV.

Some sample spectra are shown in fig. 7.3. The spectra were generally obtained with data collection times of 3 to 8 hours using beam intensities of $\leq 0.1 \mu\text{A}$. It is apparent from inspection of the proton spectrum that there was a large background under the peaks of interest. These background protons came from the $p(\alpha,p)\alpha$ reaction. Although the proton group from this reaction is higher in energy than the proton groups from the $^{56}\text{Fe}(\alpha,p)^{59}\text{Co}$ reaction, the protons scattered off the slits and inner walls of the magnet

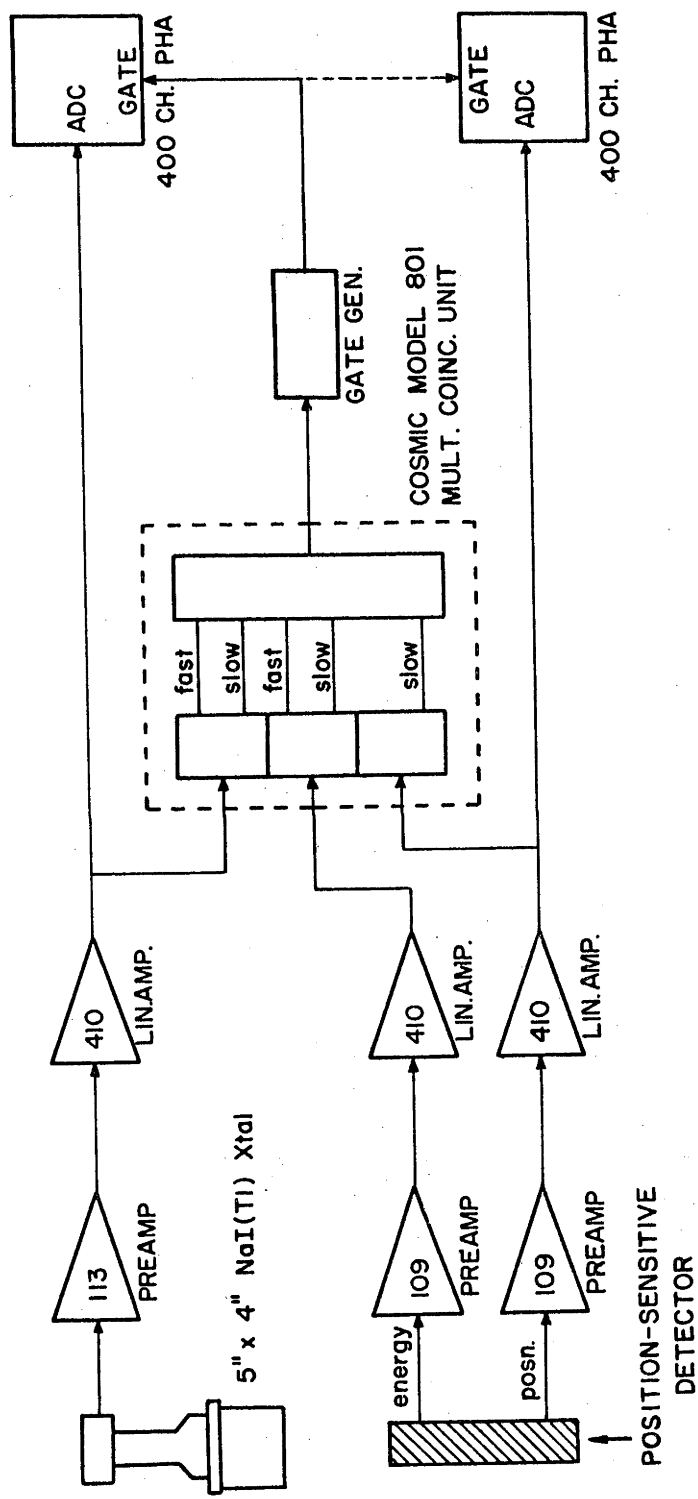


Figure 7.2: Schematic diagram of the electronics used for the branching ratio measurements (method A). The amplifiers and preamplifiers whose model numbers are shown were manufactured by Ortec and the 400-channel analysers by R.I.D.L.

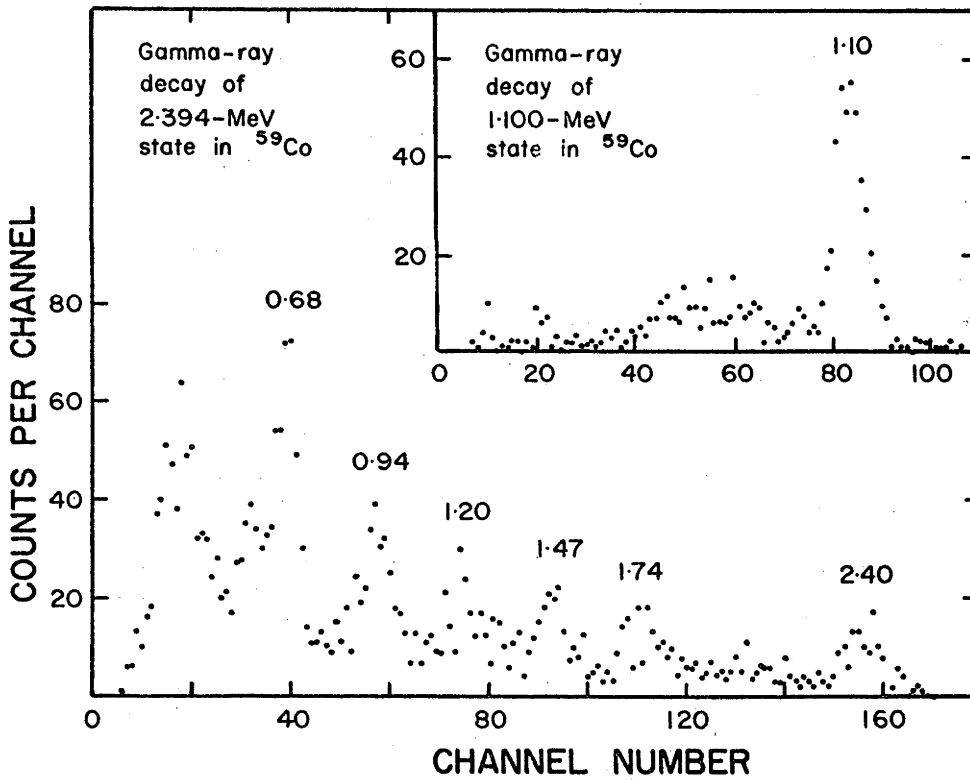
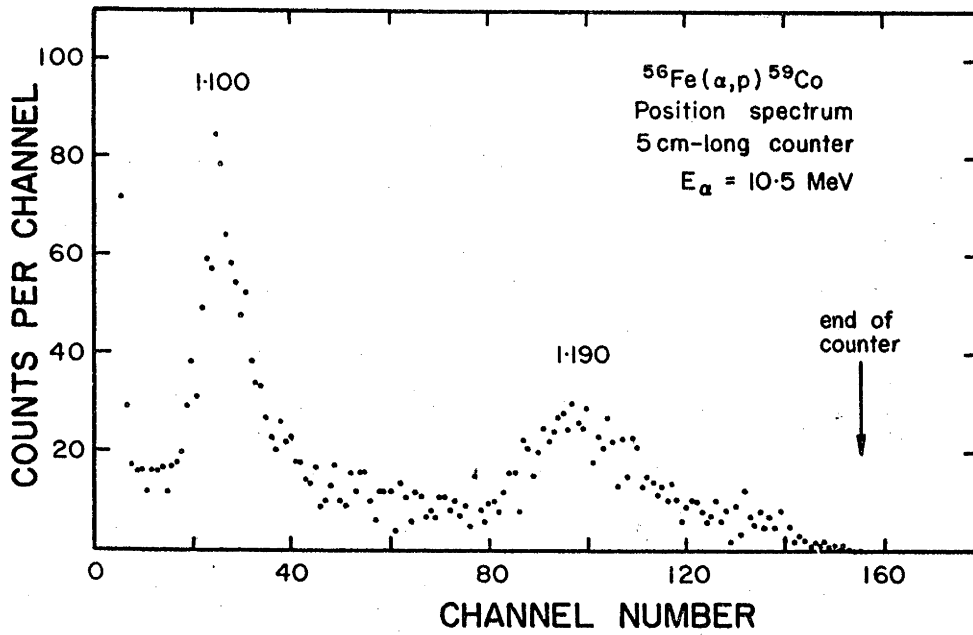


Figure 7.3: $^{56}\text{Fe}(\alpha, p\gamma)^{59}\text{Co}$ branching ratio measurements (method A).

Top: A typical proton singles spectrum.

Bottom: γ -ray decay of the 1.100 and 2.394 MeV states.

The random coincidence spectra have not been subtracted.

produce an extended tail on the low energy side of the very intense peak [Ke 69]. This large background, while not in coincidence with γ -rays, increased the random to real ratio in the coincidence spectra.

The angular correlation measurements in this configuration (protons detected at 0°) were performed using a thin walled target chamber (1.6 mm-thick stainless steel) with the NaI detector in the horizontal plane. The NaI detector mount could be positioned accurately with locating pins at intervals of 2.5° around the target chamber. The isotropy of this arrangement has been checked by Kean [Ke 69], who found the count rate of 2.61 MeV γ -rays from a ThB(ThC'') source placed in the centre of the target chamber, to be independent of angle to within 1%. To avoid background subtraction difficulties associated with the position-sensitive detector mentioned above, another 12.7 cm \times 10.2 cm NaI crystal was fixed in position at 90° to the beam direction with its face 8.5 cm from the target. The coincidence yield from this detector was used as a normalizing factor for each run. The movable 12.7 cm \times 10.2 cm NaI detector on the opposite side of the target chamber, was 10.5 cm from the target and could be rotated between 90° and 142.5° . Gain changes of up to a factor of ten were produced by the fringing field of the spectrometer when the NaI detectors were mounted at forward angles [Ke 69], so that data were recorded in the backward quadrant.

A schematic drawing of the electronics is shown in fig. 7.4. A window width of 180 ns was placed on the time-to-pulse-height converter (TPHC) spectrum; such a large resolving time was necessary because of the poor timing characteristics of the position-sensitive detector. The γ -ray random spectra were assumed to have

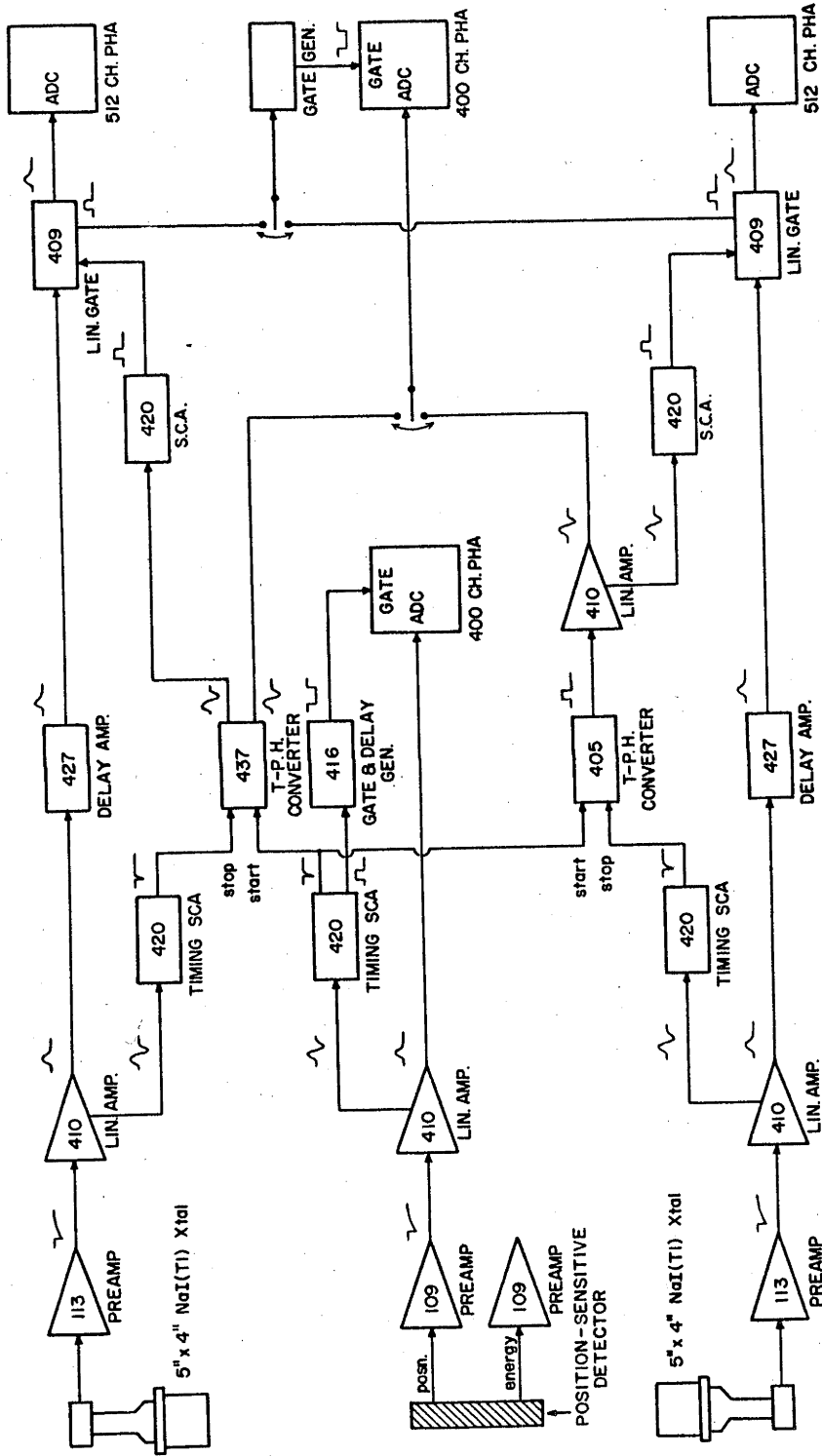


Figure 7.4: Schematic diagram of the electronics used for the angular correlation measurements (method A). The numbers refer to model numbers of the Ortec electronics. The 400 and 512 channel analysers were manufactured by R.I.D.L. and R.C.L. respectively.

the same shape as the γ -ray singles spectra at each angle. The magnitude of the random spectra was obtained from the random to real ratio observed in the ungated TPHC spectra. The correlation was obtained by normalizing the photopeak counts obtained at each angle with the movable crystal to the photopeak counts obtained with the fixed crystal.

7.3.2 Method B

During the course of these experiments, equipment became available for measuring correlations using an annular particle detector. In view of the difficulties encountered in making measurements with the magnetic spectrometer, the use of an annular counter was preferable for states that could be resolved by the detector. With the counter located at 180° there was no background from the $p(\alpha,p)\alpha$ reaction, and the solid angle subtended by the counter, being larger than that subtended by the magnetic spectrometer, increased the coincidence rate. In all of the experiments reported here, the annular counter subtended angles between 165° and 171° , corresponding to a solid angle of 0.13 sr, which was 10 times larger than the maximum angle subtended by the spectrometer.

All measurements made using the annular counter and NaI crystals were performed on the same beam line and with the same thin walled target chamber used for the correlation measurements reported in section 7.3.1. The spectrometer was rotated out of the way, and a 2 m long beam dump added at 0° . The face of the annular counter was located 2.5 cm from the target; tantalum apertures immediately in front of the counter face defined the angular acceptance. The α -particle beam was collimated by two apertures of 0.020 and 0.030

cm diameter located upstream from the target chamber at distances of 0.3 and 1.3 m respectively. As an additional precaution, a tantalum insert (ID \approx 0.25 cm) was placed through the centre of the counter to prevent the beam impinging on the counter itself. The target ladder was normally rotated $\sim 25^\circ$ from the perpendicular to the beam direction to prevent γ -ray attenuation in the steel before being detected in the NaI crystal. The 12.7 cm \times 10.2 cm NaI(Tl) detector was rotated in a forward quadrant from 90° to 22.5° at a target to crystal face distance of 20 cm. For the branching ratio measurements, the detector was fixed at 55° , 10 cm from the target. To minimize low energy γ -ray background, the crystal sides were surrounded with a 1 cm thick lead collar.

Because of the negative Q values of the $\text{Fe}(\alpha, p)$ reactions, the energy of the scattered α -particles had to be reduced so that they did not interfere with the proton groups of interest. To do this, foils were placed over the face of the counter. After a series of trials using aluminium, nickel and mylar ($\text{C}_{10}\text{H}_6\text{O}_4$) foils in front of a counter detecting protons from the $^{12}\text{C}(\text{}^3\text{He}, p)^{14}\text{N}$ reaction, it was found that, for foils of equivalent α -particle stopping power, the best resolution was obtained with mylar. Therefore mylar was used in all the measurements.

Data collection times averaged ~ 10 hrs per angle with a target of $\sim 100 \mu\text{g}/\text{cm}^2$ of Fe and with beam intensities of $\sim 0.1 \mu\text{A}$. The beam current was adjusted to maintain γ -ray count rates above ~ 80 keV constant. This was done to minimize variations in coincidence losses due to pile up. (The particle singles rate was considerably less than the γ -ray singles rate, so that coincidence losses associated with changing particle count rates were relatively

unimportant). With a count rate of $\sim 24,000$ counts/sec, assuming a Poisson distribution, 7% of the pulses from the linear amplifier (with double delay line clipping, the pulse width was ~ 3 μ sec) would overlap to some extent. Many of these pulses will have the zero cross-over point shifted out of the coincidence window, and will not be observed in the coincidence spectrum. However, assuming that any overlap causes a pulse to be lost, it is possible to put an upper limit on the coincidence losses due to pile up. With a singles rate of 25,000 counts/sec, a change in the rate of 5,000 counts/sec would change the relative coincidence yield by $< 1.5\%$.

For the first measurement of the 1.744 MeV state correlation, this effect was even smaller as an Ortec fast time pickoff unit was used on the γ -ray signal. This unit derives a signal from the leading edge of the pulse, so that the problem of coincidence losses was greatly reduced. However, pile up rejection could not be used, and it was found that the time pickoff unit provided only a marginal improvement over the cross-over timing (both gave resolving times of ~ 70 ns). For this reason the cross-over timing electronics shown in fig. 7.5 was used for all subsequent experiments. The IBM 1800 on-line data acquisition system was used in dual parameter mode to collect the data in a 128×32 array. The 128 channel X-axis provided sufficient dispersion for the γ -ray spectra, while the 32 channel Z-axis enabled more than one proton group to be studied at one time. The 90° monitor counter of method A was not needed in these experiments, since the proton singles spectra collected at the same time as the coincident protons could be used for monitoring. Proton peak intensities were obtained by fitting skewed Gaussians on a linear background to the proton spectra. Representative spectra

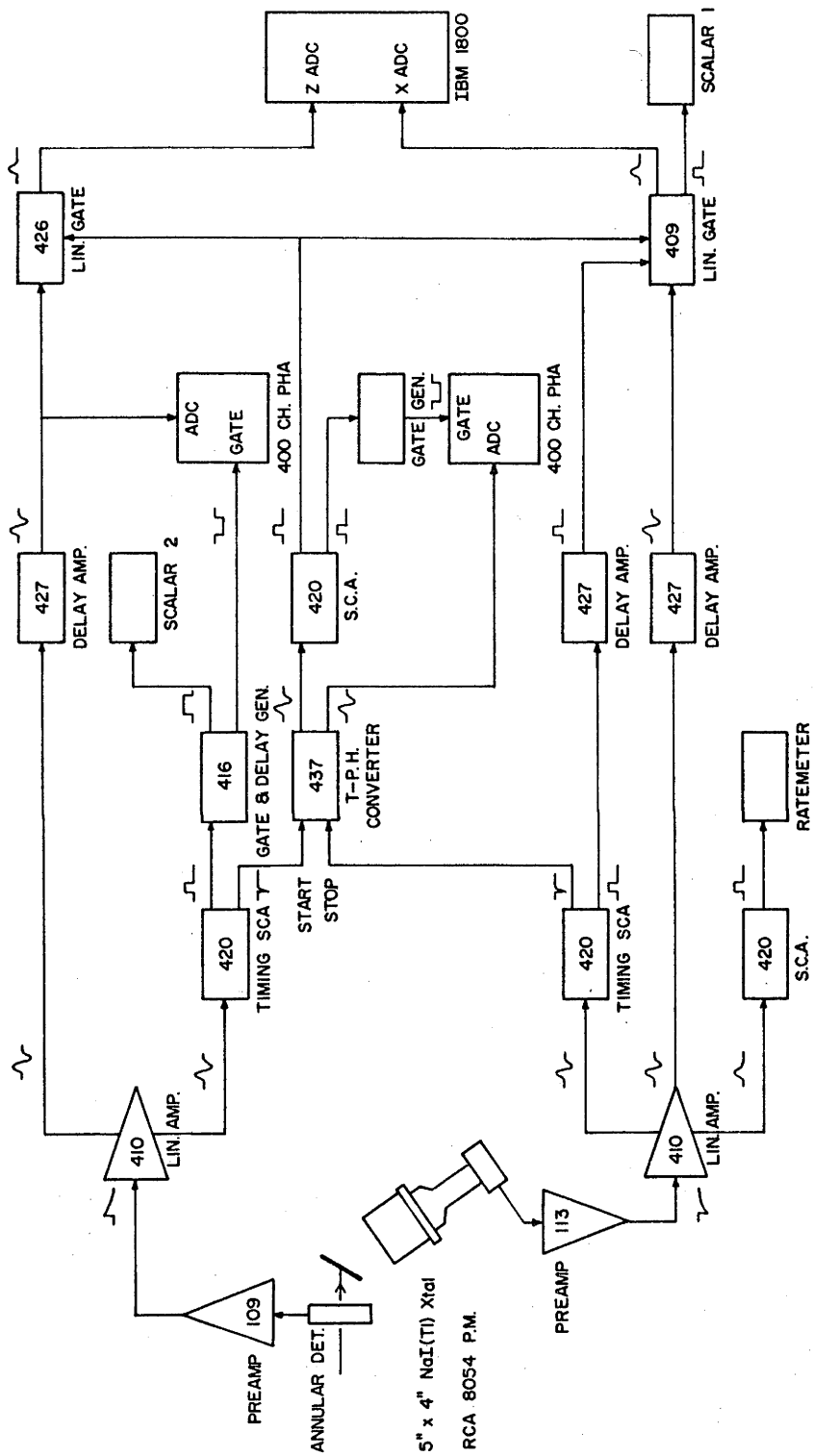


Figure 7.5: Schematic diagram of the electronics used for the particle- γ -ray coincidence measurements (method B). The IBM 1800 was used in the dual parameter mode (128 x 32 chs).

for the 1.291 and 1.100 MeV angular correlations are shown in fig. 7.6. The γ -ray spectra were first inspected by summing the slices where no peak overlap occurred (the hatched regions in the summed proton coincidence spectra in fig. 7.6). The total number of γ -ray-proton coincidences was obtained by normalizing each γ -ray spectrum to the number of coincident protons to the corresponding state. This latter quantity was obtained from fitting skew Gaussians to the summed proton coincidence slices. The angular correlations were then derived from the ratios of the coincident γ -rays and the total number of protons to each state observed in the singles spectra. Appropriate corrections were made for dead time, gain changes, etc.

7.3.3 Method C

Because of the poor resolution inherent in NaI γ -ray detectors, several ambiguities were found in the observed decay scheme for ^{59}Co . To resolve these ambiguities, some coincidence measurements were made with a 40 cc Ge(Li) detector and the annular counter.

A thin walled target chamber, with an insert to accommodate the Ge(Li) detector at 55° to the beam direction and with the detector face 3.4 cm from the target, was used. The face of the annular counter was ~ 0.4 cm from the target ($\sim 200 \mu\text{g}/\text{cm}^2$ of ^{56}Fe). The beam of $\sim 0.1 \mu\text{A}$ intensity was stopped on a platinum beam stop 3 m beyond the target. The γ -ray singles rate was not measured accurately but was in the range of 50 K to 80 K counts/sec. Although the high count rate reduced the full energy peak resolution, a workable coincidence rate was possible.

A schematic diagram for the electronics is shown in fig.

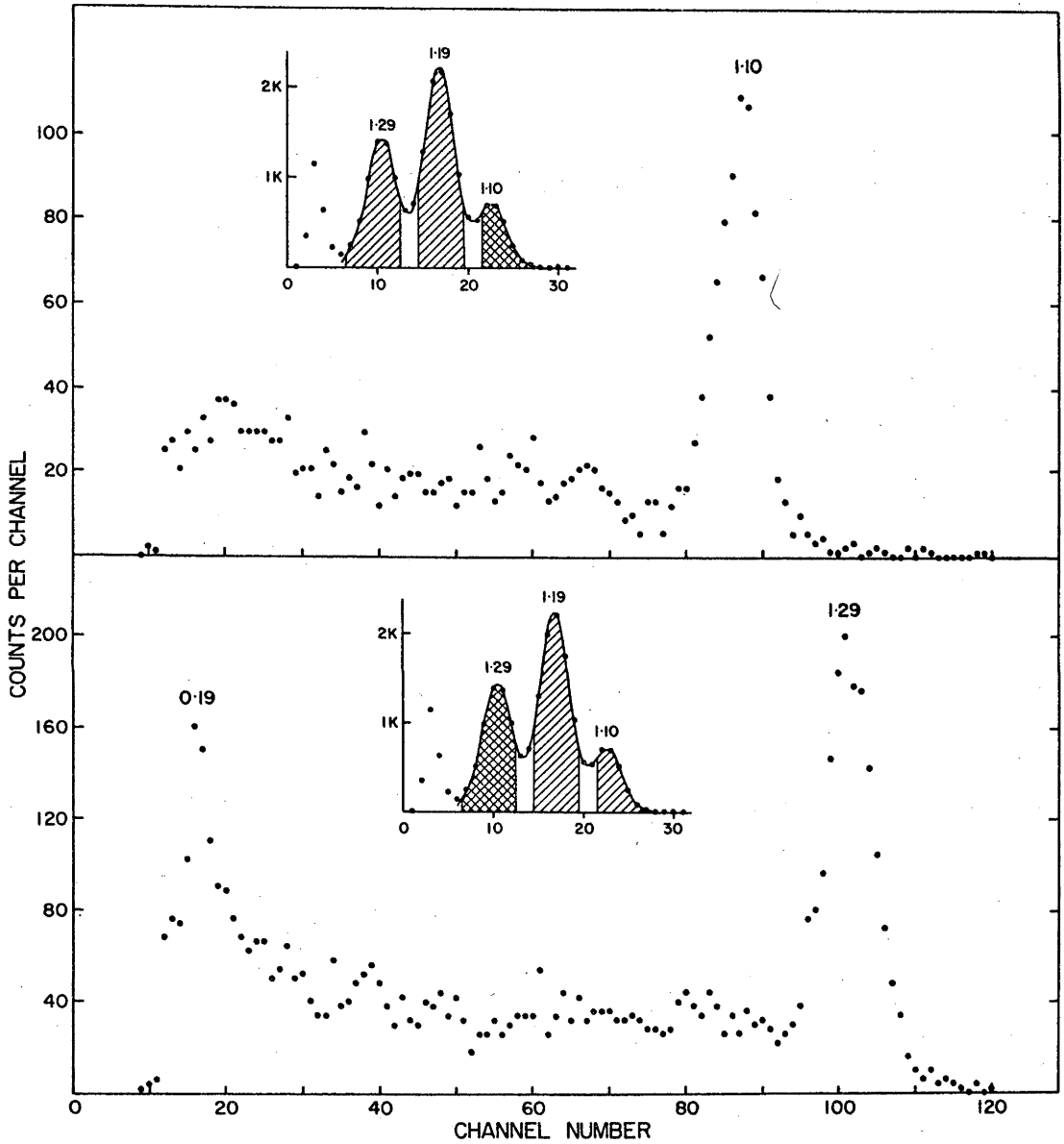


Figure 7.6: The γ -ray decay of the 1.100 and 1.291 MeV states in ^{59}Co , obtained using the $^{56}\text{Fe}(\alpha, p\gamma)$ reaction. The NaI detector was located at 57.5° . Proton coincidence spectra are shown in the insets. The cross hatched regions correspond to the summed slices of γ -ray spectra shown.

7.7. One of the amplifiers on the Ge(Li) side of the coincidence circuit was used in the RC clipping mode with long time constants (1 and 2 μ s), in order to obtain optimum energy resolution. The other amplifier was operated in the double delay line mode for optimum timing for the coincidence circuit. Nevertheless, because of the poor timing qualities associated with large coaxial Ge(Li) detectors, it was necessary to use a window width of 250 ns on the TPHC spectrum to adequately bracket the coincidence peak.

When the $^{58}\text{Fe}(\alpha, p\gamma)^{61}\text{Co}$ results were found to be too complex due to the interference of the $^{56}\text{Fe}(\alpha, p\gamma)$ reaction, branching ratio measurements were made using the $^{64}\text{Ni}(p, \alpha\gamma)^{61}\text{Co}$ reaction. The experimental arrangement was similar to the previous Ge(Li) coincidence measurements. It was found necessary to have a thin foil (4×10^{-4} cm aluminized mylar) over the face of the annular counter to exclude electrons ejected from the target by the proton beam. Although the foil reduced the α -particle resolution, an energy resolution of ~ 125 keV F.W.H.M. was obtained with a target thickness of ~ 300 $\mu\text{g}/\text{cm}^2$.

A schematic diagram of the electronic circuitry is given in fig. 7.8. The timing system for the Ge(Li) detector was the same as before, but γ -rays associated with four different α -particle groups, selected by single channel analyzers, were routed into 4×1024 channels in the Nuclear Data 2200 analyzer. The linear amplifiers on the outputs of the single channel analyzers transformed the rectangular logic pulses into shapes suitable for acceptance in the N.D. 2200 and adjusted the amplitudes to correspond to the appropriate channels of the Z A.D.C. The Nuclear Data analyzer was chosen for this experiment because the A.D.C.s could be D.C.

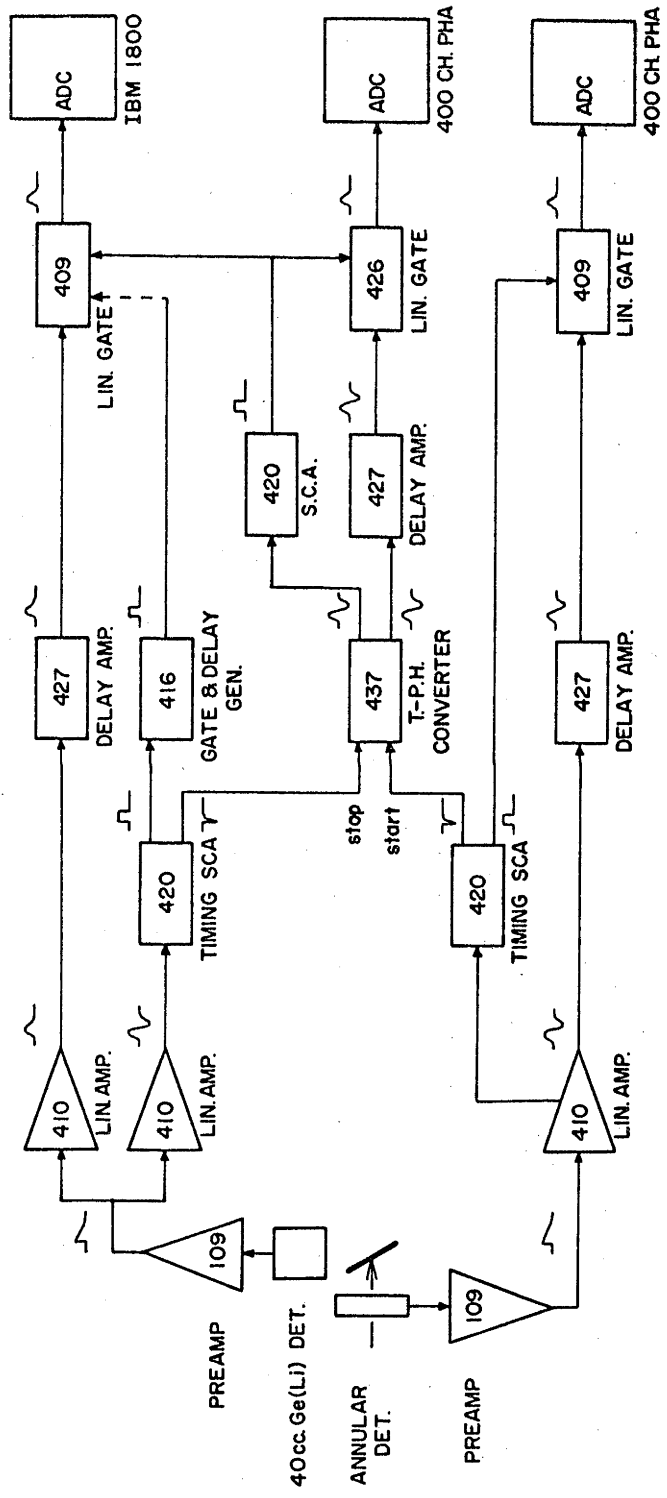


Figure 7.7: Schematic diagram of the electronics used for the $^{56}\text{Fe}(\alpha, \gamma)$ coincidence measurements performed with the Ge(Li) detector.

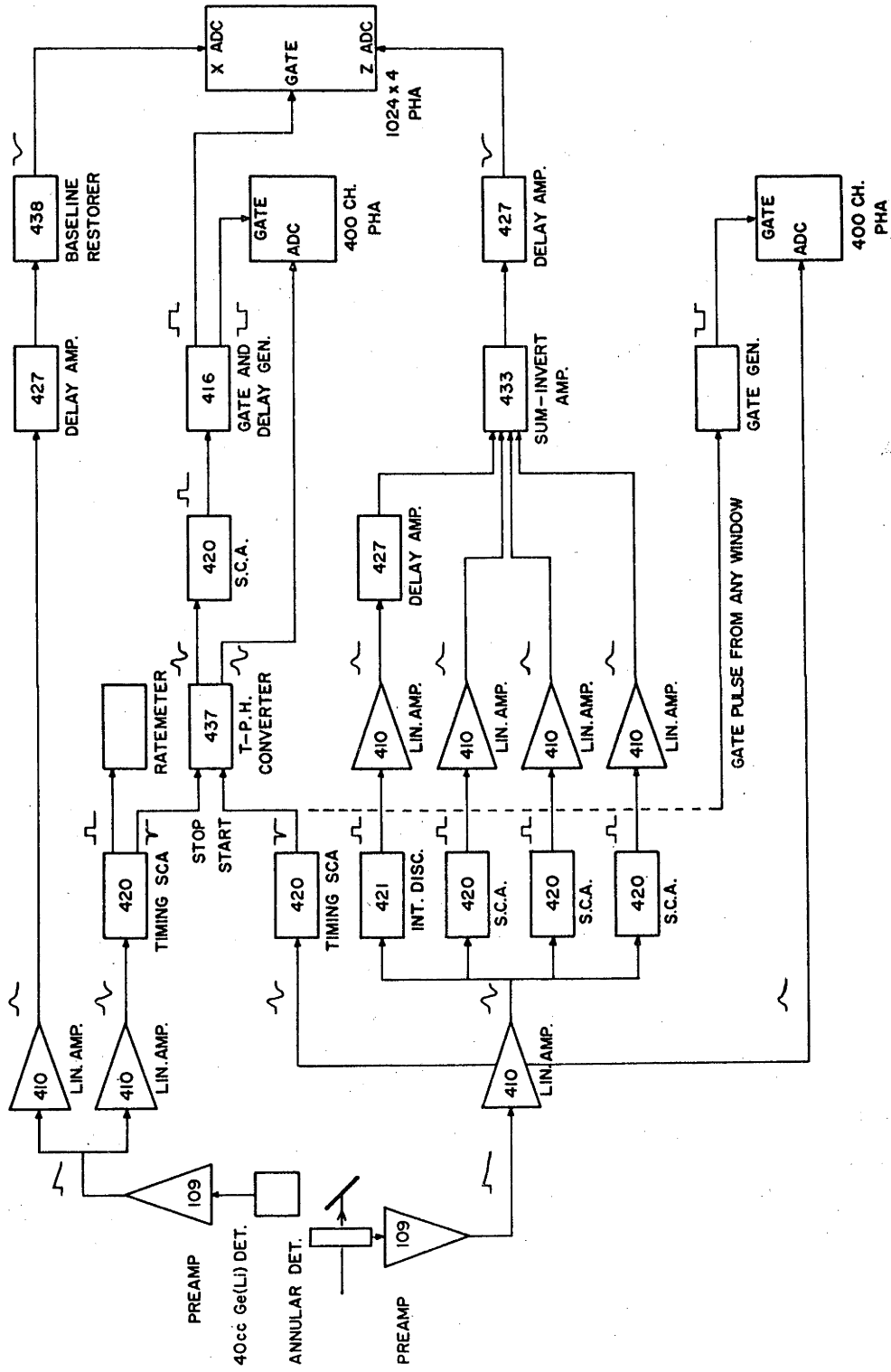


Figure 7.8: Schematic diagram of the electronics used in the $^{64}\text{Ni}(p, \alpha)^{61}\text{Co}$ experiment. The operation of the circuit is explained in the text.

coupled enabling a base line restorer to be used on the pulses from the Ge(Li) detector. With the constant count rate of ~ 50 K counts/sec, this combination provided a good compromise between full energy peak and timing resolution (12 keV and 250 ns). The high count rate was due to a large neutron background, and, in fact, a measurable decrease in the energy resolution arising from neutron damage to the detector was noted during the course of this experiment.

7.4 ^{59}Co RESULTS

7.4.1 γ -Ray Branching Ratios

Branching ratio measurements were made for states in ^{59}Co at 1.190, 1.291, 1.744, 2.394, 2.476 and 2.581 MeV excitation using the $^{56}\text{Fe}(\alpha, p\gamma)$ reaction. At the time of these measurements, little was known about the decay modes of the last four states. Subsequently, the stronger transitions from some of these states were obtained in an $(n, n'\gamma)$ experiment reported by Daniels and Felsteiner [Da 68].

All five of the above states were studied using the magnetic spectrometer (method A, section 7.3.1), and sample γ -ray spectra for the 1.100 and 2.394 MeV state decays are shown in fig. 7.3; random coincidence counts have not been subtracted. Photopeak counts were obtained by fitting the spectra with line shapes interpolated from a standard set (0.511, 0.661, 1.173 and 2.365 MeV) measured in this laboratory [Op 68]. The relative photopeak efficiency curve for the 12.7 cm diam. \times 10.2 cm long NaI detector was assumed to be the same as that measured by Coop and Grench [Co 65] for a 10.2 cm diam. \times 10.2 cm long NaI detector. The errors quoted

by these authors were increased by 3% to allow for the possible inaccuracy of this assumption. Although the γ -ray spectra generally identified the main decay features of the levels studied, in some cases poor statistics made extraction of accurate branching ratios impossible. Further information on these levels was obtained by the other methods mentioned below.

While obtaining some of the dual parameter coincidence spectra for the angular correlation experiments using the annular counter and NaI detectors (method B, section 7.3.2), some spectra were obtained for the group of 5 states near 2.1 MeV excitation. The level spacing of the 5 states, being much less than the proton resolution, prohibited any extraction of branching ratios. However, by making a slice by slice comparison of the spectra, the more intense γ -rays could be identified with particular levels. In the analysis of the spectra, use was made of the data of Daniels and Felsteiner [Da 68], in which two γ -rays from this group of 5 states had been attributed to two individual levels. The transitions identified are shown in fig. 7.9 and tabulated in table 7.1. The data shown are a summary of the results from all the branching ratio measurements, including the branching ratios extracted from the angular correlation data with the aid of Legendre polynomial fits. The data for the higher energy states, and some of the lower energy states, were obtained with the Ge(Li) detectors as reported below.

In the early stages of the experiments, it was not known whether the low energy transition from the 1.744 MeV state involved the 1.463 MeV or the 1.482 MeV state or both. To answer this question, a coincidence measurement was made using the annular counter and the 40 cc Ge(Li) detector (method C, section 7.3.3). In addi-

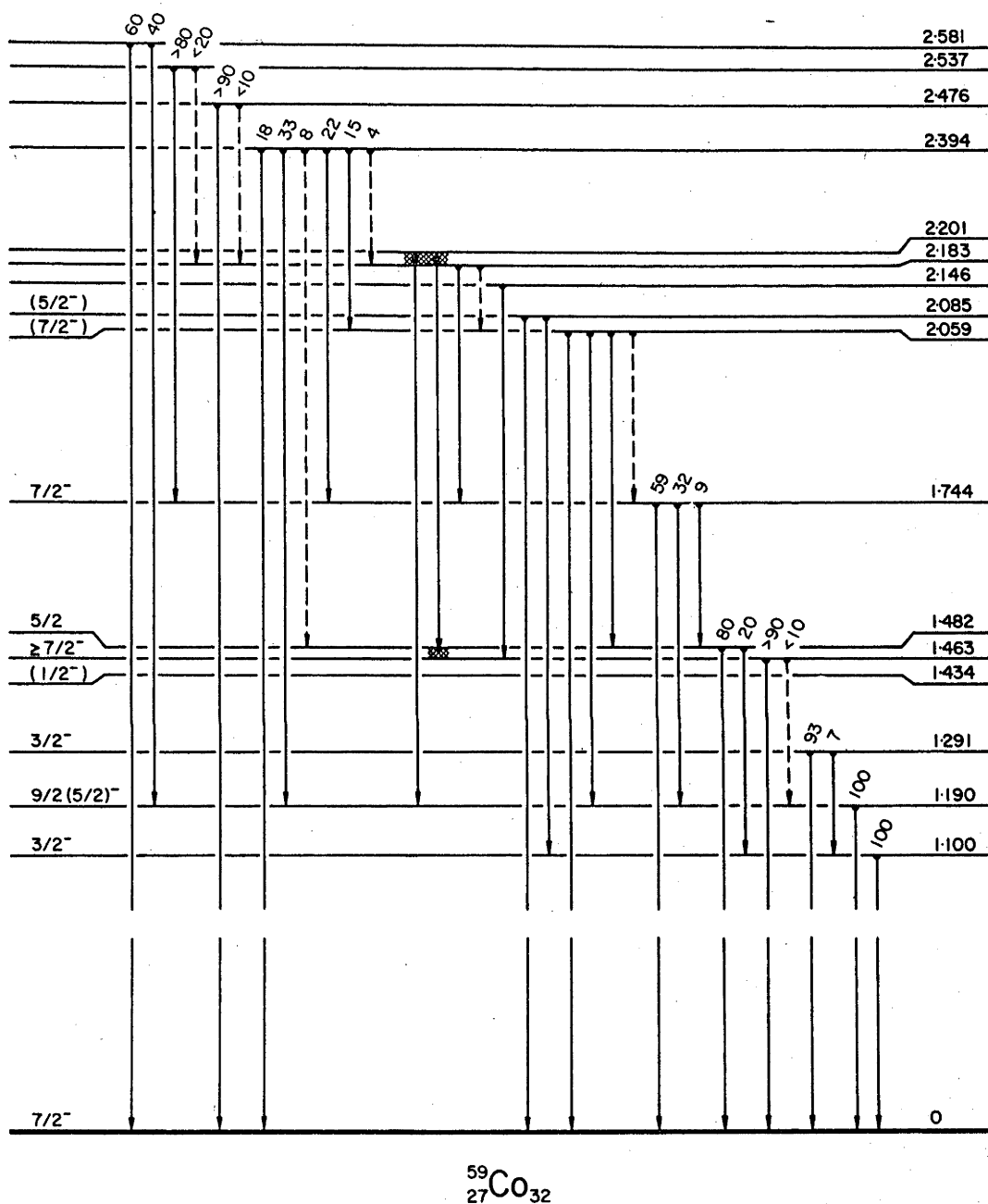


Figure 7.9: The decay scheme of ^{59}Co deduced in the present experiment. The J^π values were obtained from the present and previous experiments.

Table 7.1
 γ -ray branching ratios for ^{59}Co

Initial state (MeV)	Final state (MeV)	Branching ratios			
		This exp.	[Be 67]	[No 67]	[Da 68]
1.100	0.0	100	100	100	100
1.190	0.0	100		100	100
1.292	0.0	93 ± 4	5		6
	1.100	7 ± 4	95		94
1.463	0.0	> 90		90	100
	1.190	< 10		10	
1.482	0.0	80 ± 3	72		80
	1.100	20 ± 3	28		20
1.744	0.0	59 ± 4			60
	1.190	32 ± 2			30
	1.482	9 ± 2			10
2.059	0.0	*(weak)			
	1.190	*			
	1.482	*(strong)			*
	1.744	*(weak)			
2.085	0.0	*			
	1.100	*			
2.146	1.463	*			*
2.183	1.744	*(strong)			
2.183 or 2.201	1.190	*			
	1.463 or	*			
	1.434				
2.394	0.0	18 ± 9			*
	1.190	33 ± 9			
	1.482	8 ± 7			
	1.744	22 ± 6			
	2.059	15 ± 5			
	2.183	4 ± 2			
2.476	0.0	> 90			
	2.183	< 10			
2.537	1.744	> 80			
	2.183	< 20			
2.581	0.0	60 ± 8			
	1.190	40 ± 8			

* γ -ray observed, but little or no intensity information available.

The errors shown for the branching ratios are standard errors.

tion, a measurement was made with a window set on the proton groups populating the states at 2.394, 2.476, 2.537 and 2.581 MeV. These groups were unresolved but were adequately separated from adjacent proton groups. Because of the large number of peaks present in the γ -ray spectrum, the data were much more difficult to analyze than in the case of the 1.744 MeV state. However, most of the stronger transitions have been identified. To aid in the analysis of the data (particularly for the quartet of states), the coincidence γ -ray spectra were smoothed using the technique described by Yule [Yu 67]. The original and smoothed spectra are shown in fig. 7.10. The energies of the peaks which have been fitted into the decay scheme are indicated; many of the smaller bumps are due to the smoothing program, and are not indicative of γ -ray peaks. The branching ratios were obtained using the efficiency curves of Huang [Hu 68] and Black *et al.* [Bl 68] for the detector. As small amplitude pulses are more likely to be lost from the system because of pile up effects [Co 69], the errors were increased to account for the losses associated with the high count rates. It can be seen that the 1.744 MeV state has a branch to the 1.482 MeV state, and no detectable branch to the 1.463 MeV state. This agrees with the results of Daniels and Felsteiner [Da 68].

7.4.2 Angular Correlation Measurements

A discussion of the theory of angular correlation measurements and the modifications required to meet the present experimental limitations is contained in the Appendix. Briefly, the formulae and tables of Rose and Brink [Ro 67a] were used to analyze the data. At 0° the reaction populates only the $|M_1| = 1/2$ substates,

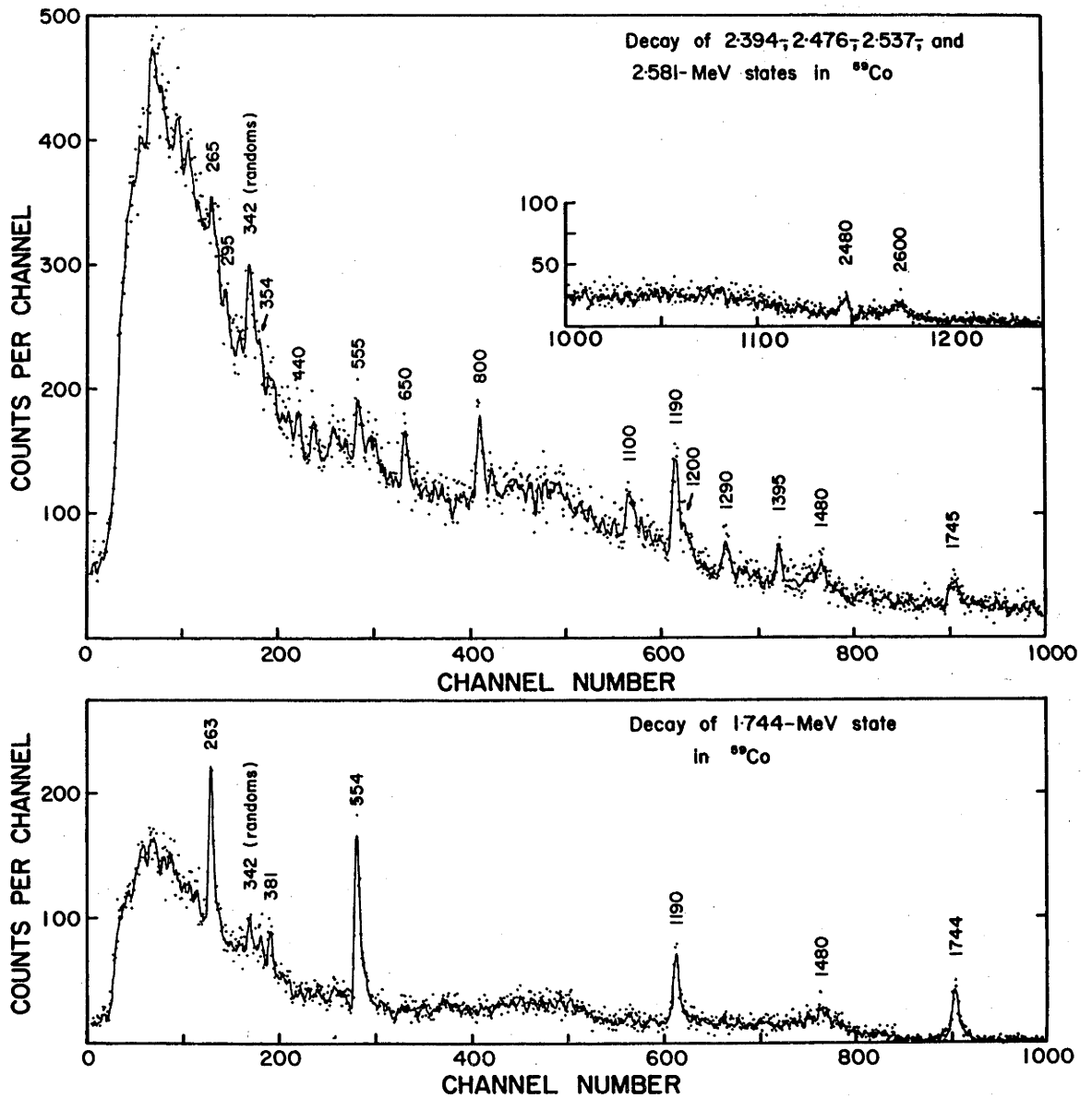


Figure 7.10: Ge(Li) spectra of the decay states in ^{59}Co obtained using the $^{56}\text{Fe}(\alpha, \gamma)$ reaction. (The random coincidence spectra have not been subtracted.) The continuous curves are the result of smoothing the spectra using the method outlined in Yule [Yu 67]. The energies (keV) of the γ -rays which were placed in the decay scheme are shown near the full energy peaks.

but to allow for the finite range of angles subtended by the detectors about 0° or 180° , it was assumed that $|M_1| = 3/2$ substates could also be populated to a small extent.

The correlations were fitted by the equation given in the Appendix for various values of initial state spin J_1 , final state spin J_2 and the mixing ratio δ . For given values of the spins, least squares fits were made to the data and χ^2 values for each fit were obtained. The well established ground state spin of $7/2$ [N.D.S.] was used for all fits, while the spins of the initial states were varied from $1/2$ to $13/2$. The fitting program was valid for multipolarities up to and including octupole. Values of χ^2 were computed with the program by dividing the weighted sum of the squares of the residuals by $(M-N)$, where M is the number of angles and N is the number of free parameters. The confidence limits for the normalized χ^2 values were taken from the tabulations of Nijght *et al.* [Ni 59]. With regard to these confidence limits, the general criteria adopted were that the theoretical correlation curves did not fit the data for values of χ^2 well outside the 1% confidence limit, and for values of χ^2 near or inside the 10% confidence limit, the fit was considered to be satisfactory. For values of χ^2 between these ranges, the fit was generally considered indeterminate. It is recognized that these criteria are arbitrary; however, it is felt that they are reasonable ones to use for the data presented. Fits to the data were also made with $P(3/2)/P(1/2) = 0.1$, and in some cases 0.3; these fits were considered when the mixing ratios and errors were deduced.

Five different sets of data (labelled A to E) were taken using the configurations of method A (section 7.3.1) or method B

(section 7.3.2) and various bombarding energies as set out in table 7.2. The fits to these data sets are considered below under the appropriate energy state heading. A summary of the final spins and mixing ratios deduced is contained in table 7.8.

Table 7.2

Conditions under which the $^{56}\text{Fe}(\alpha, p\gamma)$ angular correlation measurements were made

Data set	Exp. method	E_{α} (MeV)	Angles measured	χ^2 confidence limits	
				1%	10%
A	A	10.15	$90^{\circ}, 102.5^{\circ}, 115^{\circ}, 127.5^{\circ}, 140^{\circ}$	3.7	2.2
B	A	10.40	$90^{\circ}, 117.5^{\circ}, 130^{\circ}, 142.5^{\circ}$	3.3	1.9
C	B	10.66	$90^{\circ}, 62.5^{\circ}, 50^{\circ}, 37.5^{\circ}, 22.5^{\circ}$	3.7	2.2
D	B	10.66	$90^{\circ}, 57.5^{\circ}, 40^{\circ}, 22.5^{\circ}$	3.3	1.9
E	B	10.92	$90^{\circ}, 57.5^{\circ}, 40^{\circ}, 22.5^{\circ}$	3.3	1.9

Data set C was taken using the fast time pickoff unit, while D and E were taken with the cross-over timing as described in section 7.3.2.

1.100 MeV State

For a first attempt at measuring angular correlations, the first excited state of ^{59}Co was selected. Although there had been some discrepancies in the work of previous experimentalists in assigning a J^{π} value to the level, an assignment of $3/2^{-}$ from the (t, α) work appeared to be correct [N.D.S.]. Thus, the state would be expected to decay by a pure E2 transition to the $7/2^{-}$ ground state, and should yield a definite, predictable correlation. The

measurement of this correlation was, therefore, considered primarily as a test of the equipment and technique to be used for subsequent measurements involving states whose J^π assignments were less certain, or not known at all.

The first measurement with the magnetic spectrometer (data set A) was beset with difficulties associated with the monitor counter, so that the correlation measurement was repeated using the annular counter (data set E). The latter correlation, and the best fit to it, are shown in fig. 7.11. The results of the fits to both measurements are summarized in table 7.3. While not as definite as desired, the correlations do give good fits for the predicted $3/2 \rightarrow 7/2$ transition for $\delta = 0$ (pure E2), and indicated that the experimental method could be useful for assigning J values to other states.

Table 7.3

Summary of the theoretical fits to the
1.100 MeV angular correlations

Spin sequence	$\frac{P(3/2)}{P(1/2)}$	χ^2_{\min}	Values of the mixing ratio at confidence limits					Data set
			1%	10%	min.	10%	1%	
1.100 to 0.0 MeV								
3/2-7/2	0.0	0.1	-.31	-.24	0.0	2.6	3.1	A
1/2-7/2		0.8						A
3/2-7/2	0.0	0.1	-.18	-.15	-.07	0.03	0.06	E
3/2-7/2	0.1	0.1	-.18	-.16	-.05	0.06	0.11	E
1/2-7/2		1.6						E

$P(3/2)/P(1/2)$ is the ratio of the population of the $|M_1| = 3/2$ to $|M_1| = 1/2$ substates used in the theoretical correlation. χ^2_{\min} is the value of χ^2 at the minimum of the χ^2 vs. δ curve. The mixing ratio is that defined by Rose and Brink [Ro 67a] for the two lowest order multipolarities which can occur in the transition.

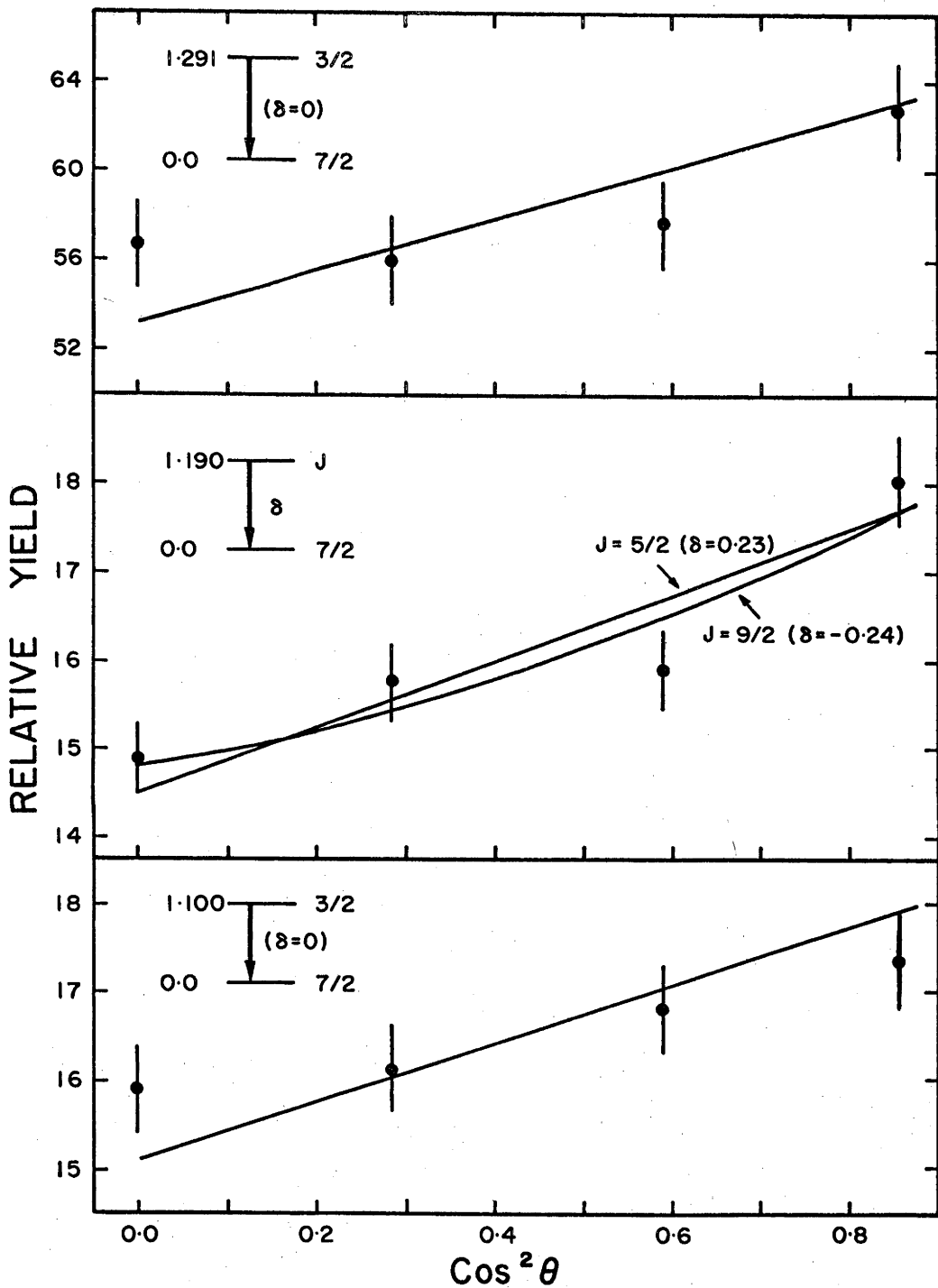


Figure 7.11: The $^{56}\text{Fe}(\alpha, p\gamma)$ angular correlations for the 1.100, 1.190 and 1.291 MeV states obtained using the annular counter (data set E). The curves are the theoretical correlations for the initial spin J and mixing ratio δ shown in the insets.

1.190 MeV State

The 1.190 MeV state is not populated in β decay, but has been observed in a number of reactions [N.D.S.], including $^{59}\text{Co}(^{16}\text{O},^{16}\text{O}'\gamma)$ [No 67]. As a result of the $(^{16}\text{O},^{16}\text{O}'\gamma)$ experiment the J^π of the level has been limited to $5/2^-$, $7/2^-$ or $9/2^-$ with the $5/2^-$ choice the most improbable. The 1.190 MeV state decays entirely to the ground state with a mean life, $\tau = 0.08 \pm 0.01$ ps [No 67].

The 1.190 MeV state was investigated both by direct α -particle population and through cascade γ -rays from the 1.744 MeV state. The angular correlations obtained using the magnetic spectrometer and annular counter to detect the 1.190 MeV state α -particle group, are shown in figs. 7.12 and 7.11 respectively. A summary of the fits to this data is contained in the first part of table 7.4. A typical spectrum obtained in the 1.744 MeV state correlations is shown in fig. 7.13, and it can be seen that both the 1.190 MeV state population γ -ray (0.55 MeV) and the decay γ -ray could be extracted from the data. The curve in fig. 7.13 is the fit to the spectrum obtained with a standard set of line shapes as described in section 7.4.1. The cascade correlations obtained from data sets C and D are shown in figs. 7.14 and 7.15 respectively; a summary of the theoretical fits to them is contained in table 7.4. In these fits it was assumed that the 1.744 MeV state had a spin of $7/2$ which was the spin deduced for it in the present experiments.

All of the correlations involving the 1.190 MeV state decay are fitted well for both $J = 5/2$ and $9/2$, but do not exclude $J = 7/2$. However, the fits to the two measurements involving the 1.744 MeV to 1.190 transition both give values of χ^2 outside the 1% confidence limit for $J = 7/2$. These fits can be improved by assum-

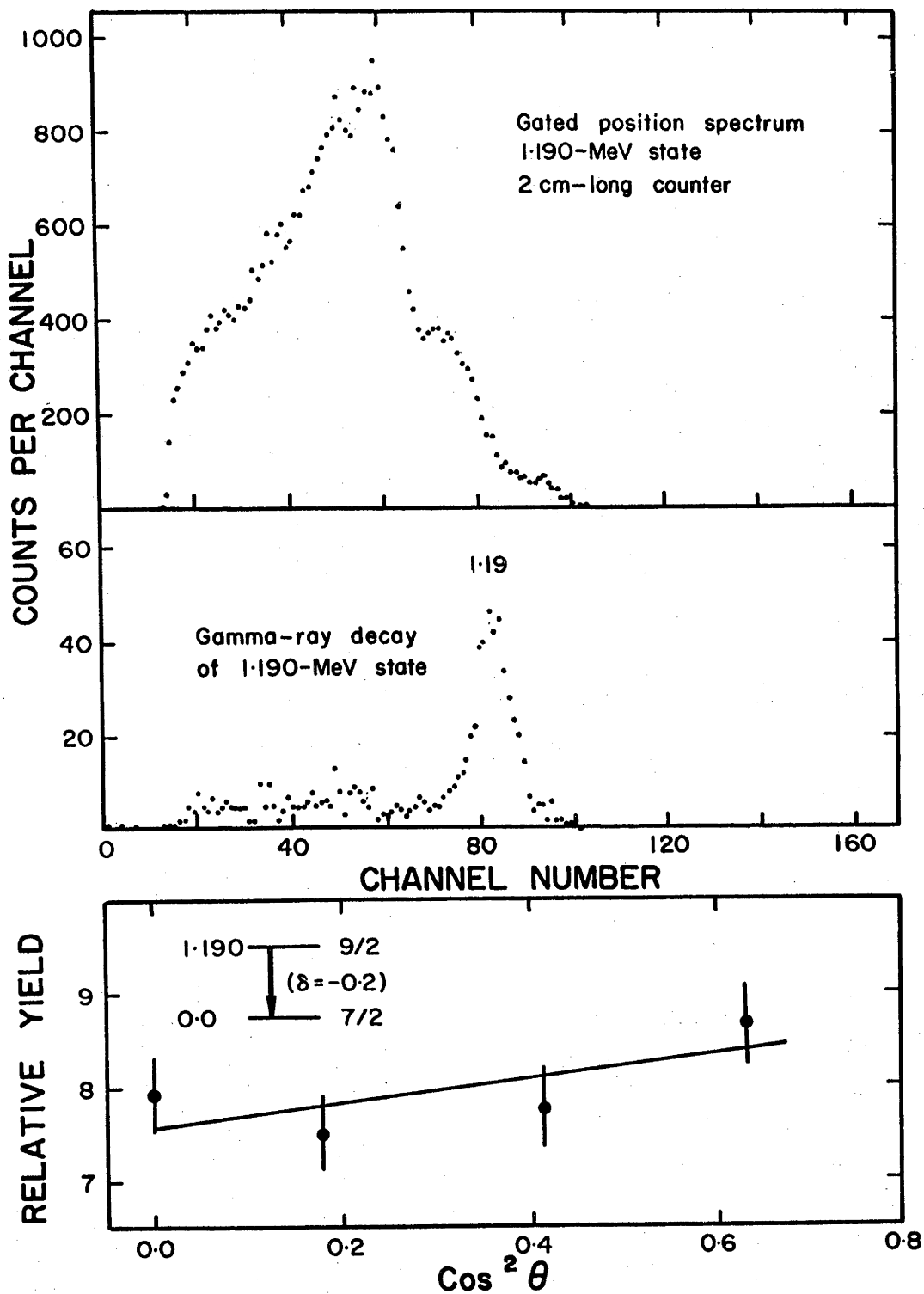


Figure 7.12: $^{56}\text{Fe}(\alpha, p\gamma)$ spectra and angular correlation for the spectrometer measurement (data set B) involving the 1.190 MeV state in ^{59}Co . (The random coincidence spectra have not been subtracted.)

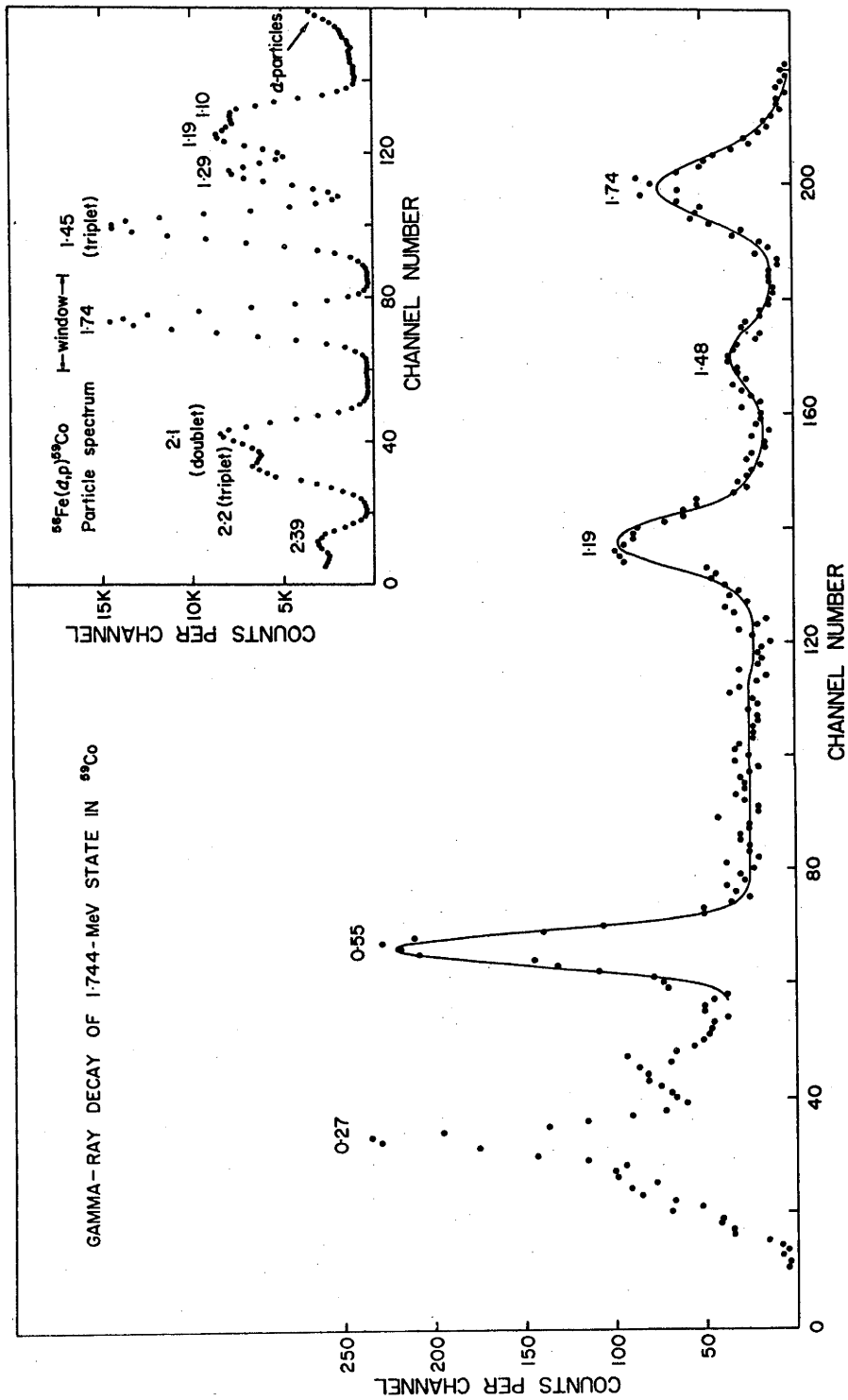


Figure 7.13: The γ -ray decay of the 1.744 MeV state in ^{59}Co obtained during the angular correlation measurements (data set C). The curve is the fit obtained with a standard set of line shapes. Normal γ -ray energies are shown near the photopeaks. A typical particle singles spectrum is shown in the inset.

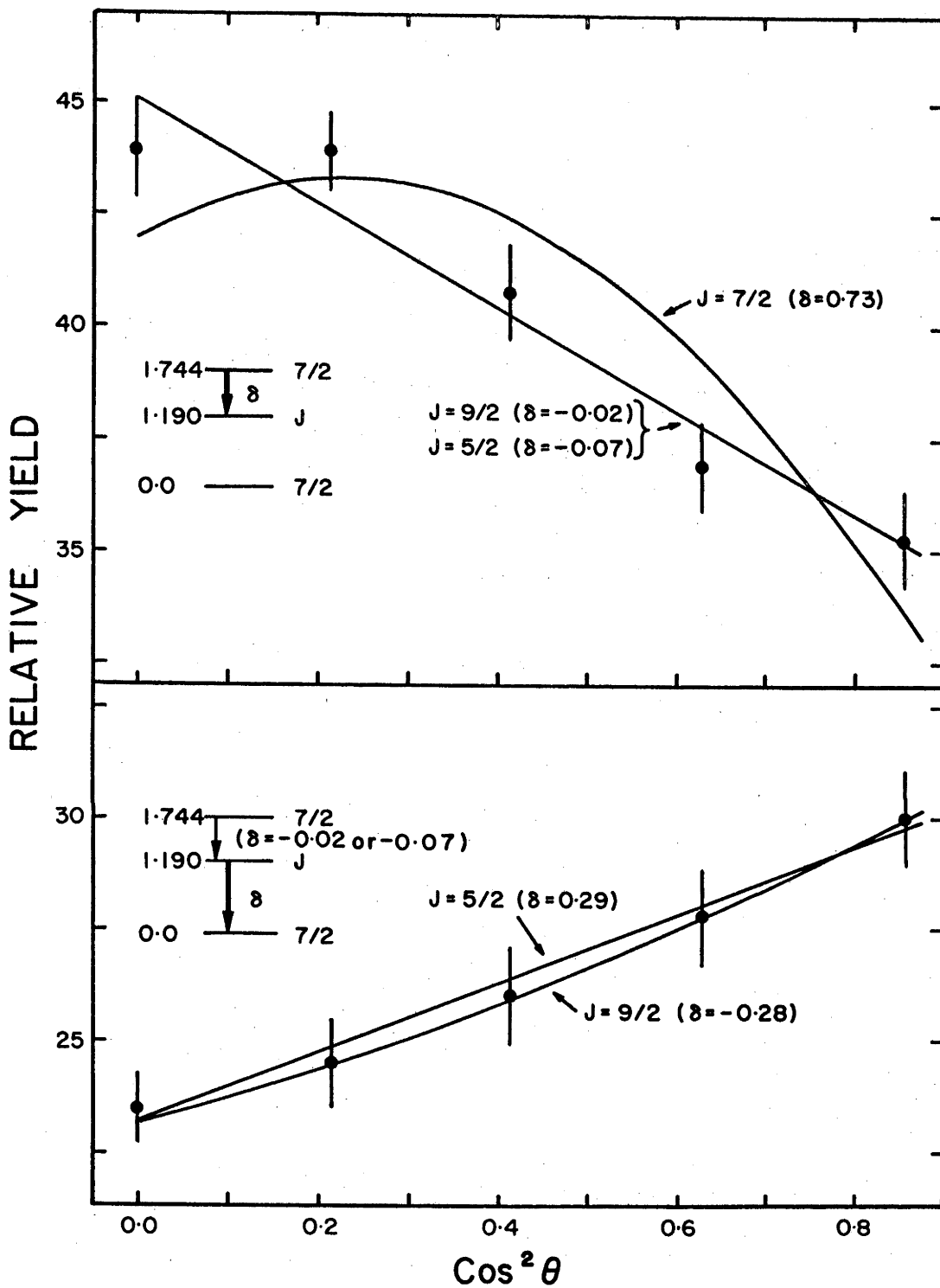


Figure 7.14: $^{56}\text{Fe}(\alpha, p\gamma)$ angular correlations (data set C) involving the $1.744 \rightarrow 1.190 \rightarrow 0.0$ MeV cascade. The heavy arrows in the insets indicate the γ -ray involved.

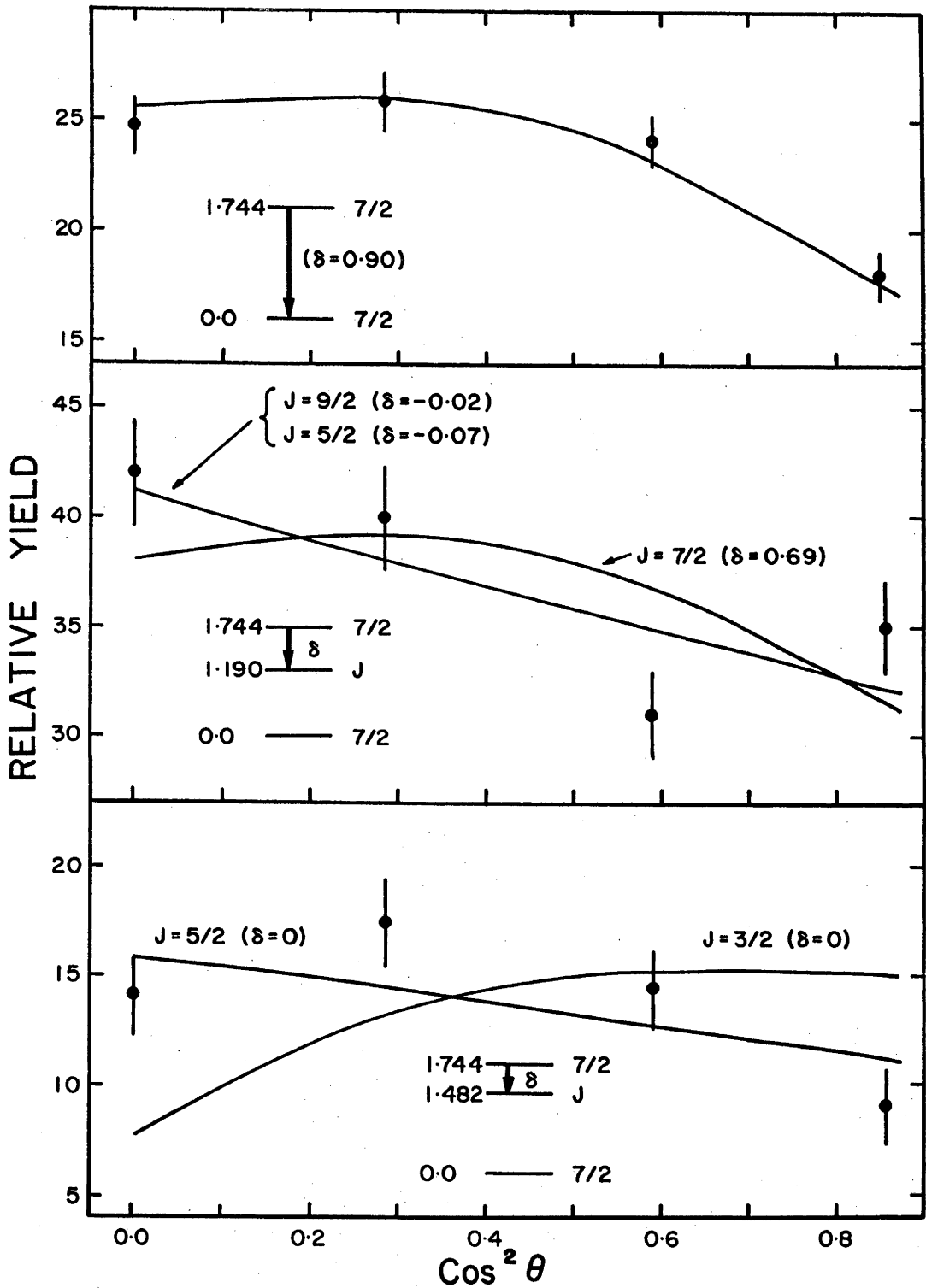


Figure 7.15: $^{56}\text{Fe}(\alpha, p\gamma)$ angular correlations (data set D) for γ -ray decays from the 1.744 MeV state.

Table 7.4

Summary of the theoretical fits to the
angular correlations involving the 1.190 MeV state

Transition and spin sequence	$\frac{P(3/2)}{P(1/2)}$	χ_{\min}^2	Values of the mixing ratio at confidence limits					Data set
			1%	10%	min.	10%	1%	
1.190 to 0.0 MeV								
9/2-7/2	0.0	0.5	-.43	-.37	-.23	-.11	-.06	B
7/2-7/2	0.0	2.6	∞		-4.5		-2.2	B
	0.0	0.8	0.06	0.16	0.38	0.68	0.88	B
5/2-7/2	0.0	0.6	-.04	0.02	0.18	0.41	0.55	B
	0.0	0.4	1.23	1.57	2.7	5.5	9.0	B
13/2-7/2	0.0	99.						E
($\delta=0$)	0.3	93.						E
11/2-7/2	0.0	40.			∞			E
	0.3	28.			∞			E
9/2-7/2	0.0	0.9	-.29	-.27	-.24	-.20	-.18	E
7/2-7/2	0.0	2.6	0.27		0.33		0.39	E
	0.1	2.4	0.26		0.33		0.39	E
5/2-7/2	0.0	1.3	0.13	0.17	0.21	0.26	0.28	E
	0.0	0.9	2.2	2.4	2.8	3.2	3.6	E
3/2-7/2	0.0	1.3						E
($\delta=0$)								
1/2-7/2		7.8						E
1.744 to 1.190 MeV								
7/2-9/2	0.0	1.1	-.07	-.05	-.02	0.01	0.03	C
	0.1	1.1	-.08	-.06	-.03	0.01	0.03	C
7/2-7/2	0.0	3.4			0.73			C
	0.1	2.8	0.68		0.74		0.81	C
7/2-5/2	0.0	1.1	-.11	-.10	-.07	-.05	-.04	C
	0.1	1.1	-.11	-.10	-.07	-.04	-.03	C
7/2-9/2	0.0	2.1	-.10	-.04	-.02	0.0	0.07	D
	0.1	2.1	-.11	-.04	-.02	0.0	0.07	D
	0.0	1.4	5.4	7.1	14.	60.		D
7/2-7/2	0.0	4.7			0.69			D
	0.1	4.4			0.69			D
7/2-5/2	0.0	2.1	-.15	-.09	-.08	-.06	-.01	D

Table 7.4 (cont'd)

Transition and spin sequence	$\frac{P(3/2)}{P(1/2)}$	χ_{\min}^2	Values of the mixing ratio at confidence limits					Data set
			1%	10%	min.	10%	1%	
1.744 (δ_1) to 1.190 to 0.0 MeV 2nd member								
9/2-7/2 ($\delta_1 = -.02$)	0.0 0.1	0.1 0.1	-.37 -.39	-.36 -.37	-.28 -.29	-.22 -.22	-.20 -.21	C C
7/2-7/2 ($\delta_1 = 0.73$)	0.0 0.0	0.5 0.3	-2.6 -.04	-2.2 0.03	-1.6 0.18	-1.2 0.33	-1.0 0.39	C C
5/2-7/2 ($\delta_1 = -.07$)	0.0 0.1 0.0	0.1 0.1 0.1	0.15 0.15 1.5	0.19 0.19 1.6	0.29 0.29 2.2	0.41 0.43 3.0	0.48 0.50 3.3	C C C

ing a contribution from the $|M_1| = 3/2$ substates, but even for $P(3/2)/P(1/2) = 0.1$ they are still poor, especially for data set D, which remains outside the 1% limit. Since the 1.744 MeV state can and does decay by dipole transitions to several different states, it is highly improbable that its lifetime is longer than 10^{-11} sec. Therefore, it is improbable that a $P(3/2)/P(1/2) > 0.1$ is needed to account for the attenuation of the 1.744 \rightarrow 1.190 correlation, and a spin of 7/2 can be fairly confidently ruled out for the 1.190 MeV state.

The choice between 5/2 and 9/2 cannot be made on the basis of the correlation data. The mixing ratios obtained for the 1.190 \rightarrow 0.0 transition are in satisfactory agreement with those obtained by Nordhagen *et al.* [No 67] from B(E2) and lifetime measurements, and with those obtained in the ($^{16}\text{O}, ^{16}\text{O}'\gamma$) correlation measurements. (It is to be noted that they have used a different

phase convention). However, they have argued against $J = 5/2$ on the basis of comparisons with $B(E2)$ values obtained in ^{59}Co and neighbouring nuclei. Also, since the 1.190 MeV state has negative parity [No 67], it could be populated by an allowed β decay from the ^{59}Fe ($3/2^-$) ground state if its spin were $5/2$. This state has not been observed in β decay while higher energy states with $J^\pi = 1/2^-, 3/2^-$ and $5/2^-$ have been.

Thus $9/2^-$ remains the most probable J^π assignment for the level, in agreement with the Hauser-Feshbach calculations of the $(n,n'\gamma)$ cross sections by Daniels and Felsteiner [Da 68].

1.291 MeV State

This state is thought to have a J^π of $3/2^-$ [N.D.S. and No 67], although Daniels and Felsteiner [Da 68] have assigned a spin of $5/2$ on the basis of Hauser-Feshbach fits to $(n,n'\gamma)$ cross sections. A typical γ -ray spectrum from the angular correlation measurement (method B, data set E) is shown in fig. 7.6, and the correlation obtained, with a fit for $J = 3/2$ (pure E2 transition), is contained in fig. 7.11. The fit is not very satisfactory, and, as can be seen from the summary of fits in table 7.5, a spin of $5/2$ could fit the data just as well. Because of the long lifetime of the 1.291 MeV state ($\tau_{1/2} = 0.6$ ns), some perturbation due to hyperfine interactions might be expected, and somewhat better fits can be obtained by assuming a contribution from the $|M_1| = 3/2$ substates. However, the data are not accurate enough to definitely conclude that the correlation is perturbed. No further information on this state could be obtained from the 1.290 - 1.100 MeV transition, because it was not possible to accurately extract the 1.10 or 1.19 MeV γ -rays.

Table 7.5
Summary of the theoretical fits to the 1.291 MeV
angular correlation

Spin sequence	$\frac{P(3/2)}{P(1/2)}$	χ_{\min}^2	Values of the mixing ratio at confidence limits					Data set
			1%	10%	min.	10%	1%	
1.291 to 0.0 MeV								
5/2-7/2	0.0	0.7	.09	.10	.16	.23	.25	E
	0.1	0.7	.09	.10	.16	.23	.26	E
	0.3	0.7	.07	.10	.17	.24	.29	E
3/2-7/2	0.0	0.7	-.19	-.15	-.06	0.03	0.07	E
	0.1	0.7	-.19	-.15	-.04	0.06	0.13	E
	0.3	0.7	-.21	-.15	0.01	0.21	0.40	E
	0.0	0.7	1.25	1.37	1.6	2.0	2.2	E
1/2-7/2		2.1						E

1.482 MeV State

The population of the 1.482 MeV state in β decay by an allowed or first forbidden transition ($\log ft = 7.25$) has been observed by Beraud *et al.* [Be 67], so that it must have a spin of 1/2, 3/2 or 5/2. The 1/2 possibility is highly unlikely, since the state has a large branch to the $7/2^-$ ground state as well as being populated from the 1.744 MeV state ($J^\pi = 7/2^-$).

If the 1.482 MeV state has a spin of 3/2, then the 1.744 \rightarrow 1.482 transition would be expected to be a pure quadrupole transition; the predicted correlation is strongly anisotropic, increasing by a factor of 2 between 90° and 40° . On the other hand, a 7/2 to 5/2 transition (quadrupole/dipole mixture) would be considerably different for most values of the mixing ratio. Thus it was anticipated that a short correlation measurement, involving the 0.26

MeV γ -ray from the 1.744 MeV state, might yield a definite spin value for the 1.482 MeV state.

As can be seen from fig. 7.13, the 0.26 MeV γ -ray could be extracted from the 1.744 MeV angular correlation measurements, although large errors were involved in background subtraction. The correlation obtained along with the fits for $J = 3/2$ ($\delta = 0$) and $J = 5/2$ ($\delta = 0$) is shown in fig. 7.15. A summary of the fits is contained in table 7.6. Although the fit for a spin of 5/2 was outside the 1% confidence limit, the shape of the 3/2 correlation precluded a J of 3/2, and it was concluded that the 1.482 MeV state has a spin of 5/2.

Table 7.6

Summary of the theoretical fits to the
1.744 \rightarrow 1.482 MeV transition angular correlation

Spin sequence	$\frac{P(3/2)}{P(1/2)}$	χ_{\min}^2	Values of the mixing ratio at confidence limits					Data set
			1%	10%	min.	10%	1%	
1.744 to 1.482 MeV								
7/2-5/2	0.0	2.4	-.15		-.02		0.10	D
	0.1	2.4	-.15		-.02		0.10	D
7/2-3/2	0.0	4.2			0.5			D
	0.1	3.2	0.40		0.7		1.7	D
($\delta=0$)	0.0	10.2						D
($\delta=0$)	0.1	9.7						D

A parity assignment to this state is not possible with the existing experimental data. With a $\delta = 0$ for the 1.744 ($7/2^-$) \rightarrow 1.482 ($5/2$) transition, the multipolarity could be either E1 or M1.

If the mixing ratio is non-zero, then the most probable assignment is negative, as an M2/E1 mixture is unlikely to occur.

1.744 MeV State

The angular distribution of the α -particle group populating the 1.744 MeV state in the $^{60}\text{Ni}(t,\alpha)$ reaction [Bl 66], is thought to be characteristic of an $\ell = 3$ pickup pattern. This limits the J^π value of the state to $5/2^-$ or $7/2^-$ [N.D.S.]. If the assumptions of Blair and Armstrong [Bl 66] regarding the (t,α) reaction mechanism and the configuration of the ^{61}Ni ground state are correct, then $7/2^-$ is the most probable assignment. The level is populated in a number of other reactions, but has not been seen in β decay studies [N.D.S.]. This would also favour the $7/2^-$ assignment.

As the 1.744 MeV state is at least 250 keV from its nearest neighbour, it is particularly amenable to study using the annular counter (method B, section 7.3.2). Two separate measurements were made, and the ground state correlations obtained are shown in fig. 7.15 (data set D) and fig. 7.16 (data set C). From the plots of χ^2 vs. $\tan^{-1} \delta$ shown in fig. 7.16, it is clear that the only satisfactory fit is obtained with a J of 7/2 for the 1.744 MeV state. A summary of the theoretical fits for both measurements is contained in table 7.7.

The results of the $^{56}\text{Fe}(\alpha,p\gamma)$ correlation measurements are summarized in table 7.8.

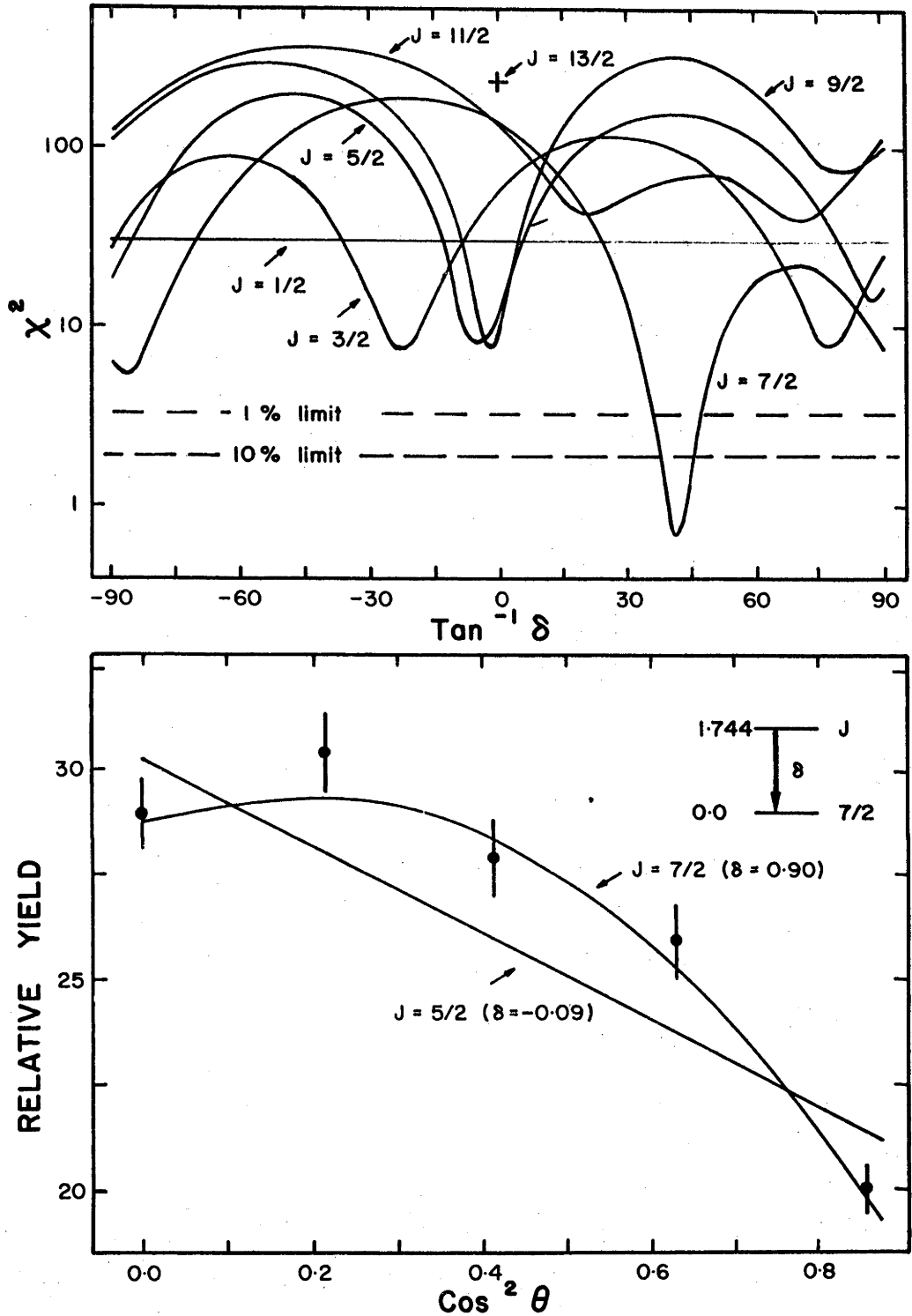


Figure 7.16: $^{56}\text{Fe}(\alpha, p\gamma)$ angular correlation obtained for the ground state decay of the 1.744 MeV state (data set C).

Top: Plots of χ^2 vs. $\tan^{-1}\delta$. The curves are labelled with the spin value used for the initial state.

Bottom: The curves shown are the calculated correlations obtained with the J and δ indicated.

Table 7.7

Summary of the theoretical fits to the 1.744 MeV
angular correlation

Spin sequence	$\frac{P(3/2)}{P(1/2)}$	χ_{\min}^2	Values of the mixing ratio at confidence limits					Data set
			1%	10%	min.	10%	1%	
1.744 to 0.0 MeV								
13/2-7/2	0.0	235.						C
($\delta=0$)	0.3	228.						C
11/2-7/2	0.0	40.			2.7			C
	0.3	28.			2.7			C
9/2-7/2	0.0	7.7			-.02			C
	0.1	7.6			-.02			C
7/2-7/2	0.0	0.7	0.74	0.78	0.88	1.02	1.09	C
	0.1	0.9	0.76	0.81	0.91	1.05	1.13	C
5/2-7/2	0.0	7.6			-.09			C
	0.1	7.6			-.09			C
3/2-7/2	0.0	7.6			-.41			C
1/2-7/2		31.						C
7/2-7/2	0.0	0.3	0.58	0.63	0.85	1.10	1.30	D
5/2-7/2	0.0	3.2	-.11		-.06		0.01	D
	0.1	3.2	-.13		-.06		-.02	D

7.5 ^{61}Co RESULTS

Initial attempts at measuring the decay scheme of levels in ^{61}Co , using the $^{58}\text{Fe}(\alpha, p\gamma)$ reaction, were made in two experiments, one with the magnetic spectrometer and NaI detector, and the other with the annular counter and Ge(Li) detector. Both experiments were unsuccessful because of low yields and interference from the $^{56}\text{Fe}(\alpha, p)$ reaction. (The target contained 16% ^{56}Fe , and the (α, p) cross section for this isotope was generally several times larger than for ^{58}Fe .)

Table 7.8

Spins and mixing ratios deduced in the
 $^{56}\text{Fe}(\alpha, p\gamma)$ correlation measurements

Initial state		Mixing ratio	Final state	
Energy	Deduced J^π			
1.100	Consistent with $3/2^-$, pure E2 transition	0.0		$7/2^-$
1.190	$9/2^-$	-0.25 ± 0.05	0.0	$7/2^-$
	$(5/2^-)$	$0.22 \begin{matrix} + 0.09 \\ - 0.06 \end{matrix}$		
1.291	Consistent with $3/2^-$, pure E2 transition	0.0		$7/2^-$
1.482	$5/2^-$			
1.744	$7/2^-$	$0.89 \begin{matrix} + 0.25 \\ - 0.17 \end{matrix}$	0.0	$7/2^-$
		-0.02 ± 0.05	1.190	$9/2^-$
		$-0.07 \begin{matrix} + 0.03 \\ - 0.04 \end{matrix}$		$(5/2^-)$
		-0.02 ± 0.13	1.482	$5/2^-$

The mixing ratios were obtained from simultaneous fits to all data sets; the limits were obtained from the 1% confidence limits of the χ^2 vs. δ plots. (The fits for both $P(3/2)/P(1/2) = 0.0$ and 0.1 were considered and the largest $\Delta\delta$ compatible with either fit is shown above.)

A more successful approach was made by comparing two-dimensional coincidence spectra obtained with an ^{56}Fe target (99.9% ^{56}Fe) and an ^{58}Fe target (82% ^{58}Fe , 16% ^{56}Fe). The configuration and electronics used were those of method B (section (7.3.2) with the NaI detector at 55° , 10 cm from the target. Initial measurements were made with the 1.65 MeV doublet in ^{61}Co . As discussed in

section 6.3.3, it was not known which of these two states is populated in β decay. The state observed in β decay studies [N.D.S.] decays entirely to the ground state, so that a measurement of the branching ratios from the doublet could resolve this question.

After an excitation function was measured, a bombarding energy of 11.27 MeV was chosen because the annular counter spectrum showed a relatively high yield of protons to the 1.65 MeV doublet from the $^{58}\text{Fe}(\alpha, p)$ reaction, compared to the yield to the interfering states in ^{59}Co from the $^{56}\text{Fe}(\alpha, p)$ reaction. This is demonstrated in fig. 7.17 where particle spectra are shown for both the ^{56}Fe and ^{58}Fe targets. Two two-dimensional coincidence spectra were obtained - one containing information on the ^{59}Co and ^{61}Co states, and the other containing information on only the ^{59}Co states.

The γ -ray slices, summed over the region of interest, are shown in fig. 7.18. Three γ -rays can be seen to be associated with ^{61}Co ; their energies are 1.65 ± 0.04 , 1.29 ± 0.03 , and 0.35 ± 0.02 MeV. The spectra therefore demonstrate that one of the pair of levels at 1.65 MeV has a large branch to the 1.287 MeV state which then decays to the ground state. To determine which member of the doublet decays through the 1.287 MeV state, the summed γ -ray spectrum (slices 15 - 17), shown in the upper diagram of fig. 7.18 was divided into two spectra - slices 15 and 16 in coincidence with proton pulses of lower amplitude were summed and compared with slice 17 which was in coincidence with higher energy protons. These two spectra are shown in fig. 7.19. By comparing the counts in the 0.35 and 1.29 MeV photopeaks with those in the 1.65 MeV photopeak, it could be deduced that the lower member of the doublet (1.623 MeV) branches to the 1.287 MeV state. This is confirmed by addi-

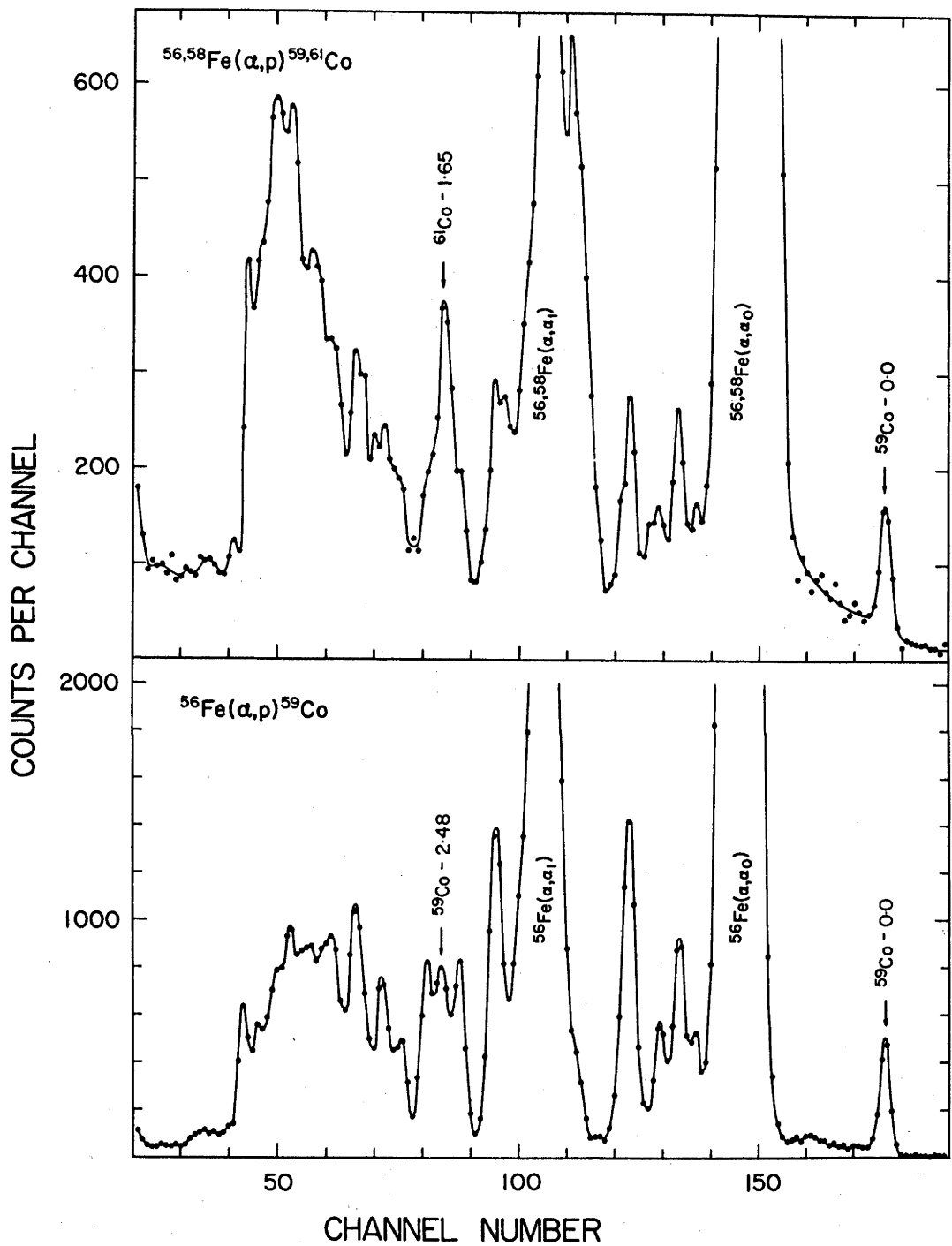


Figure 7.17: Particle singles spectra obtained in the annular counter.

Top: From an enriched ^{58}Fe target.

Bottom: From an enriched ^{56}Fe target.

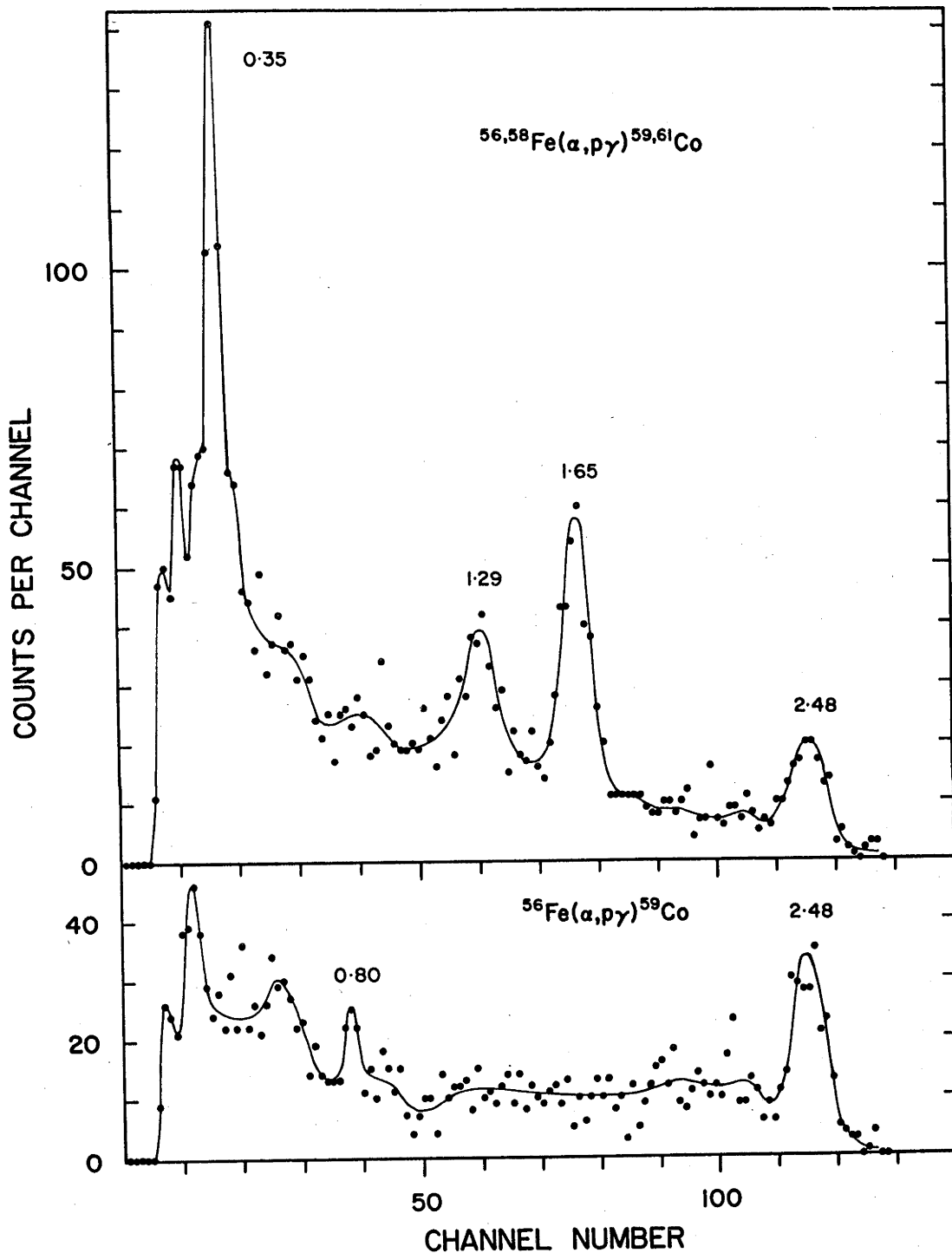


Figure 7.18: γ -ray decay of states in ^{59}Co and ^{61}Co obtained using the $(\alpha, p\gamma)$ reaction.

Top: From an enriched ^{58}Fe target.

Bottom: From an enriched ^{56}Fe target.

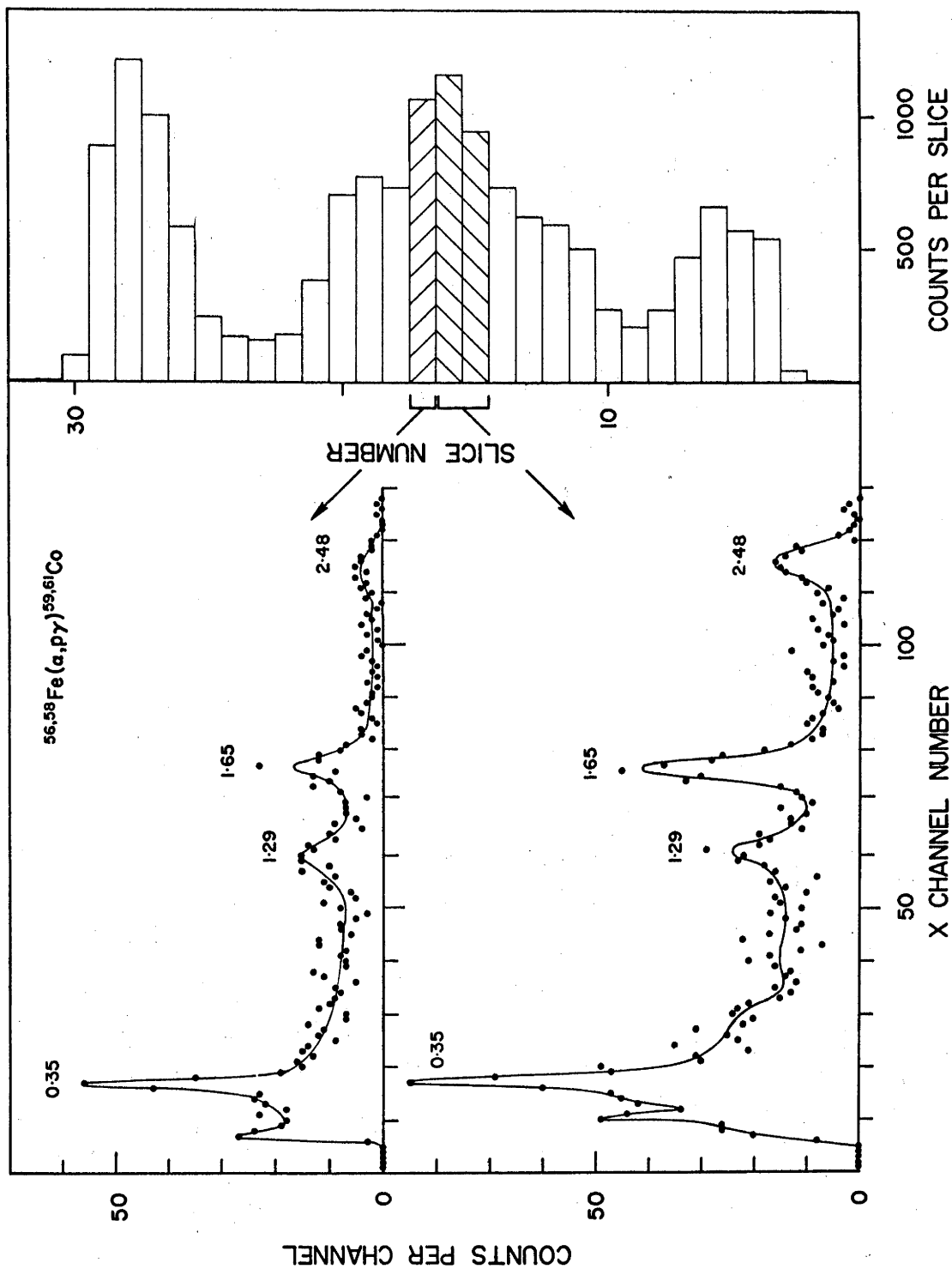


Figure 7.19: γ -decay of states in ^{59}Co and ^{61}Co obtained using the $(\alpha, p\gamma)$ reaction with an enriched ^{58}Fe target. The proton coincidence spectrum is shown on the r.h.s. of the diagram. The γ -ray spectra were obtained as indicated.

tional results obtained with a Ge(Li) detector discussed later in this section. Thus, the 1.655 MeV level is populated in β decay and therefore has a spin of $3/2$ or $5/2$. This conclusion is in contradiction to the current assignment in Nuclear Data Sheets [N.D.S.], where the compilers assumed that the 1.623 MeV level was populated and on this basis assigned a spin of $(5/2)^-$.

Attempts were made to look at higher energy states of ^{61}Co using the same procedure, but the data acquired were too complex for analysis with a reasonable investment of time.

After some trials, it was found possible to use the 40 cc Ge(Li) detector and an annular counter to detect coincidence γ -rays in the $^{64}\text{Ni}(p, \alpha\gamma)$ reaction (method C, section 7.3.3). A bombarding energy of about 10 MeV or more is required if the outgoing α -particles of interest are to be near or above the top of the Coulomb barrier. However, large neutron and γ -ray backgrounds, which increase rapidly with increasing bombarding energy, can be expected with proton induced reactions at these energies. The actual coincidence run was performed at 10.00 MeV using the timing electronics shown in fig. 7.8.

Coincident γ -rays from four different α -particle groups were selected by four windows on the annular counter spectrum, as indicated in fig. 7.20. The windows were set on:

- (a) the ground state group to collect the random spectra;
- (b) the 1.65 MeV doublet;
- (c) the 1.887, 1.953 and 2.015 MeV states; and
- (d) the 2.230, 2.302 and 2.343 MeV states.

Because the discriminator cut-offs were smeared somewhat, a large part of the 2.015 MeV state was excluded from window (c). Likewise,

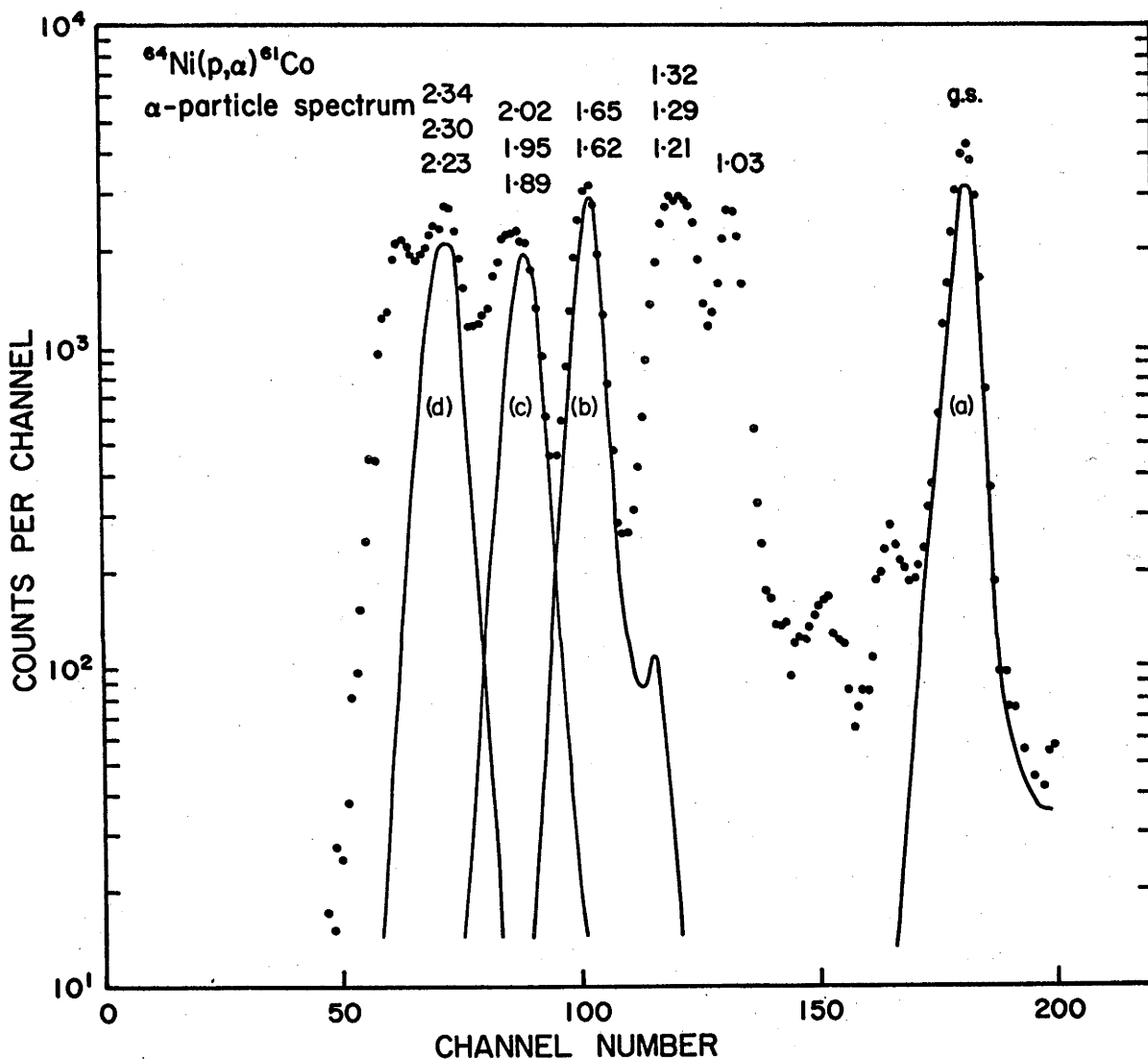


Figure 7.20: A typical particle spectrum obtained in the annular counter from the $^{64}\text{Ni}(p,\alpha)^{61}\text{Co}$ reaction. The solid lines indicate the shape of the gated spectra obtained in the four windows described in the text. The α -particle groups are labelled by the excitation energy (MeV) of the states populated in ^{61}Co .

the 2.343 MeV state, and to a lesser extent the 2.302 MeV state, might have been excluded from window (d). The coincidence spectra were accumulated for a total time of 30 hours with a beam of 0.2 μA . During this time the resolution of the detector decreased measurably due to neutron damage.

The γ -ray detection system was calibrated with ^{228}Th and ^{60}Co sources before and after the measurement. A fairly large deviation from a straight line calibration was observed for the lower γ -ray energies, so that a parabola was fitted to the 0.239, 0.511 and 0.583 MeV calibration points to provide a calibration curve below 0.5 MeV. The relative full energy efficiencies determined by Huang [Hu 68] and Black *et al.* [Bl 68] were used to obtain relative γ -ray intensities. The efficiency curves were corrected at the low energy end to allow for attenuation in the perspex wall of the target chamber. (The corrections were determined by a subsidiary experiment with a ^{228}Th source.)

For display purposes the 1024 channel spectra have been compressed to 512 channels; they are shown in fig. 7.21. For the purposes of discussion, the energies of levels as deduced in chapter 6 will be used, even though the values obtained in the present experiment are more accurate. These energy level values and the branching ratios deduced, are listed in table 7.9; the branching ratios are also shown schematically in fig. 7.22.

The 1.623 and 1.655 MeV States (Slice (b))

Examination of slice (b) in fig. 7.21 reveals that both members of the doublet have branches to the ground state. In agreement with the $(\alpha, p\gamma)$ experiment, the 1.623 MeV state was observed to

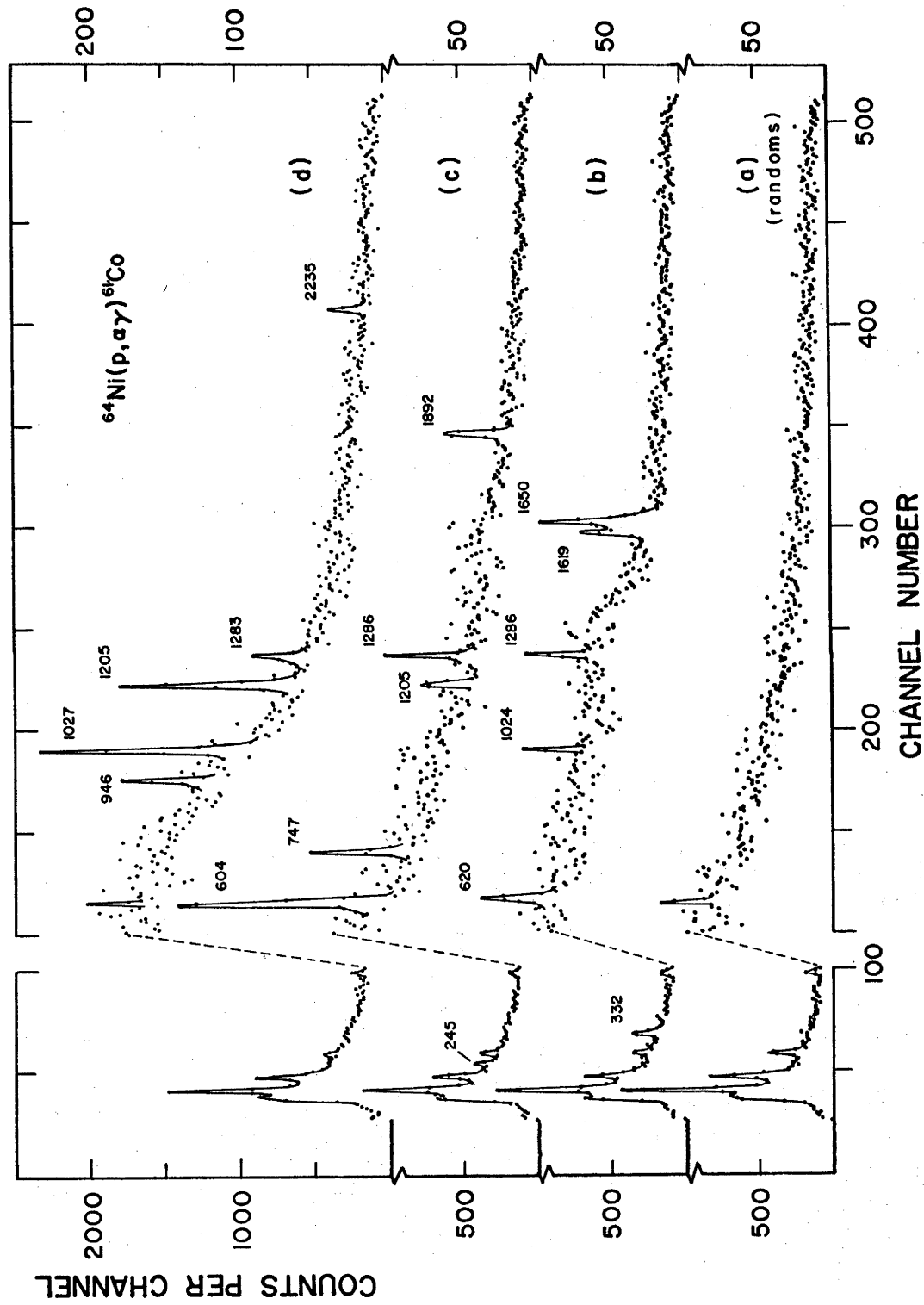


Figure 7.21: The γ -ray spectra obtained in the $^{64}\text{Ni}(p, \gamma)^{61}\text{Co}$ reaction. The energies of the γ -rays are shown near the full energy peaks.

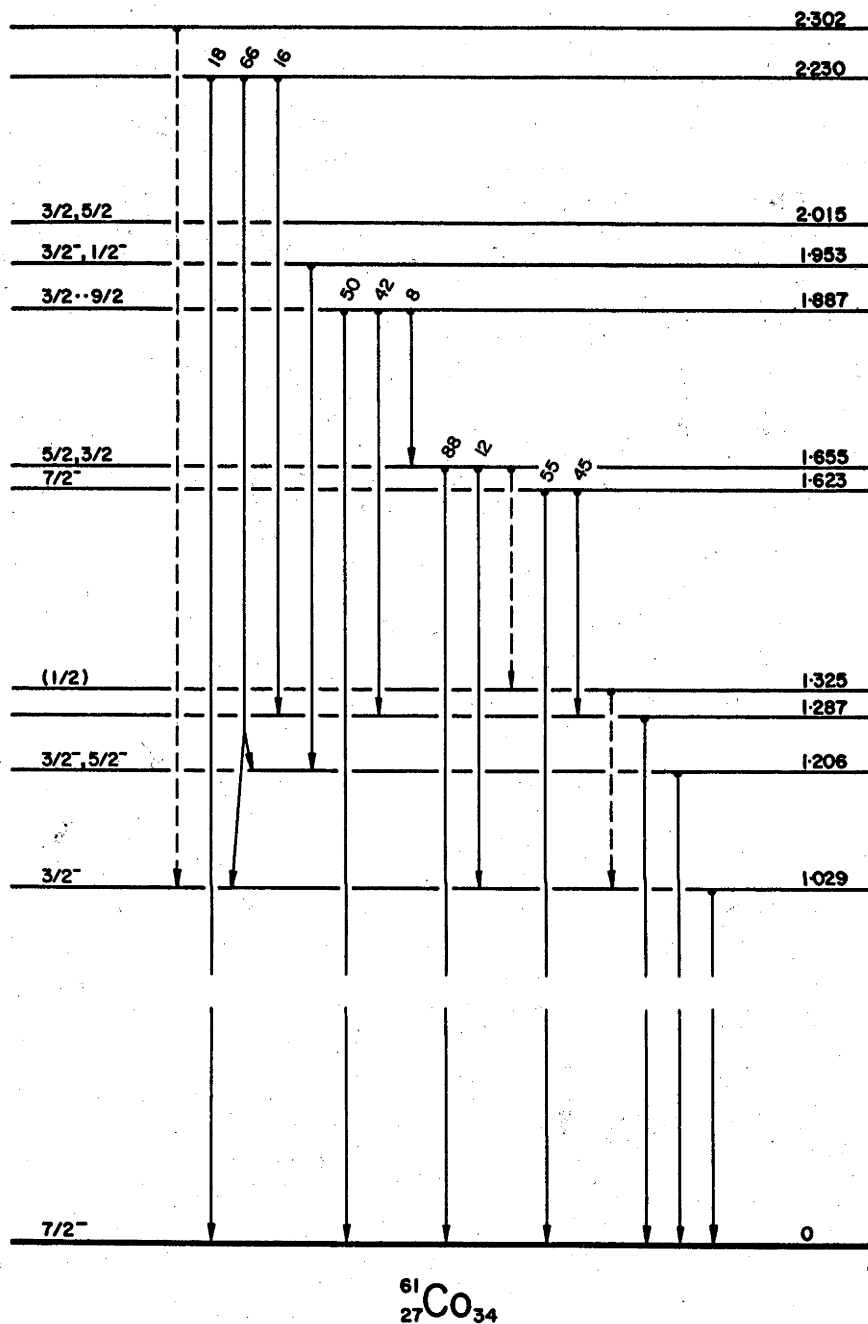


Figure 7.22: The decay scheme of ^{61}Co as determined in the present experiment. The J^π values were obtained from the present and previous experiments.

Table 7.9
 γ -ray branching ratios for ^{61}Co

Initial state energy obtained from (p, α) experiment	Initial state	Final state	Branching ratios	
	Energies from chapter 6		Present exp. \pm standard error	[N.D.S.]
1.025	1.029	0.0	100	100
1.205	1.206	0.0 1.029	100	96 4
1.285	1.287	0.0	100	
	1.325	0.0 1.029 1.206		80 20
1.619	1.623	0.0 1.287	55 \pm 8 45 \pm 8	100
1.647	1.655	0.0 1.029	88 \pm 4 12 \pm 4	
1.891	1.887	0.0 1.287 1.655	50 \pm 8 42 \pm 8 8 \pm 3	
1.952	1.953	0.0 1.206	< 20 100	100
	2.015	0.0		
2.232	2.230	0.0 1.029 or) 1.206) 1.287	18 \pm 7 66 \pm 9 16 \pm 5	100
	2.302	1.029	(tentative assignment)	

have a large branch to the 1.287 MeV state, which in turn decays to the ground state. A small branch (12%) from the 1.655 MeV state to the 1.029 MeV state was also observed. This again raises the question of which member of the doublet is populated in β decay, since,

in the β decay studies of Grench *et al.* [Gr 67], and others, only a 1.65 MeV \rightarrow ground state transition is reported. However, in the Ge(Li) spectrum of Grench *et al.* the 0.34 MeV γ -ray (1.623 to 1.287) would have had a relative intensity of $\sim 7\%$, and would have been readily apparent if present, while the 0.63 MeV γ -ray (1.655 to 1.029), with a relative intensity of $\sim 1.2\%$, would not have been seen. Therefore, it appears that the J^π of the 1.623 MeV state is $7/2^-$, as reported in the (t, α) and (t,p) studies [Bl 66, Hu 71]. The 1.655 MeV level could have a spin of $3/2$ or $5/2$ on the basis of its population in β decay, although the (t, α) and (t,p) data favour a spin of $5/2^-$.

The 1.887, 1.953 and 2.015 MeV States (Slice (c))

The decay modes of the 1.887 and 1.953 MeV states are deduced from slice (c) of fig. 7.21; no γ -rays were observed which can be attributed to the 2.015 MeV state. The 1.887 MeV state was seen to decay to the $7/2^-$ ground state, to the 1.287 MeV state and to the $5/2^-$ ($3/2^-$) 1.655 MeV state. Thus the possible spin assignments are $3/2$, $5/2$, $7/2$ and $9/2$, assuming dipole or quadrupole transitions. The 1.953 MeV state decays to the 1.206 MeV state with an upper limit of 20% placed on a possible ground state branch. This is consistent with the $3/2^-$ assignment from the (t, α) studies [Bl 66], since the 1.206 MeV state is considered to have $J^\pi = 3/2^-$ or $5/2^-$.

Although the decay of the 2.015 MeV state was not observed here, its decay can be inferred from the present data and β decay studies. Since the 1.953 MeV state decays primarily by a cascade to the 1.206 MeV state, it follows that the 2.015 MeV state is populated

in β decay and decays primarily to the ground state. The spin of the 2.015 MeV state can then be limited to $3/2$ or $5/2$ ($1/2$ is improbable because of the ground state decay).

Grench *et al.* [Gr 67] saw a very weak 1.20 + 0.80 MeV pair of coincident γ -rays in their β decay studies, but did not consider the transition definitely established. It is possible that this was an indication of a weak population of the 1.953 to 1.206 cascade in β decay.

The 2.230 MeV State (Slice (d))

The main γ -rays observed in slice (d) of fig. 7.21 were all attributed to the 2.230 MeV state, although there was some evidence for a possible weak transition from the 2.302 MeV state to the 1.029 MeV state. The evidence was based on the broadening of the 1.287 MeV full energy peak. As mentioned above, the window on the α -particle spectrum probably excluded most of the α -particle pulses corresponding to the population of this state.

In addition to the ground state decay of the 2.230 MeV state, branches were observed to the 1.287 MeV state and to either the 1.029 or 1.206 MeV states, or to both. It was not possible to distinguish between the last two possibilities, since both give rise to pairs of γ -rays of the same energies (within experimental error). Because the intensities of both members of the cascade were equal, they cannot be attributed to decays from higher energy states.

A state near 2.230 MeV has been observed in both (t, α) and (t,p) studies [Hu 71]. However, the (t, α) work indicated a state at 2.250 MeV with a spin of $1/2^+$ while the (t,p) angular distributions indicated a state at 2.240 MeV with negative parity. Both assign-

ments are unambiguous, so that it appears that the present (p, $\alpha\gamma$) work populated one member of a close doublet at this energy. (In the (p, α) spectrometer measurements there was no evidence for a doublet with a separation of > 5 keV). The decay of the 2.230 MeV level observed here, to the $3/2^-$ 1.029 MeV state, is consistent with both assignments. However, decay to the $7/2^-$ ground state would require an E3 (or M4) transition, which on the basis of the Weisskopf single particle estimates, is about a factor of 10^8 slower than possible E1 transitions to other states (e.g. the 1.029 MeV state). An E3 enhancement of more than 10^2 can be ruled out [N.D.S.], and an E1 retardation of at least 10^6 , which is required for the E1 and E3 transitions to compete, though possible, is unlikely [Go 66]. Thus the evidence is that the state populated in the (p, α) reaction is the negative parity state observed in the (t,p) studies.

The other decay mode of the 2.230 MeV state is through the 1.287 MeV state, whose spin is not known. The 1.287 MeV level has been seen in the (t,p) reaction, but is only weakly populated in the (t, α) reaction, and has not been observed in β decay studies. This, along with the population of the level through transitions from the $7/2^-$, 1.623 MeV state and the 1.887 MeV state (which could be $7/2$ or $9/2$), and the non-population by transitions from states with known spins of $3/2$ or $5/2$, is consistent with a high spin assignment ($\geq 9/2$) for the 1.287 MeV level. This would definitely rule out a spin of $1/2^+$ for the 2.230 MeV level, since transitions slower than octupole would have lifetimes longer than the resolving time of the coincidence circuit used in the present experiment.

A consistent set of spin assignments can now be suggested to fit the observed decays. Allowing dipole and quadrupole transi-

tions, the spin of the 1.287 MeV state can be $9/2$, $11/2$ or $13/2$, so that the spins of both the 1.887 and 2.230 MeV states can be $5/2$, $7/2$ or $9/2$. However, these assignments are only conjectural and no more can be said without more information on the spin and parity of the 1.287 MeV state.

7.6 DISCUSSION

The level schemes for ^{59}Co and ^{61}Co are shown in fig. 7.23. The J^π values and modes of decay obtained in the present and previous experiments [N.D.S.], for some of the levels are indicated. Also shown is the level scheme for ^{59}Co calculated by Satpathy and Gujrathi [Sa 68]. The calculated level scheme for ^{61}Co is similar and is shown in fig. 6.5.

The dashed lines in fig. 7.23 connect levels in the two nuclei which have energy ratios of $E(^{59}\text{Co})/E(^{61}\text{Co}) \approx 1.08$, as discussed in chapter 6. It can be seen that the 4 lower pairs of levels have similar decay schemes and possibly the same J^π values. However, this similarity is not carried on to the other four pairs of levels connected by dashed lines. The decays from the 2.085 - 1.953 MeV pair and the 2.183 - 2.015 MeV pair have no common features. There are some similarities in the decays of the states at 2.394 (^{59}Co) and 2.230 (^{61}Co) MeV, but a transition to the 1.623 MeV state is missing in ^{61}Co , while that to the low lying $3/2$ or $5/2$ state, which appears in ^{61}Co , is not present in ^{59}Co . Information on the decay of the 2.302 MeV state in ^{61}Co is insufficient to allow an adequate comparison to be made with that of the 2.476 MeV state in ^{59}Co . However, if the 2.302 MeV state decays to the 1.029 MeV

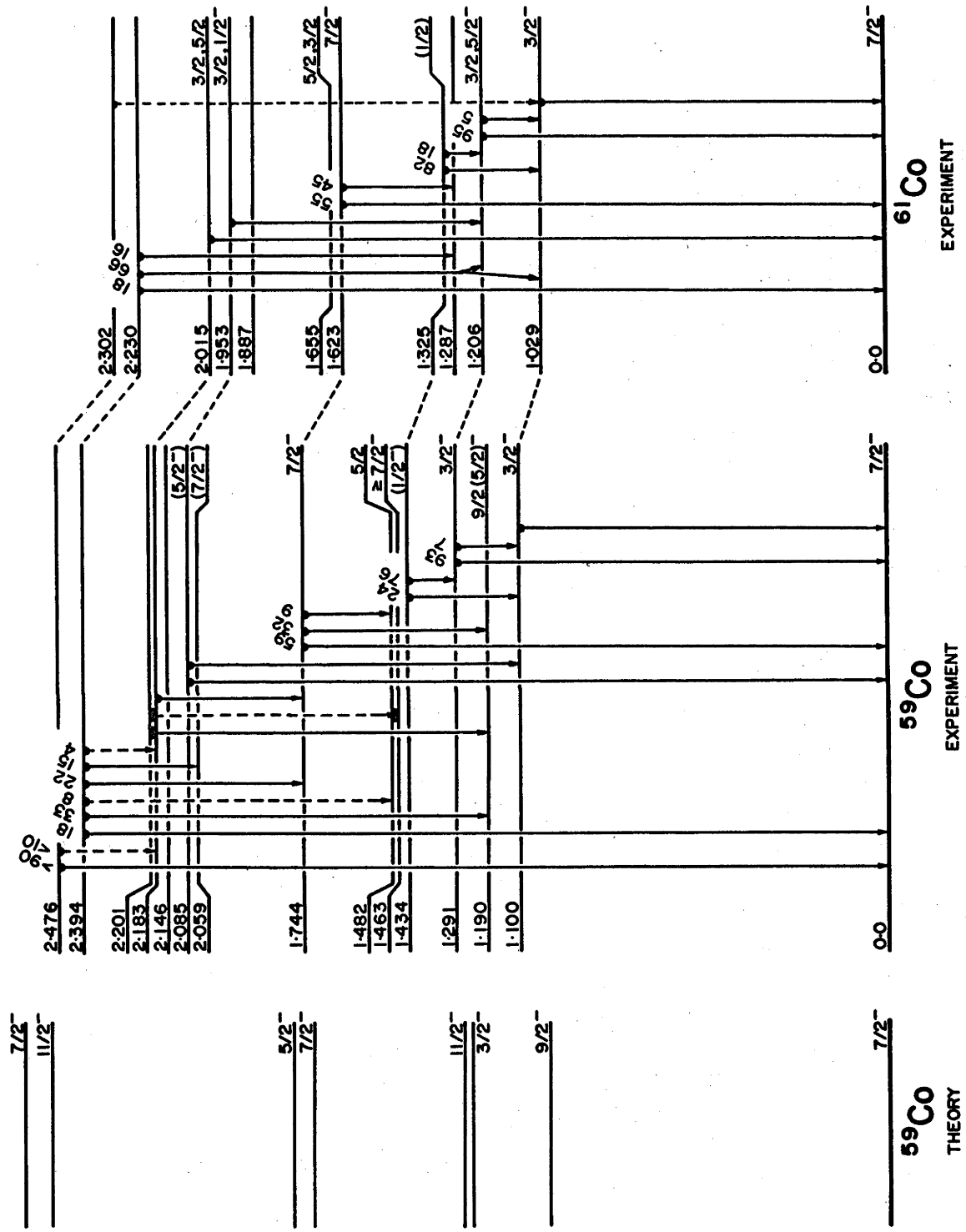


Figure 7.23: Energy level diagrams of ^{59}Co and ^{61}Co obtained from the results of the present and previous experiments. Also shown are the calculated energy levels of ^{59}Co [Sa 68].

state, as tentatively indicated, then the decay schemes of the pair of levels are obviously different.

Further evidence for similarities in level structure for the low lying states of ^{59}Co and ^{61}Co , gained from (t,α) and $(^3\text{He},d)$ data, is discussed in relation to the other odd-mass cobalt nuclei in chapter 8.

Unfortunately, the calculations of Satpathy and Gujrathi [Sa 68] did not include the extraction of mixing and branching ratios, although such calculations can be made within the framework of the model used. Theoretical values for these quantities would be useful in correlating the experimentally determined states with the calculated ones, and would also serve as a further check on the model. Corello and Manfredi [Co 71] have made similar calculations for ^{57}Co , and their theoretical values for E2/M1 mixing ratios agree well with the experimental values of Coop *et al.* [Co 70].

Satpathy and Gujrathi [Sa 68] predicted two low-lying high-spin states in ^{61}Co ($9/2^-$ and $11/2^-$). The present experiment has provided evidence for only one (1.287 MeV). The only other likely candidate is the 1.887 MeV state which is well away from the predicted position. Another serious discrepancy exists in ^{59}Co , where the doublet which appears in both ^{57}Co and ^{61}Co , should appear in ^{59}Co at ~ 1.75 MeV. Branching ratios taken at different bombarding energies indicate that the level observed in 1.744 is a single isolated state. There are, therefore, still some apparently unreconcilable differences between the calculated and theoretical level schemes for ^{59}Co and ^{61}Co .

CHAPTER 8

CONCLUSIONS

The purpose of this chapter is to discuss the systematics in the level structure of the odd-mass cobalt nuclei, ^{57}Co , ^{59}Co and ^{61}Co . The low lying levels of the three nuclei are shown in fig. 8.1, together with the level scheme for ^{55}Co [Ro 70] and the scheme obtained for ^{63}Co from $^{64}\text{Ni}(t,\alpha)$ experiments [Bl 66].

There is now a large body of information available on the low lying levels of $^{55,57,59,61}\text{Co}$, and, to a lesser extent, ^{63}Co . The lowest excited states of ^{55}Co appear at relatively high excitation and are widely spaced - properties to be expected in a nucleus differing by one nucleon from a doubly closed shell. The addition of two neutrons into the $2p$ or $1f$ shell to form ^{57}Co , produces a marked decrease in excitation energy for the lowest levels and an increase in level density. With the addition of further pairs of neutrons, the energy of the first excited state continues to decrease, but it is not immediately obvious that this is the case for low lying levels in general. In a simple approach, one would expect any pure proton hole states to be little affected by the addition of the neutron pairs. Blair and Armstrong, in their (t,α) studies [Bl 66], observed that the excitation energies of the $(2s_{1/2})^{-1}$ and $(1d_{3/2})^{-1}$ states, which appear at several MeV excitation, decrease with increasing mass number.

It was noted in chapter 6, that the $(^3\text{He},d)$ reaction, proceeding largely via a simple stripping mechanism, is expected to preferentially populate states which have a strong single particle character. The states identified in this way were found to be the

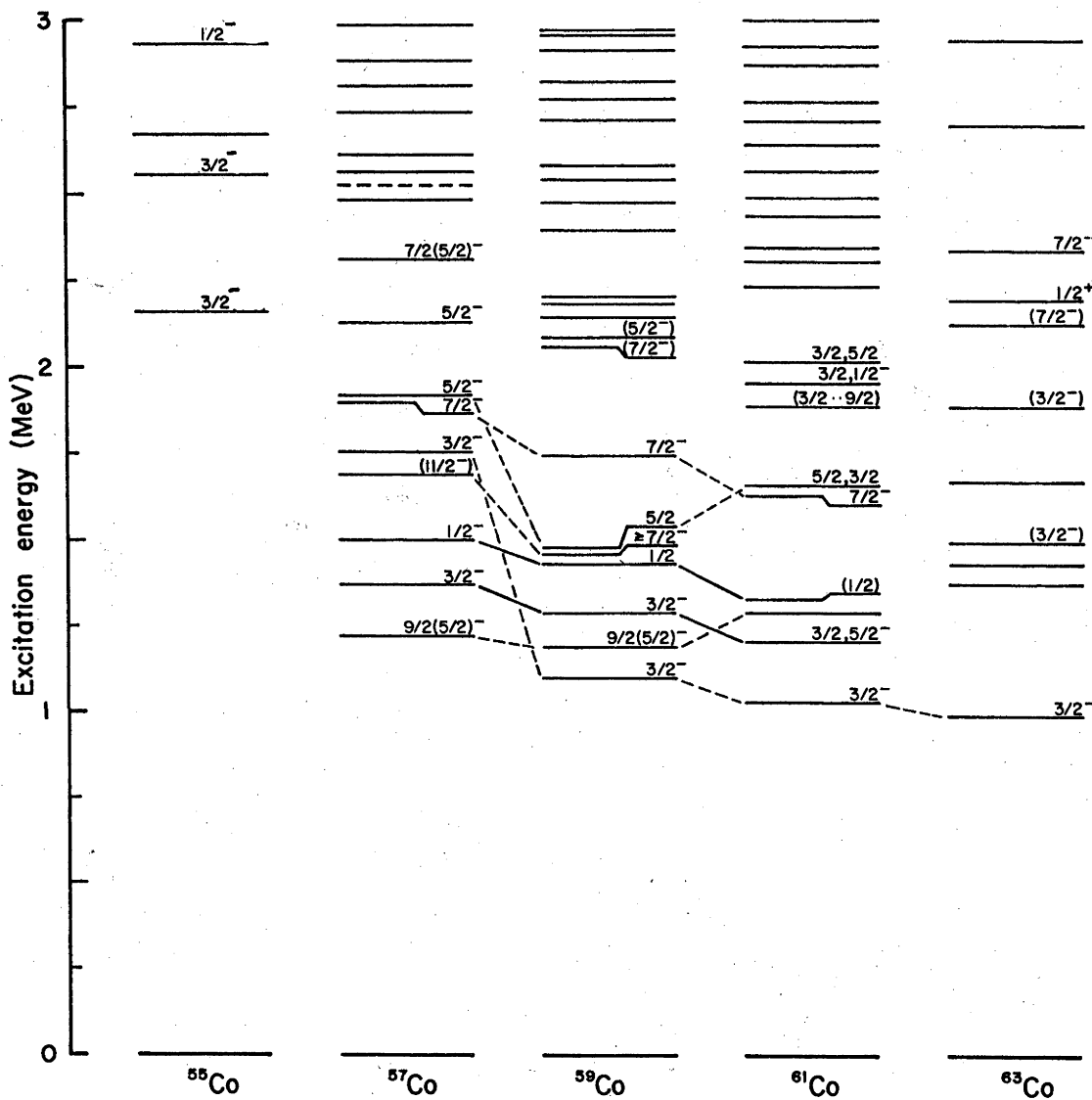


Figure 8.1: Energy levels of the odd mass cobalt nuclei, $^{55-63}\text{Co}$. The information regarding the levels in ^{55}Co , ^{57}Co and ^{63}Co was obtained from Roussel *et al.* [Ro 70], Coop *et al.* [Co 70] and Blair and Armstrong [Bl 66] respectively. The level schemes for ^{59}Co and ^{61}Co are those deduced in the present work.

states not described by the collective model calculations of Satpathy and Gujrathi [Sa 68]. On the other hand, the (t,α) reaction tends to populate states which can be described in terms of the target nucleus coupled to a proton hole. Owing to the large number of final states populated in these reactions on the Ni isotopes [Bl 66], many of these hole states must be coupled to an excited or deformed core (the basis of the calculations of Satpathy and Gujrathi). In fact, Nordhagen *et al.* [No 67] have observed that states in ^{59}Co which are enhanced in the (t,α) reaction, were found to be highly collective in character from (d,d') and $(^{16}\text{O},^{16}\text{O}')$ reaction studies; also, in general, states strongly populated in the (t,α) reactions [Bl 66], are weakly, or not at all, populated in the $(^3\text{He},d)$ reactions [Ro 67], and vice versa. Thus, states that are strongly populated in the (t,α) reaction, might be expected to have substantial collective components.

In fig. 8.1, levels in $^{57,59,61}\text{Co}$ which appear to have the same J^π values and similar γ -ray decay schemes, are connected by solid and dashed lines. States which may have single particle components on the above criteria are joined by solid lines, while those states of suspected collective nature are joined by dashed lines. Some of these similarities between states in ^{57}Co and ^{59}Co have been pointed out previously by Nordhagen *et al.* [No 67] and Gatrousis *et al.* [Ga 69]. The latter authors have also suggested that there are different major configurations for some of the states in ^{57}Co ; on the basis of the available evidence, this suggestion would appear to be valid for ^{59}Co and ^{61}Co as well. In this regard, the decays of the $J = 5/2$ levels which are connected by dashed lines, are worthy of note - all have ground state branches and branches to $J = 3/2$

levels connected by dashed lines, but have no branches to the $J = 3/2$ levels connected by solid lines. In contrast, the $5/2^-$ state at 2.127 MeV in ^{57}Co , which was strongly populated in the $(^3\text{He},d)$ reaction [Ro 67] and would therefore appear to have a strong single particle character, decays to the single particle $1/2^-$ and $3/2^-$ states, but not to any of the other complex states.

The systematic change in energy of the states connected by solid lines suggests the presence of two states in ^{63}Co at 1.1 and 1.3 MeV excitation. Because of the suggested single particle character of these levels, the (t,α) reaction would not be expected to excite them at the 15 MeV bombarding energy used by Blair and Armstrong [Bl 66]. However, evidence for their existence might be obtained at lower bombarding energies, where the compound nucleus mechanism is more important.

In the intermediate coupling calculations of Satpathy and Gujrathi [Sa 68], the schemes for the low lying negative parity states were very similar in the four nuclei, ^{57}Co , ^{59}Co , ^{61}Co and ^{63}Co , showing a decrease in excitation energy for increasing mass number, but keeping the same ordering of the states. However, the suggested collective states in the experimentally determined level schemes of $^{57,59,61}\text{Co}$, joined by dashed lines in fig. 8.1, show no such systematic trend. The linking of these states was based on levels which could have the same J^π values, have similar decay schemes, and have similar spectroscopic factors as measured in the (t,α) reactions [Bl 66]. Support for assigning a collective nature to these levels comes from Corello and Manfredi's calculations [Co 71] on the quintet in ^{57}Co . They performed a similar calculation to that of Satpathy and Gujrathi [Sa 68], coupling the $f_{7/2}$,

$s_{1/2}$ and $d_{3/2}$ proton hole states to quadrupole and octupole vibrations of the ^{58}Ni core, and derived mixing ratios for transitions between the levels which agree well with the experimental values of Coop *et al.* [Co 70]. In the case of ^{59}Co , further support for the division of levels comes from the (d,d') measurements of Nordhagen *et al.* [No 67]. This reaction strongly excites collective vibrational levels, and it was found that the reaction excited the five states in ^{59}Co which are indicated as being collective in fig. 8.1, but did not excite the $3/2^-$ and $1/2^-$ single particle states.

Continuing the assignments up to ^{61}Co and ^{63}Co is more difficult. The $3/2^-$ first excited states have the same (t, α) spectroscopic factors as the first excited state of ^{59}Co , but apart from this, further assignments in ^{63}Co are not possible without more data. The $5/2$, $7/2$ doublet at 1.65 MeV in ^{61}Co has a similar decay scheme to the 1.90 MeV doublet in ^{57}Co if the 1.287 MeV state is taken to be the $9/2^-$ member of the "collective quintet" in ^{61}Co . Accepting this interpretation, there are then no levels in ^{61}Co below 2.2 MeV which can be associated with the ($11/2^-$) states in ^{57}Co and ^{59}Co . However, if the 1.287 MeV state is $11/2^-$, then the 1.887 MeV state is the only likely $9/2^-$ candidate. Further experimental study is required to settle this problem.

The labelling of states in these nuclei as either single particle or collective is not completely justified as there could be mixing of configurations in these states. Hudson and Glover [Hu 71] in their (t,p) and (t, α) studies of ^{61}Co , observed that, although the two reaction mechanisms were different, many states were excited in both reactions. They interpreted this as evidence of mixing of neutron and proton configurations. Similarly, from an examination

of the ($^3\text{He},d$) and (t,α) results [Ro 67, Bl 65 and Bl 66], there may be some admixing of configurations into the single particle states in ^{57}Co and ^{59}Co . In particular, the "single particle" $3/2^-$ state in ^{57}Co appears to have a purer single particle configuration than the $3/2^-$ state in ^{59}Co , while the "collective" $3/2^-$ state in ^{59}Co has a larger share of the $3/2^-$ strength in the ($^3\text{He},d$) reaction than its equivalent in ^{57}Co .

Some indication of the magnitude of the admixture into the $3/2^-$ 1.291 MeV state in ^{59}Co comes from the calculations of Agarwal *et al.* [Ag 67]. The 1.375 (^{57}Co) and 1.291 (^{59}Co) MeV levels have lifetimes of $T_{1/2} = 0.03$ and 0.6 ns, respectively [Be 67a and Ag 67]. This large difference in lifetimes cannot be explained by the energy differences alone, and, in fact, the ^{59}Co 1.291 MeV E2 transition to ground is retarded considerably in comparison to a single particle estimate. Agarwal *et al.* accounted for this by assuming an admixture of a $p_{3/2}$ single particle state and a $3/2^-$ state obtained by coupling an $f_{7/2}$ hole to the 2^+ excitation of the ^{60}Ni core. The wave functions of the two ^{59}Co $3/2^-$ states were then written as:

$$\psi_1(1.100 \text{ MeV}) = \alpha |f_{7/2}; 2^+ : 3/2^- \rangle + \sqrt{1 - \alpha^2} |p_{3/2} \rangle$$

$$\text{and } \psi_2(1.291 \text{ MeV}) = \sqrt{1 - \alpha^2} |f_{7/2}; 2^+ : 3/2^- \rangle - \alpha |p_{3/2} \rangle .$$

A value of $\alpha = 0.9$, i.e. a single particle admixture of about 80%, was needed to fit the observed lifetime. This value was then used to calculate other properties of the 1.100 and 1.291 MeV states, and good agreement with experimental results was achieved. A similar calculation on the $3/2^-$ levels in ^{57}Co (where the 1.375 MeV E2

transition is only retarded by a factor of 4 [Be 67a] as compared with a factor of 50 for the ^{59}Co state), would be expected to lead to a purer single particle configuration.

Thus it would appear that the systematic decrease of excitation energies of the collective quintet with increase in mass, as calculated by Satpathy and Gujrathi [Sa 68], is modified by single particle admixtures. The general trend is reproduced by the experimental results, and in particular, the $7/2^-$ states are near the calculated values (2.01, 1.73 and 1.57 MeV). The $7/2^-$ levels would be expected to be the purest collective states, since they have the highest transition strengths in the (t,α) reactions. However, it is obvious that another theoretical approach is necessary to attempt to account for the known low lying levels of these isotopes and their decay properties. The calculations would need to describe the apparent strong single-particle character of some levels, and the more complex character of others. Larner [La 70] has performed calculations on nuclei in this region, (^{51}Ti , ^{53}Cr , ^{55}Fe , $^{61,63,65}\text{Cu}$) using an intermediate coupling model developed by Thankappan and True [Th 65]. In general, Larner achieved a good agreement between the theory and experimental data for both the single particle strengths and the collective properties. The calculations of Satpathy and Gujrathi [Sa 68] for the odd-mass cobalt isotopes are similar to those of Larner [La 70], and it is possible that the calculations of the former authors could be successfully extended by including additional single particle configurations.

This study of the level schemes for the low lying states of ^{57}Co , ^{59}Co and ^{61}Co has indicated that there are many similarities between the nuclei. Additional data for some of the states

concerned and for higher excited states are needed before further comparisons can be made; however, the acquisition of such data becomes increasingly difficult as excitation energies and level densities increase. It would also be useful to have more information on the levels in ^{63}Co , so that it could be compared with the other three odd-mass cobalt isotopes. The main need though, is for an improved theoretical approach to explain the properties already observed in these nuclei.

APPENDIX

CONSIDERATIONS INVOLVED IN ANGULAR CORRELATION MEASUREMENTS

The theory of γ -ray angular correlations has been discussed at length by Litherland and Ferguson [Li 61] and Rose and Brink [Ro 67a]. The latter authors developed a phase defined theory from first principles, so that experimentally measured and theoretically predicted signs of mixing ratios could be compared. This was necessary, since previous treatments differed in their sign conventions for some cases. The formulae and tables calculated by Rose and Brink were used to analyze the results of the angular correlation measurements reported in this thesis.

The formula for γ -ray angular distributions is given (without the coefficients Q_k) by Rose and Brink [Ro 67a] as:

$$W(\theta) = \sum_k B_k(J_1) P_k(\cos\theta) Q_k \times \left[\frac{R_k(LLJ_1J_2) + 2\delta R_k(LL'J_1J_2) + \delta^2 R_k(L'L'J_1J_2)}{1 + \delta^2} \right]$$

which is valid for the case when only the two lowest multipolarities, L and $L' = L + 1$, contribute to the γ -ray transition between the initial state of spin J_1 and the final state of spin J_2 ; this condition is assumed to be valid for measurements reported in this thesis. θ is the angle between the direction of the particle beam (which is taken as the axis of symmetry) and the outgoing γ -ray. The quantity δ is the γ -ray mixing ratio defined in eq. 3.39 of ref. [Ro 67a]; it can, *in modulus*, be interpreted as the square root of the ratio of the partial γ widths for the two multipolarities occur-

ing in the transition. The coefficients $B_{\kappa}(J_1)$ describe the alignment of the initial state J_1 , while the coefficients R_{κ} are independent of the alignment and depend only upon the spins of the initial and final states, and the multipolarities involved in the transition; the coefficients R_{κ} are tabulated in ref. [Ro 67a]. The coefficients Q_{κ} account for the attenuation of the angular correlation due to the finite size of the NaI detector; they were calculated using the method outlined by Rose [Ro 53]. Finally, the coefficients P_{κ} are the Legendre polynomials.

For the case where the second member of a γ -ray cascade is observed, the above equation can be made applicable by including a coefficient U_{κ} (tabulated in ref. [Ro 67a]), which is dependent upon the initial and final state spins of the unobserved γ -ray, and upon the mixing ratio of the transition between these two states. In this case, the coefficient B_{κ} refers to the alignment of the initial state of the unobserved γ -ray. Thus the product $B_{\kappa} U_{\kappa}$ effectively determines the alignment of the initial state of the second (observed) member of the cascade.

For reactions of the type $X(\underline{a}, \underline{b}\gamma)Y$, where \underline{b} is not detected, the system is cylindrically symmetric about the beam axis. If the beam and target nuclei are unpolarized, and if the initial state J_1 has definite parity, the population of each $+M_1$ substate is equal to the population of the $-M_1$ substate; i.e. the state J_1 is aligned. This simplifies the B_{κ} coefficients so that they can be written as:

$$B_{\kappa}(J_1) = \sum_{M_1=0 \text{ or } 1/2}^{M_1=J_1} \omega(M_1) \rho_{\kappa}(J_1 M_1) ,$$

where the ρ_κ are the statistical tensor coefficients (tabulated in ref. [Ro 67a]), and the $\omega(M_1)$ are the population parameters of the M_1 substates which are normalized so that:

$$\sum_{M_1} \omega(M_1) = 1 .$$

This limits the values of κ , since the B_κ coefficients are zero for odd κ . A further limit on the values of κ is determined by the triangular conditions governing the Clebsch-Gordan and Racah coefficients used in the definitions of B_κ and R_κ ; namely, $\kappa \leq \min(2J_1, 2L, 2L')$.

In order to calculate the angular correlation in the above case, a complete knowledge of the reaction mechanism is required to predict the population parameters $\omega(M_1)$ uniquely. However, if the particle \underline{b} is detected at 0° or 180° , then neither the cylindrical symmetry nor the alignment condition is destroyed, and there is a further restriction on the population parameters. Because of the detection of \underline{b} coaxial with \underline{a} no contributions to the possible M_1 values can come from orbital angular momenta. Thus, the only population parameters which can contribute, must fulfil the condition $|M_1| \leq J_x + s_a + s_b$ where J_x is the target spin, and s_a and s_b are the spins of the incident and outgoing particles, respectively. For reactions such as (α, p) on targets of zero spin, the condition on $|M_1|$ reduces to $|M_1| = 1/2$ and the alignment is unique.

However, in practice, when angular correlations are measured between the protons and coincident γ -rays, the proton detector subtends a finite range of angles about 0° or 180° . If the detector is an annular counter, the cylindrical symmetry of the problem is

preserved, but, because of the finite range of angles subtended, substates other than $|M_1| = 1/2$ may now contribute to the population of the state J_1 . In the magnetic spectrometer measurements, the maximum half angle subtended is considerably less than that subtended by the annular counter (6° compared to 15°), so that this effect should be substantially reduced. However, a further complication arises from the rectangular acceptance slits of the instrument; the axial symmetry which is, strictly speaking, required for the above formulae to be applicable, is not preserved. In this regard, Litherland [Li 64] has pointed out that certain misalignments of the particle counter do not affect the angular correlations; Kean [Ke 69] has discussed this problem in relation to the A.N.U. spectrometer and has argued that the errors introduced are negligible.

In general, the relative population of substates contributing to the correlation depends not only on the angles subtended by the detector, but also depends upon the specific process by which the state is formed. Litherland and Ferguson [Li 61] have indicated that the relative population of higher substates contributing to the correlation is proportional to ϕ^2 , where ϕ is the half angle subtended by the detector. For small values of ϕ , most experimenters assume that the contributions from substates $|M_1| > 1/2$, due to the finite size of the particle detector, are small and can be neglected for reactions such as $(\alpha, p\gamma)$.

Another problem in determining the population parameters of the magnetic substates arises if the alignment of the initial state is significantly changed before the emission of the γ -ray. For sufficiently long lived states, the relative population of the

magnetic substates may be altered by the interaction of the electric and magnetic moments of the nucleus with the electric and magnetic fields generated by the atomic electrons. This effect is usually assumed to be negligible for lifetimes shorter than approximately 10^{-10} sec [Fe 65]; however, a recent study by Ben Zvi *et al.* [Be 68] has shown that, under certain conditions, states with lifetimes as short as 10^{-12} sec may be appreciably affected by the hyperfine fields generated in highly ionized, recoiling atoms. With the conditions pertaining in the present experiments, it is unlikely that the hyperfine fields will be as large as those observed by Ben Zvi *et al.*, but for states with longer lifetimes, some attenuation of the correlations might be expected.

In the $^{56}\text{Fe}(\alpha, p\gamma)$ correlation measurements, there are some internal checks regarding these problems. The 1.291 and 1.100 MeV states have lifetimes of 6×10^{-10} and 2×10^{-12} sec respectively. Both states have a spin of $3/2^-$, and the ground state transitions are almost certainly pure E2 ($\delta = 0$). Therefore, the correlation is dependent only upon the relative contribution of the $|M_1| = 1/2$ and $|M_1| = 3/2$ substates. Unfortunately, the predicted correlations for the $|M_1| = 1/2$ and $3/2$ cases are not strongly anisotropic, and the errors involved in the measurements are large compared with the expected changes in the pure $|M_1| = 1/2$ correlation. Hence, even the presence of rather large contributions from the $|M_1| = 3/2$ substates is difficult to detect.

Coop [Co 69] has made measurements on the ^{56}Fe and $^{64}\text{Ni}(\alpha, \alpha'\gamma)$ reactions to investigate this effect. Angular correlations were made on 2^+ to 0^+ transitions from states with known lifetimes, under similar experimental conditions to those used in the

present Fe(α, γ) experiments. The 2^+ to 0^+ transitions are pure E2 and have the desirable feature of being strongly anisotropic. Coop's results indicated that the attenuation of the angular correlation due to the finite size of the particle detector and the hyperfine interactions, could be accounted for by assuming that only the two lowest magnetic substates contributed to the correlation.

For the (α, γ) measurements, it was concluded that a population ratio of 0.1 or less for the $|M_1| = 3/2$ to $1/2$ substates would generally account for the observed attenuation. The lifetimes of the levels investigated by Coop [Co 69] were of the order of $\sim 10^{-11}$ sec, and this was considered the limit of the applicability of the above conclusion. As most states investigated can decay by E2/M1 admixtures, this is not a particularly restrictive assumption. (The Weisskopf estimates for a 1.5 MeV γ -ray transition in cobalt are $\tau(M1) \approx 10^{-14}$ sec and $\tau(E2) \approx 10^{-11}$ sec.) Of the three lifetimes known for states in ^{59}Co , two are below this limit (1.100 MeV - 2×10^{-12} sec and 1.190 MeV - 5×10^{-14} sec). The other, the 1.291 MeV state has a lifetime of 6×10^{-10} sec. This long lifetime is quite unusual, being two orders of magnitude greater than the Weisskopf estimate for a pure E2 transition ($3/2^-$ to $7/2^-$). For other states in ^{59}Co where such an inhibition might be expected to occur (low lying states with $J \leq 3/2$ or $\geq 11/2$), due note is taken in the discussion of the analysis (section 7.4.2).

Thus the general procedure followed here was to fit the data for both $P(3/2)/P(1/2) = 0.0$ and 0.1 , and to consider both results when making spin assignments and determining possible mixing ratio values. In some cases where long lifetimes might have been expected, the effects of assuming $P(3/2)/P(1/2) = 0.3$ were also investigated.

REFERENCES

- Ag 67 Y.K. Agarwal, C.V.K. Baba and S.K. Bhattacharjee, Nucl. Phys. A99 (1967) 457.
- Aj 69 F. Ajzenberg-Selove, "Energy levels of light nuclei: A = 13" (Lemon aid preprint, May 1969), and Nucl. Phys. A152 (1970) 1.
- Ba 61 F.C. Barker, Nucl. Phys. 28 (1961) 96.
- Ba 66 F.C. Barker, J.R. Patterson, J.M. Poate and E.W. Titterton, Phys. Lett. 21 (1966) 318.
- Ba 67 H. Bakhru and I.L. Preiss, Phys. Rev. 154 (1967) 1091.
- Be 67 R. Beraud, I. Berkes, J. Daniere, M. Levy, G. Marest and R. Rougny, C.R. Acad. Sc. Paris, t265B (1967) 1354.
- Be 67a R. Beraud, I. Berkes, G. Marest and R. Rougny, Nucl. Phys. A98 (1967) 154.
- Be 68 I. Ben Zvi, P. Gilad, M. Goldberg, G. Goldring, A. Schwarzschild, A. Sprinzak and Z. Vager, Nucl. Phys. A121 (1968) 592.
- B1 65 A.G. Blair and D.D. Armstrong, Phys. Rev. 140 (1965) B1567.
- B1 66 A.G. Blair and D.D. Armstrong, Phys. Rev. 151 (1966) 930.
- B1 68 J.L. Black, W.J. Caelli and R.B. Watson, private communication (1968).
- B1 68a S.L. Blatt, A.M. Young, S.C. Ling, K.J. Moon and C.D. Porterfield, Phys. Rev. 176 (1968) 1147.
- B1 69 J.L. Black, W.J. Caelli and R.B. Watson, "Interim report on the A.N.U. ten inch NaI(Tl) γ -ray spectrometer", A.N.U. internal report ANU-P/483 (1969), unpublished.

- B1 70 J.L. Black, W.J. Caelli, W.F. Davidson and R.B. Watson,
Nucl. Phys. A153 (1970) 233.
- Bo 36 N. Bohr, Nature 137 (1936) 344.
- Bo 68 N. Bouchard and B. Cujec, Nucl. Phys. A108 (1968) 529.
- Br 56 C.P. Browne and W.W. Buechner, Rev. Sci. Instr. 27 (1956)
899.
- Br 64 D.M. Brink, R.O. Stephen and N.W. Tanner, Nucl. Phys. 54
(1964) 577.
- Ca 69 W.J. Caelli, D.F. Hebbard, W.J. Lamberth and T.R. Ophel,
Proceedings of Fourth Australian Computer Conference
(1969), p.557.
- Ca 70 T.A. Cahill, F.P. Brady, S. Corbett, W. Hammontree,
K. Isaacs and E. Young, Nucl. Instr. Meth. 87 (1970)
151.
- Co 57 B.C. Cook, Phys. Rev. 106 (1957) 300.
- Co 65 K.L. Coop and H.A. Grench, Nucl. Instr. Meth. 36 (1965)
339 and erratum 45 (1966) 359, Lockheed Report
LMSC-6-75-65-37.
- Co 65a S. Cohen and D. Kurath, Nucl. Phys. 73 (1965) 1.
- Co 69 K.L. Coop, Ph.D. thesis, Australian National University
(1969), unpublished.
- Co 70 K.L. Coop, I.G. Graham and E.W. Titterton, Nucl. Phys.
A149 (1970) 463.
- Co 71 A. Covello and V.R. Manfredi, Phys. Lett. 34B (1971) 584.
- Cr 64 W.G. Cross, Phys. Canada 20 #2 Abstr. 7.5 (1964) 36.
- Da 68 J.M. Daniels and J. Felsteiner, Can. J. Phys. 46 (1968)
1849.

- Di 63 J.K. Dickens, D.W. Haner and C.N. Waddell, Phys. Rev. 132
(1963) 2159.
- Ea 62 B.R. Easlea, Phys. Lett. 1 (1962) 163.
- E1 66 F. El-Batanoni and A.A. Kresnin, Nucl. Phys. 89 (1966) 577.
- E1 68 R.V. Elliott, K.W. Carter and R.H. Spear, Nucl. Instr.
Meth. 59 (1968) 29, and R.V. Elliott, Ph.D. thesis,
Australian National University (1968), unpublished.
- Er 60 T. Ericson, Advances in Physics 9 (1960) 425.
- Er 63 T. Ericson, Ann. Phys. (N.Y.) 23 (1963) 390.
- Fe 65 A.J. Ferguson, "Angular correlation methods in gamma ray
spectroscopy" (North-Holland Publ. Co., Amsterdam,
1965).
- Fi 63 P.S. Fisher, D.F. Measday, F.A. Nikolaev, A. Kalmykov and
A.B. Clegg, Nucl. Phys. 45 (1963) 113.
- Ga 69 C. Gatrousis, R.A. Meyer, L.G. Mann and J.B. McGrory,
Phys. Rev. 180 (1969) 1052.
- Gi 70 M. Girod, Nguyen Van Sen, J.P. Longequeue and
Tsan Ung Chan, Journal de Physique 31 (1970) 125.
- Go 66 N.B. Gove, in "Nuclear spin-parity assignments", ed. by
N.B. Gove and R.L. Robinson (Academic Press, New York,
1966) p.83.
- Gr 67 H.A. Grench, K.L. Coop and H.O. Menlove, Phys. Rev. 161
(1967) 1118.
- He 70 J.O.V. Hellström, Ph.D. thesis, Australian National
University (1970), unpublished.
- Hu 68 F.C.P. Huang, Ph.D. thesis, Australian National University
(1968), unpublished.
- Hu 71 F.R. Hudson and R.N. Glover, Nucl. Phys. A160 (1971) 482.

- Ja 51 H.A. Jahn and H. van Wieringen, Proc. Roy. Soc. A209
(1951) 502.
- Ke 69 D.C. Kean, Ph.D. thesis, Australian National University
(1969), unpublished.
- Ku 63 I. Kumabe, H. Ogata, T. Komatuzaki, N. Inoue, S. Tomita,
Y. Yamada, T. Yamaki and S. Matsumoto, Nucl. Phys. 46
(1963) 437.
- Ku 64 Hsin-Min Kuan, T.W. Bonner and J.R. Risser, Nucl. Phys.
51 (1964) 481
- Ku 71 N. Kumar, private communication (1971).
- La 66 T. Lauritsen and F. Ajzenberg-Selove, Nucl. Phys. 78
(1966) 1.
- La 70 D. Larner, Phys. Rev. C2 (1970) 522.
- Le 64 K.J. Le Couteur, Phys. Lett. 11 (1964) 53.
- Li 61 A.E. Litherland and A.J. Ferguson, Can. J. Phys. 39 (1961)
788.
- Li 64 A.E. Litherland, in "Radiative transitions in nuclear
structure and electromagnetic interactions", ed. by
N. MacDonald (Oliver and Boyd, Edinburgh, 1964) p.108.
- Li 67 E.W.A. Lingemann, J. Konign, F. Diederik and B.J. Meijer,
Nucl. Phys. A100 (1967) 136.
- Me 63 D.F. Measday, P.S. Fisher, A. Kalmykov, F.A. Nikolaev and
A.B. Clegg, Nucl. Phys. 44 (1963) 98.
- Me 65 D.F. Measday, A.B. Clegg and P.S. Fisher, Nucl. Phys. 61
(1965) 269.
- Mo 67 P.A. Moldauer, Phys. Rev. Lett. 18 (1967) 249.
- N.D.S. Nuclear Data Sheets, ed. by Nuclear Data Group ORNL
(Academic Press, New York).

- Ni 59 G.J. Nijght, A.H. Wapstra and R. von Lieshout, "Nuclear spectroscopy tables" (North-Holland, Amsterdam, 1959).
- No 67 R. Nordhagen, B. Elbek and B. Herskind, Nucl. Phys. A104 (1967) 353.
- Op 68 T.R. Ophel, private communication (1968).
- Op 70 T.R. Ophel, "Notes on nuclear spectroscopy instrumentation", A.N.U. internal report ANU-P/502 (1970), unpublished.
- Os 64 D.R. Osgood, J.R. Patterson and E.W. Titterton, Phys. Lett. 10 (1964) 75.
- Ov 62 J.C. Overly and W. Whaling, Phys. Rev. 128 (1962) 315; G.D. Symons and P.B. Treacy, Nucl. Phys. 46 (1963) 93; H.L. Jackson and A.L. Galonsky, Phys. Rev. 89 (1953) 370; M. Lambert and M. Durand, Phys. Lett. 24B (1967) 287; V. Gomes, R.A. Douglas, T. Polga and O. Sala, Nucl. Phys. 68 (1965) 417.
- Pa 65 J.R. Patterson, J.M. Poate and E.W. Titterton, Proc. Phys. Soc. 85 (1965) 1085.
- Pa 65a J.R. Patterson, J.M. Poate, E.W. Titterton and B.A. Robson, Proc. Phys. Soc. 86 (1965) 1297.
- Pa 66 J.R. Patterson, J.M. Poate and E.W. Titterton, Proc. Phys. Soc. 88 (1966) 641.
- Pe 63 R.W. Peterson and N.W. Glass, Phys. Rev. 130 (1963) 292.
- Pi 66 C.J. Piluso, D.O. Wells and D.K. McDaniels, Nucl. Phys. 77 (1966) 193.
- Po 67 J.M. Poate, Ph.D. thesis, Australian National University (1967), unpublished.
- Ri 68 E.M. Rimmer and P.S. Fisher, Nucl. Phys. A108 (1968) 561.
- Ro 53 M.E. Rose, Phys. Rev. 91 (1953) 610.

- Ro 67 B. Rosner and C.H. Holbrow, Phys. Rev. 154 (1967) 1080.
- Ro 67a H.J. Rose and D.M. Brink, Rev. Mod. Phys. 39 (1967) 306.
- Ro 70 P. Roussel, G. Bruge, A. Bussiere, H. Faraggi and
J.E. Testoni, Nucl. Phys. A155 (1970) 308; J.N. Mo,
B. Cujec, R. Dayras, I.M. Szoghy and M. Toulemonde,
Nucl. Phys. A147 (1970) 129, and references contained
therein.
- Sa 68 L. Satpathy and S.C. Gujrathi, Nucl. Phys. A110 (1968) 400.
- Sc 56 J.P. Schiffer, T.W. Bonner, R.H. Davis and F.W. Prosser,
Phys. Rev. 104 (1956) 1064.
- Sc 66 E.F. Scarr, M.Sc. thesis, Australian National University
(1966), unpublished.
- Sc 67 D.K. Scott, P.S. Fisher and N.S. Chant, Nucl. Phys. A99
(1967) 177.
- Sh 71 Y.M. Shin, C.F. Wong and H.S. Caplan, Nucl. Phys. A166
(1971) 162.
- Si 66 P.P. Singh, B.A. Watson, J.J. Kroepfl and T.P. Marvin,
Phys. Rev. Lett. 17 (1966) 968.
- Si 70 J. Singh, Nucl. Phys. A155 (1970) 453.
- Sk 67 D.J. Skyrme, Nucl. Instr. Meth. 57 (1967) 61.
- St 66 J.E. Strain and W.J. Ross, J. Inorg. Nucl. Chem. 28 (1966)
2075.
- Su 68 M. Suffert, W. Feldman, J. Mahieux and S.S. Hanna, Nucl.
Instr. Meth. 63 (1968) 1.
- Ta 60 I.J. Taylor, F. de S. Barros, P.D. Forsyth, A.A. Jaffe and
S. Ramavataram, Proc. Phys. Soc. 75 (1960) 772.
- Th 65 V.K. Thankappan and W.W. True, Phys. Rev. 137 (1965) B793.

- Wi 62 C. Williamson and A.J. Boujot, "Tables of range and rate of energy loss of charged particles of energy 0.5 to 150 MeV", C.E.A.-2189 (1962) and C.E.A.-R3042 (1966).
- Wi 66 D.H. Wilkinson, J.T. Sample and D.E. Alburger, Phys. Rev. 146 (1966) 662.
- Yu 67 H.P. Yule, Nucl. Instr. Meth. 54 (1967) 61.